








A Compendium of Key Seismic and Geological Aspects for Characterizing the Upper Aptian Carbonate Reservoirs in the Brazilian Pre-Salt

Nathalia Martinho S. M. da Cruz ¹, Thais P. Bispo Moreira ¹, Adler Nascimento ¹,
Leonardo Teixeira ¹, Jose Marcelo Cruz ¹, Alexandre Maul ¹, and Wagner Lupinacci ²

¹Petrobras, Rio de Janeiro, RJ, Brazil

²Universidade Federal Fluminense - UFF, Niterói, RJ, Brazil

*Corresponding author email: nathalia.martinho@petrobras.com.br

ABSTRACT. The Aptian carbonate reservoirs within the pre-salt section of the Santos Basin, such as the principal reservoirs of the Tupi Field, exhibit considerable heterogeneity in reservoir quality. This variability is influenced by several factors, including the widespread presence of magnesium clay minerals and diagenetic processes, which hampers hydrocarbon production. Given the lack of comprehensive reservoir-scale historical references, we revisit the reservoir zoning, inherent individualizations, facies distributions, seismostratigraphic, and tectonic features of the Barra Velha Formation within the Tupi Field. We spatially map key elements, decipher facies association profiles, and pinpoint porosity classes tied to facies and depositional or diagenetic characteristics from a multi-scale dataset comprising rock samples, well logs, and seismic data. A pragmatic seismostratigraphic zoning approach was employed to define intervals BVE100, BVE200, and BVE300 and their subzones. Reservoir quality was then linked with lake retraction periods, identified by an increase in well-developed shrubs displaying higher porosities and permeabilities, properties further amplified by dissolution phenomena. We also discuss the influence of structural positioning on facies distribution, associating higher carbonates with clay minerals proportions to structural lows, and reworked carbonates reservoirs to the structural highs and edges. We argue that only the BVE100 displays sag-type features, suggesting a mixed tectonic setting for BVE200. Furthermore, we characterized Feature X, a unique BVE100 high acoustic impedance signature associated with wells sampling elevated proportions of low-energy facies within structural flanks and lows. These insights carry significant implications for exploration and exploitation strategies in the studied area and can be applied to other pre-salt regions of any basin.

Keywords: seismostratigraphy, facies associations, reservoir zoning, tectonic context, seismic facies, diagenetic processes, porosity and permeability relationship, reworked carbonates reservoirs, Mg-clay minerals.

INTRODUCTION

The Santos Basin pre-salt, located in the southeast region of the Brazilian Coast, stands as the leading oil-producing province in Brazil. This prominent status is further underscored by the exceptional results achieved in the Tupi, Sapinhoá, Búzios, Mero, and Iara Complex oil fields, which together account for nearly 75% of Brazil's oil production (ANP, 2024). The considerable economic value, ultra-deep-water location, complex sedimentary deposition characteristics, and unique geological, petrophysical, and geophysical features of the Santos Basin's carbonate reservoirs demand the use of advanced seismic data acquisition, ultimate processing techniques, and detailed, continuous up-to-date interpretation and modeling.

The main hydrocarbon reservoirs in the Santos Basin pre-salt section are the carbonate rocks of the Barra Velha Formation (in-situ carbonates, reworked carbonates, and carbonates with dissolution features) and the Itapema Formation (bioclastic agglomerates/coquinas). Despite a significant and available body of academic literature on the pre-salt section, the complexities of the intrinsically tectono-stratigraphic evolution, as well as the varied depositional and diagenetic elements that shaped its expansive reservoirs, are still not fully comprehended (Moreira et al., 2007; Teixeira et al., 2017; Artagão, 2018; Pedrinha et al., 2018; Artagão, 2019; Cruz, 2019; Dias et al., 2019; Penna et al., 2019; Mello, 2020; Cruz et al., 2021a; Cruz et al., 2021b; Castro and Lupinacci, 2022; Mello and Lupinacci, 2022; Pedrinha et al., 2024). Moreover, most of the

published material focuses on separate, frequently regionally purposed, sedimentological, diagenetic, or geophysical aspects, without a more pragmatic reservoir-scale characterization and exploitation perspective.

Specifically, regarding the Barra Velha Formation, several topics remain debated in the literature, presenting various geological and geophysical challenges that require further investigation. Key questions include the nature of the depositional environment, which could be lacustrine, marine, or influenced by marine conditions. There are uncertainties about the tectonic context and its role in orienting reservoir predispositions, with interpretations ranging from sag and rift portions to mixed tectonic settings (Figure 1). The origin of the deposits is also a point of contention, with possibilities including chemical, biological, biochemical, or biologically influenced processes. Moreover, there are ongoing disputes over the best criteria for reservoir zoning and the individualization of the Barra Velha Formation, with various facies nomenclatures (e.g., Pedrinha et al., 2018; Figure 2) and associated depositional and diagenetic models being proposed (Moreira et al., 2007; Wright and Barnett, 2015; Artagão, 2018; Pedrinha et al., 2018; Artagão, 2019; Gomes et al., 2020; Magalhães et al., 2020; Silva et al., 2021; Cruz et al., 2021a; Cruz et al., 2021b; Carramal et al., 2022; Castro and Lupinacci, 2022; Mello and Lupinacci, 2022; Pedrinha et al., 2024; Pedrinha and Artagão, 2024).

The distribution of magnesium clay minerals and the delineation between reservoir, non-reservoir, and transitional zones are critical aspects, as is the presence of lesser-known seismic features and facies, such as Feature X (Figure 3), which requires broader correlation with well data. Moreover, prior to the Tupi Nodes Pilot, there was significant skepticism regarding the effectiveness of time-lapse seismic for proactive monitoring of low compressibility reservoirs in the Santos Basin pre-salt (Cruz et al., 2021a; Cruz et al., 2021b). These topics represent the main geological and geophysical uncertainties and challenges impacting the characterization, exploration, and exploitation of the Barra Velha Formation reservoirs and are mostly addressed in this work.

Accordingly, we outline the requisite data and methodology for obtaining continuous and robust facies association profiles essential for effective seismostratigraphic zoning. Our approach involves the identification and detailed description of key lithologies, geological markers, and their associated seismic horizons, alongside other significant seismic and geological features crucial for characterizing and modeling pre-salt reservoirs. Specifically, our analysis focuses on the stratigraphic intervals named BVE100 and BVE200 – reservoir zones that adhere to the nomenclature established by Pedrinha et al. (2018), Minzoni et al. (2021), Pedrinha et al. (2024), and Pedrinha and Artagão (2024). These analyses are designed to guide geological-geophysical interpretations that facilitate the identification of areas predominantly containing reservoir, non-reservoir, and transition facies

within the Barra Velha Formation, while also being applicable to additional geological units of interest.

We have adopted and elaborated on a few premises, including the reservoir zoning terminology – BVE100, BVE200, and BVE300 (Pedrinha et al., 2018; Pedrinha et al., 2024; Pedrinha and Artagão, 2024) – and the lacustrine depositional environment (Wright & Barnett, 2015; Pedrinha et al., 2018; Gomes et al., 2020; Carramal et al., 2022; Pedrinha and Artagão, 2024). We also discuss several key themes, such as the tectonic context, analyzed through seismic thickness observations during detailed seismostratigraphic mapping at the Tupi Field. However, it is important to note that discussing the origin of the deposits is not within the scope of this work. For reservoir zoning criteria and the individualization of the Barra Velha Formation, we consolidate and detail the primary criteria from the literature, applying them within the geological context of our study area, enriched with multi-scale interpretative details. Our methodology describes a pragmatic, step-by-step seismostratigraphic and rock-supported approach, incorporating seismic facies analysis, extensive rock and log data interpretations, and a review of major findings from previous studies, such as the main fluid-flow paths and baffles identified in the 4D seismic interpretation of the Tupi Nodes Pilot and their correlation to Feature X (Cruz et al., 2021a; Cruz et al., 2021b). Regarding facies nomenclature and depositional models, we have adopted and adapted proposals from Pedrinha et al. (2018) and Pedrinha and Artagão (2024), integrating a

revised tectonic context and placing greater emphasis on the correlation between local log patterns and seismic responses.

To better understand the distribution of magnesium clay minerals and the differentiation between reservoir, non-reservoir, and transitional zones in the Tupi Field and the pre-salt section of the Santos Basin, we conducted various petrogeophysical studies. Refer to Wyman (1981), Lebedev et al. (2009), Rosa (2010); Rosa (2018), Vasquez et al. (2021), and Cruz (2023) for the terminology. These studies represent a comprehensive integration of geological, petrophysical, and seismic data, allowing us to elucidate the vertical and lateral variations and distributions of depositional facies and diagenetic elements observed in the Tupi Field wells. Additionally, we explored the extension of these elements beyond the wells' immediate surroundings by leveraging various seismic attributes. By defining key effective porosity classes and analyzing seismic amplitude, thickness, and impedance characteristics, we pinpointed regions and intervals with enhanced reservoir quality.

Furthermore, all cited seismic features and facies were analyzed and extensively correlated with well data, with special attention given to Feature X. We present a detailed workflow for the seismostratigraphic characterization of the Tupi Field, outlining key steps in rock-log-seismic correlations and highlighting intermediate products that aid in understanding the overall work. This step-by-step approach can be replicated in any pre-salt field and analogous situations. We consolidate the results and

provide a concluding discussion that summarizes and highlights the main structural, facies, and seismic characteristics of the BVE100, BVE200 and BVE300 stratigraphic intervals, which comprise the Barra Velha Formation in the Tupi Field.

General Geological Overview

The terms "pre-salt layer" or "pre-salt section" commonly refer to the set of Brazilian pre-salt Aptian carbonate reservoirs located beneath a saline evaporitic sequence, comprising salt layers that vary from homogeneous to stratified. Meanwhile, the terms "pre-salt province" or "pre-salt play" typically denote the oil fields established in an offshore area spanning approximately 150,000 km², encompassing the Santos, Campos, and Espírito Santo basins (Formigli, 2007; Carminatti et al., 2008; Chang et al., 2008; Gomes et al., 2020). Additionally, "pre-salt play" can signify a set of features or prospects that show the potential for hydrocarbons (Riccomini et al., 2012). The saline evaporitic sequence in question serves as the primary seal for these hydrocarbon accumulations and can vary in thickness from a few meters to kilometers (Teixeira et al., 2020). On November 8th, 2007, Petrobras, the Brazilian oil operator, officially used the term "pre-salt" for the first time in a letter to the press (Machado, 2018).

The reservoirs of interest for this study are set within the geological context of the pre-salt layer of the Santos Basin. The Santos Basin is the largest Brazilian offshore basin, located in the

southeastern region of the Brazilian continental margin, between the parallels 23° and 28° south latitude. It spans an area of approximately 350,000 km² and extends to a bathymetric depth of over 3000 m. The basin's formation is associated with the breakup of the Gondwana supercontinent and the opening of the South Atlantic Ocean around 135 million years ago (Ma) (Mio et al., 2005; Thiede et al., 2010; Buckley et al., 2015).

The lithostratigraphic detailing of the Santos Basin began with the work of Ojeda and Cesero (1973). In the 1970s, Ponte and Asmus (1978) classified it as a passive margin basin, describing its evolution based on tectono-sedimentary mega-sequences separated by regional unconformities. Later, Pereira and Feijó (1994) sought to establish a chrono-lithostratigraphic framework emphasizing depositional sequences, which was updated by Moreira et al. (2007) due to the large volume of well and seismic data acquired by Petrobras' exploratory campaigns in the early 2000s (Artagão, 2018). Distinct interpretations proposed for the tectono-stratigraphic evolution of the Santos Basin, focusing on the Barra Velha Formation, are depicted in Figure 1.

Moreira et al. (2007) categorized the sedimentary record of the Santos Basin into supersequences demarcated by regional unconformities. These divisions are associated with the primary stages of the basin's tectonic evolution, occurring within the context of the Western Gondwana breakup (Milani et al., 2007). The identified stages encompass the rift (Hauterivian - Lower Aptian), post-rift (Aptian),

and drift (from the Albian to the present). According to Moreira et al. (2007), the rift stage aligns with the lower portion of the Guaratiba Group, comprising volcanic rocks (Camboriú Formation), predominantly siliciclastic sediments (Piçarras Formation), and bioclastic carbonates and siliciclastic rocks (Itapema Formation). These formations were deposited during an era of intense tectonic activity, where active normal faults regulated sediment accommodation. This activity resulted in substantial topographic variations – regional depocenters and structural highs – and significant fluctuations in sediment thickness, with erosion or non-deposition towards the economic basement's structural elevations. The volcanic rocks of the Camboriú Formation, assumed here as the economic basement, are mainly tholeiitic basalts correlated to the outflows of the Paraná-Etendeka Magmatic Province. The Piçarras Formation is characterized by sandstones and polymictic conglomerates in proximal regions, associated with alluvial fan activity, and talc-stevensite pelites, sandstones, and dark organic matter-rich shales in distal sections. In certain areas, intercalations of igneous rocks may be present, dating between 121 and 130 Ma. The basin's post-rift phase record commences with a notable erosive regional unconformity, known as the Pre-Alagoas Unconformity (PAU) (Figure 1), dated at 123.1 Ma. The sedimentary record of this tectonic phase comprises various carbonate rocks (Barra Velha Formation) and an overlying salt layer (Ariri Formation). These upper deposits are from the Aptian period and associated with a tectonic regime of low activity, predominantly

thermal subsidence, displaying a regional sag-type filling pattern.

The Barra Velha Formation, the main subject of this work, will be explored in greater detail in the upcoming section, specifically titled "The Barra Velha Formation: A Review and Insights into its Geological, Stratigraphic, and Petrogeophysical Aspects". The Ariri Formation was deposited in a shallow marine setting, where the paleo-relief limited the circulation of ocean waters from the south, thus favoring the creation of an extensive evaporitic basin. This basin was primarily filled with massive salt deposits, including halite (comprising around 80%) and a mixture of complex salts, referred to as high-velocity (anhydrite and gypsum, for instance) and low-velocity (such as tachyhydrite, carnallite, and sylvite) salts (Moreira et al., 2007; Gambôa et al., 2009; Maul et al., 2018; Teixeira et al., 2020). Nonetheless, there is ongoing discourse regarding the earliest significant marine influence, possibly preceding the salt deposition in the adjacent Campos Basin (Silva-Telles et al., 1994; Dias, 2005). Tedeschi et al. (2017) also proffered an alternative timeframe for the deposition of the salt evaporites, possibly connected with the early Aptian Oceanic Anoxic Event 1a (OAE 1a), around 120 or 125 Ma. Contrastingly, Szatmari et al. (2021) offered a new radiometric age of 110.64 ± 0.34 Ma (lowermost Albian) for the correlating salts in the northeastern Sergipe Basin (Carramal et al., 2022).

The Barra Velha Formation: A Review and Insights into its Geological, Stratigraphic, and Petrogeophysical Aspects

Numerous studies have explored the pre-salt section of the eastern Brazilian and western African basins, significantly enhancing our understanding of the depositional, diagenetic, structural and petrophysical characteristics of these unique and complex deposits. These investigations have provided valuable insights into their main geological features (Moreira et al., 2007; Terra et al., 2010; Wright and Barnett, 2015; Saller et al., 2016; Ceraldi and Green, 2016; Herlinger, 2016; Lima and De Ros, 2019; Gomes et al., 2020; Carramal et al., 2022; Pedrinha and Artagão, 2024).

The chart proposed by Moreira et al. (2007) remains the primary reference for the tectonic-litho-stratigraphic description of the Santos Basin pre-salt. However, with the ongoing and rapid acquisition of new seismic and well data in the pre-salt play, alternative interpretations have surfaced and warrant consideration, particularly concerning the upper Barra Velha Formation depositional tectonic context (Figure 1). Within the Lower Cretaceous Aptian stage, the upper limit of the Barra Velha Formation corresponds to the 113 Ma base of salt evaporites from the Ariri Formation (Moreira et al., 2007; Carramal et al., 2022). According to Moreira et al. (2007), the Barra Velha Formation was deposited in a transitional environment between continental and marine settings and is composed of stromatolitic limestones, sometimes enriched in talc and Mg-clays, microbial laminites, grainstones, and packstones formed by fragments of stromatolites and occasionally ostracode bioclasts. Carbonate shales occur in the structurally deepest portions, while

sandstones and conglomerates typical of alluvial fans are common on the edges.

To standardize the various existing classifications for the carbonate rocks of Brazilian basins, primarily based on observed depositional textures, Terra et al. (2010) proposed a new nomenclature for the Aptian carbonates from the Brazilian pre-salt. They suggested a subdivision into four major classes: (1) unbound elements during formation (mudstones, wackestones, packstones, grainstones, floatstones, rudstones, bioaccumulates, and breccias); (2) elements bound during formation or in-situ (boundstones, stromatolites, arborescent stromatolites, shrub-like stromatolites, dendritic stromatolites, thrombolites, dendrolites, leiolites, spherulitic, travertines, and tufas); (3) elements bound or unbound during formation (laminites, smooth laminites, and crenulated laminites); and (4) rocks with unrecognizable depositional texture (crystalline limestones and dolomites). The authors provided various macroscopic and microscopic examples of rock samples from the Barra Velha Formation. According to these authors, the term 'boundstone', proposed in Dunham's classification (Dunham, 1962), defines an in-situ formed carbonate rock where the original framework components were bound during deposition. Moreover, the term 'stromatolite', modified from Riding (2000), is defined as a laminated and generally convex deposit, which may exhibit growth characteristics or branches towards the top, most commonly of microbial origin.

The use of the terms microbial and stromatolite by Moreira et al. (2007) and Terra et al. (2010) suggests a preference for a predominantly biological explanation for the formation of the carbonate rocks of the Barra Velha Formation, an interpretation widely adopted at the outset of exploration and development activities in the Santos Basin pre-salt section (Moreira et al., 2007; Carminatti et al., 2009; Terra et al., 2010; Muniz and Bosence, 2015; Machado, 2018). Conversely, Wright and Barnett (2015), among others (Herlinger et al., 2017; Lima and De Ros, 2019; Gomes et al., 2020), argue that there is scarce evidence of microbial processes to support a dominantly biological origin, favoring an abiotic perspective. Wright and Barnett (2015) suggest that deposition occurred in a highly alkaline lacustrine environment and that it is possible to observe metric to decametric sedimentary cycles related to the physicochemical evolution of the lake. These authors questioned the origin of these rocks (biotic or abiotic) and the depositional environment (marine or lacustrine).

In terms of the depositional environment, there is a range of authors who suggest a significant marine influence during the sedimentation of the Barra Velha Formation, particularly due to its position directly beneath a thick evaporite section typical of a proto-oceanic environment (Cainelli and Mohriak, 1999; Moreira et al., 2007; Carminatti et al., 2008; Faria et al., 2017). However, for this work, we adopt a more recent model that favors a predominantly lacustrine depositional environment (Wright and Barnett, 2015; Muniz and Bosence, 2015; Pietzsch et al.,

2018; Herlinger et al., 2017; Artagão, 2018; Pedrinha et al., 2018; Lima and De Ros, 2019; Gomes et al., 2020; Pedrinha et al., 2024; Pedrinha and Artagão, 2024).

The dominantly lacustrine origin interpretation put forward by Wright and Barnett (2015) is the result of an extensive rock data analysis (core samples), where the authors pointed out: (i) scarce fossil content, with the sporadic occurrence of non-marine ostracodes and phosphatic fragments; (ii) absence of typical marine fossils from a restricted marine environment (e.g., miliolid foraminifera); (iii) abundant presence of Mg-clay minerals, common in alkaline lakes under the influence of volcanic terrains; and (iv) absence of intercalated sulfates, such as anhydrite or gypsum, typical in restricted marine environments.

The abundant presence of syngenetic Mg-clay minerals as an indicator of a stressful lacustrine environment with high salinity and alkalinity was also presented by Calvo et al. (1995). Saller et al. (2016), Ceraldi and Green (2016), and Herlinger (2016) concluded a predominantly lacustrine environment when analyzing the rocks of the sag section of the Kwanza and Campos basins, chronocorrelated to the deposits of the Barra Velha Formation and with characteristics quite like those described by Wright and Barnett (2015). Such features were specifically observed in the core samples from three wells in the Tupi Field, studied in detail by Artagão (2018). The geochemical analysis conducted by Pietzsch et al. (2018), which includes radiogenic strontium data, further supports the conclusion that the Barra Velha carbonates were deposited in a

lacustrine environment, as evidenced by the high radiogenic signals present in the pre-salt carbonates.

Considering both genetic and environmental implications – particularly energetic conditions, water depth, water chemistry, and additional factors such as porosity, permeability, and fluid flow capacity – Pedrinha et al. (2018), Pedrinha et al. (2024), and Pedrinha and Artagão (2024) proposed a reservoir exploitation clustering of the lithologies identified in the Barra Velha Formation of the Tupi Field. Despite minor nomenclature differences among these three publications, the lithologies can be categorized into major seven facies associations. These include: (i) Carbonates with dissolution features, attributable to subaerial exposure and/or the action of ascending hydrothermal fluids; (ii) Carbonates with well-developed arborescent features or in-situ shrubs, indicative of moderate to high-energy environments; (iii) Carbonates with incipient development of arborescent and/or crust-like features or in-situ incipient shrub-like facies, associated with moderate-energy environments; (iv) Reworked carbonates, generally found in moderate to high-energy environments; (v) Reworked carbonates with detrital siliciclastic content, present in high to moderate-energy areas, such as those experiencing subaqueous traction or gravitational flow, or in exposed areas; (vi) Lithologies associated with low-energy environments, or low-energy facies in general; and (vii) Clayey facies where porosity is completely or intensely obliterated, also

indicating low-energy environments, though more often related to the presence of Mg-clays.

Pedrinha et al. (2018) suggest that the precipitation of in-situ facies is driven by increased alkalinity and salinity in the lake. Notably, the well-developed shrub constituents are believed to have a predominantly chemical genesis. Environmental conditions of moderate to high-energy, typically found in structurally higher regions with shallower water depths, are conducive to the deposition of the in-situ shrubs facies association. Arid climatic periods and CO₂ degassing create ideal chemical conditions for the precipitation of calcium carbonate aggregates directly on the lakebed (Pedrinha et al., 2018; Pedrinha et al., 2024). The term "predominantly chemical" is frequently used by various researchers to describe the genesis of the carbonates in the Barra Velha Formation. While scientific articles often lean towards either a biotic or abiotic perspective, they do not entirely dismiss the possibility of both processes having a partial, occasional, or even rare involvement (Muniz and Bosence, 2015; Wright and Barnett, 2015; Herlinger et al., 2017; Wright and Rodriguez, 2018; Lima and De Ros, 2019; Gomes et al., 2020; Pedrinha and Artagão, 2024).

Wright and Rodriguez (2018) specifically cite the uppermost stratigraphic interval of the Barra Velha Formation, equivalent to stratigraphic zone BVE110 (Pedrinha et al., 2018; Pedrinha et al., 2024; Pedrinha and Artagão, 2024), informally referred to as "Marco Lula" or "Marco Tupi" (Wright and Barnett, 2017a, 2017b; Machado, 2018; Neves et al., 2019; Vital et al.,

2023), as exhibiting typically microbial textures. This observation is made despite their leaning towards and advocacy for an abiotic origin for the entirety of the Barra Velha Formation.

Additionally, Pedrinha and Artagão (2024) discuss the sedimentary and physio-chemical processes related to low-energy facies. They assert that the genesis of more uniform laminated mudstones is primarily related to settling from suspension, while irregular laminations of carbonate levels may indicate possible microbial activity. In this context, crenulated laminations may suggest more significant microbial activity than flat ones (Demico and Hardie, 1994). They also note that the observed silica layers associated with laminated mudstones are related to syngenetic precipitation and indicate the dilution of lake waters. The input of meteoric water during wet periods causes a decrease in pH, promoting the precipitation of previously dissolved silica associated with periods of higher water concentration and alkalinity (Wright and Barnett, 2015).

Figure 2 illustrates the relationships observed between facies associations, the paleogeography of the lake (water depth and relative position to the lake margin), and energy conditions, as proposed by Pedrinha et al. (2018). The lithology/facies classification (or classes) suggested offers strong potential for rock-well logs-seismic correlations, which are fully adopted in this study. By grouping rocks considering their porosity levels and identifying distinct topographic regions of predominance, it is anticipated that a qualitative to semi-

quantitative relationship with acoustic impedance and specific seismic features/characteristics can be established. Several examples of seismostratigraphic aspects that can be explored are already present in the literature.

Teixeira et al. (2017) and Kneller et al. (2019) offer methods for differentiating clayey facies through a combination of attributes derived from seismic inversions, such as shear impedance (I_s) and the V_p/V_s ratio, supported by structural seismic mapping. Ferreira et al. (2019) highlight mound features in amplitude and acoustic impedance volumes, where well-developed shrub carbonates (in-situ shrubs) are likely to prevail. Oliveira et al. (2019) identify low amplitude and low acoustic impedance features, accentuated in horizon slices of various seismic geometric attributes, as strong indicators of carbonates with dissolution features and karstification processes. Ferreira et al. (2019) and Minzoni et al. (2021) suggest the presence of clinoform geometries and chaotic seismic facies on faulted and inclined edges as indicative of debris and reworking facies. Cruz et al. (2021a) identify a high-acoustic impedance seismic anomaly, pragmatically named Feature X for its resemblance to the letter X, as the possible seismic expression of the transition between high-moderate and low- to very low-energy facies on structural flanks, and/or the degradation of reservoir quality within relative lows. This seismic feature coincides with the fading of the 4D seismic response and a fluid flow baffle within the upper Barra Velha Formation carbonate reservoir. Lastly, Oliveira et

al. (2021) propose that onlap features denote low-energy environments in general and/or petrophysically distinct clayey/thin sediments, frequently deposited in the distal portions of the Barra Velha Formation, particularly overlying clinoform/sigmoidal geometries observed in the underlying Itapema Formation.

Besides the seismostratigraphic aspects, the facies associations proposed by Pedrinha et al. (2018) exhibit macro-textural characteristics that can be interpreted from borehole image (BHI) logs, supported by rock data (sidewall samples and cores). This enables the acquisition of continuous to nearly continuous lithofacies/facies association profiles. Muniz and Bosence (2015), who worked with the so-called 'microbiolites' of the Macabu Formation in the Campos Basin (correlatives of the Barra Velha Formation), exemplify how karstification features, carbonates with poorly and well-developed shrubs (centimeter to meter scale stromatolite textures), grainstones, and low-energy laminites can be interpreted in borehole image logs.

Moreover, the spatial organization of facies associations due to the lake's depositional dynamics is reflected in vertical facies stacking patterns and the overall behavior of gamma-ray logs. This is effectively represented by vertical proportion curves (VPCs) of facies and gamma-ray logs classes (Figure 4). VPCs are 100 percent stacked bar charts of lithofacies/facies associations (or any other categorical variable) computed layer by layer in reference to a stratigraphic surface (Pedrinha and Artagão, 2024). These curves range from 0 to 1 (or 0 to

100%), providing the vertical variation of facies proportions observed in each stratigraphic zone along drilled wells, highlighting a sequential evolution where typical log and facies signatures are obtained for each stage and environment (Deutsch and Journel, 1998; Ravenne et al., 2002; Labourdette et al., 2008; Doligez et al., 2011; Normando et al., 2022). The gamma-ray logs values' classes for the Barra Velha Formation depict the vertical percentages of cumulative deviations from the mean value within the sampling interval. This approach is similar to a classical Fischer plot (Fischer, 1964; Day, 1997; Yang et al., 2021), which evaluates thickness variations from the mean. These classes allow the observation of common gamma-ray trends across all wells within each interval or stratigraphic zone. Triangles represent cycles according to Karagodin's plot (Karagodin, 1975), with blue triangles denoting the drowning/expansion phases of the lake and red triangles indicating the retraction/dry phases (Pedrinha et al., 2018; Neves et al., 2019; Magalhães et al., 2020; Pedrinha et al., 2024; Pedrinha and Artagão, 2024).

The top limits of the facies tracts of expanding and retracting lake regimes represent medium and large-scale stratigraphic sequence boundaries that can be correlated with third and second-order system tracts (Magalhães et al., 2020). The primarily recognized medium-scale genetic sequences denote the stratigraphic/reservoir zones of the Tupi Field, where larger proportions of the in-situ shrubs facies associations and low gamma-ray logs values characterize the tops of the retracting lake

tracts (Artagão, 2018; Pedrinha et al., 2018; Magalhães et al., 2020; Pedrinha et al., 2024; Pedrinha and Artagão, 2024). These sequences do not inherently contain temporal connotations and merely correspond to similar variations in the facies stacking pattern, with varying vertical extents. However, it is important to emphasize that the changes in environmental conditions and the availability of sediment accommodation space, which are responsible for the establishment of the observed stratigraphic sequences, occurred across different temporal and spatial scales (Artagão, 2018; Pedrinha et al., 2024; Pedrinha and Artagão, 2024).

Furthermore, in addition to the origin, environment and lithofacies classification debates, the tectonic evolution and stratigraphic details of the Barra Velha Formation remain subjects of considerable discussion. Papaterra (2010) notes that various nomenclatures for the stratigraphic unconformities (erosional and/or angular) in the pre-salt section had already emerged in the first decade of the 2000s. Moreira et al. (2007) and Carminatti et al. (2009) placed the entire Barra Velha Formation within a post-rift/sag context, with its lower boundary identified by the Pre-Alagoas Unconformity (PAU). According to Papaterra (2010), the PAU had been described earlier by Dias (2005) as the Pre-Upper Aptian Unconformity and by Winter et al. (2007) as the Pre-Neo-Alagoas Unconformity. Subsequently, Wright and Barnett (2015), Buckley et al. (2015), and Neves et al. (2019) proposed dividing the Barra Velha Formation into sag (tectonic quiescence) and rift phases. According to these authors, a second

unconformity, known as the Intra-Alagoas Unconformity (IAU), marks the end of the rift phase. While Moreira et al. (2007) did not mention a specific tectonic phase subdivision for the Barra Velha Formation, they divided it into sequences K46-K48 and K44, recognizing the IAU. Additionally, Moreira et al. (2007) suggested that the contact between the terrigenous sediments of the Barra Velha Formation and the overlying Ariri Formation (113 Ma) is predominantly conformable. More recently, Castro (2019) proposed differentiating the rift phases into lower (below PAU) and upper rift (up to the IAU).

Another significant observation comes from Silva et al. (2021), who examined pre-salt sediment thickness variations in the Barra Velha Formation. Their study, which covered an area of approximately 230 km² and included data from 13 wells intersecting the pre-salt oil fields of Lapa and Sapinhoá, revealed substantial sediment thickness variations within the formation, on the order of hundreds of meters. The authors also identified geological faults that displace the base of the Ariri Formation (or the upper limit of the Barra Velha Formation). Consequently, they concluded that the observed depositional geometries do not align with a typical sag tectonic model but rather suggest a mixed tectonic context, combining thermal and mechanical subsidence processes. This transitional or mixed depositional tectonic context, in which more significant sediment thickening can be interpreted, is presented and discussed in this work (Figure 1).

For reservoir characterization and exploitation, Pedrinha et al. (2018), Pedrinha et al. (2024), and Pedrinha and Artagão (2024) proposed dividing the Barra Velha Formation of the Tupi Field into three major stratigraphic intervals – BVE300, BVE200, and BVE100 – based on a wide-ranging analysis of well data. This article aims to expand upon their concept. These major intervals, corresponding to large-scale sequences, were further subdivided by the authors into smaller zones, which are referred to as stratigraphic, production, or reservoir zones (although these terms are not always interchangeable, in the case of the Tupi Field, all stratigraphic zones are also production/reservoir zones). These subdivisions align with the primary medium-scale genetic sequences identified across the Tupi Field. Evidence suggests an increasing proportion of in-situ facies, particularly in-situ shubs, toward the upper limit of each sequence boundary, indicating variations in the lake's paleotopography resulting from gradual changes in tectonic activity and climate (Figure 4). However, their work did not provide detailed explanations on how well logs signatures can be translated into petrogeophysical or seismostratigraphic signatures that are traceable beyond the immediate vicinity of the wells, which is a key objective of our current study.

The stratigraphic intervals BVE300, BVE200, and BVE100 are arranged from the oldest to the most recent. In this study, these intervals are also referred to as BVE-I (sag context; corresponding to BVE100 zone), BVE-II (transitional context between sag and upper rift

phases; equivalent to BVE200 zone), and BVE-III (upper rift context; comparable to BVE300 zone). This nomenclature allows for some flexibility around the boundaries and ensures consistency with other publications cited in Figure 1, given that the limits of BVE300, BVE200, and BVE100 are not identical across all studies. Additionally, we emphasize the need to avoid using the term 'sag' to describe the entire tectonic context of the Barra Velha Formation or its upper portion, the K46-K48 sequence. Instead, 'upper rift' will describe the BVE-III interval, and a 'transitional' or 'mixed' tectonic context (Silva et al., 2021) will be used for the BVE-II portion, reflecting thickness variations observed in detailed seismostratigraphic and structural mapping.

During the deposition of the BVE300 stratigraphic interval, the paleorelief of the lacustrine environment was more pronounced, leading to a significant siliciclastic contribution to the facies stacking pattern of the lower zones of the Barra Velha Formation within the Tupi Field (Figure 4). The ongoing reduction of tectonic activity, coupled with the gradual increase in sedimentation rates of the in-situ shrubs facies, associated with a more arid period, progressively filled in the lake relief and reduced the water depth. This gradual infilling of the available space for sediment accumulation led to a lake with minimal relief and a notable reduction in its water depth. This change, combined with a relatively more humid climate, facilitated conditions for recurring exposure features and increased sedimentation of low-energy facies in general (laminites, spherulites), as well as in-situ

incipient facies (Pedrinha et al., 2018; Pedrinha et al., 2024). Within this depositional model and considering the vertical facies proportions presented by Pedrinha et al. (2018), the top of the BVE200 stratigraphic interval is an important stratigraphic sequence boundary. This boundary indicates considerable increases in clayey facies proportions (towards the structural lows) and reworked siliciclastic content (in basal portions). These increases could have resulted in comparatively higher average gamma-ray logs values. A significant increase in carbonates with dissolution features is also observed, especially in the upper part of the BVE220 zone or the central portion of the BVE200 interval (Figure 4).

It is worth noting that the increasing trend of in-situ facies, especially the well-developed shrubs, towards the top of the stratigraphic sequences is presented by several authors (Wright and Barnett, 2015; Muniz and Bosence, 2015; Faria et al., 2017; Lima and De Ros, 2019; Gomes et al., 2020). Pedrinha et al. (2018) suggest three elementary to small-scale stratigraphic sequences. An elementary stratigraphic sequence corresponds to the smallest recognizable cycle of environmental variation associated with a complete change in lake level. The analysis of the facies proportions trends of the elementary sequences permits the identification of small-scale sequences (Strasser et al., 1999; Strasser et al., 2006; Magalhães et al., 2020; Pedrinha et al., 2024; Pedrinha and Artagão, 2024). For the Tupi Field, these are referred to as small-scale Type 1, Type 2, and Type 3 sequences (Figure 4). The Type 1 sequence, with a higher siliciclastic contribution,

would be recurring in the lower portions of the Barra Velha Formation. The Type 2 would predominate in the BVE100 interval and the upper portion of the BVE200 zone (BVE210). The Type 3 sequence is the most common in the BVE110 zone ("Marco Lula").

Regarding the nomenclature using the prefix "BVE", for clarity, this type of mnemonic – BVE100, BVE200, BVE300 – which consists of three uppercase letters followed by a hundred, is widely adopted by geoscientists across various fields operated by Petrobras, the Brazilian oil company. The primary intention is to establish a "common stratigraphic zoning nomenclature", as Bergamaschi (2021) stated in his research at the Sapinhoá Field, where a similar nomenclature is implemented. The letters denote the lithostratigraphic unit, while the hundreds increase in accordance with the age of the interval. Therefore, BVE300 is older than BVE200, which is in turn older than BVE100. Nevertheless, it is imperative to recognize that the interpretation criteria for these intervals may vary across different oil-producing fields.

Now, it is also important to properly distinguish between the clayey facies and other generally low-energy facies associations. In a simplified manner and specifically for the Barra Velha Formation in the study area, the term "carbonates with clay minerals" refers to clayey facies with significant amounts of magnesium-rich clay minerals, although other fine sediments and/or terrigenous (non-magnesium) clays may also be present. Herlinger et al. (2020), for example, estimate that up to 2% of terrigenous clays and silt content typically mix with

magnesium clays when they occur laminated. Other authors use the term "laminites" for facies rich in diverse fine sediments (Muniz & Bosence, 2015; Lima & De Ros, 2019). Gomes et al. (2020) categorize their clayey facies as those where rock samples comprise more than 90% fine-grained components (<64 μm), including magnesium clays, microcrystalline calcite, dolomite, and silica in the same mudstone facies. Regardless of the percentage of terrigenous material or type of lamination, carbonates with Mg-clay minerals exhibit specific petrophysical behaviors, detailed in this work, and are thus not grouped by us together with the general low-energy facies association.

Petrographic studies and mineralogical data from Ramnani et al. (2021) indicate that Mg-clay minerals occur among and within carbonate components such as shubs and spherulites. Carramal et al. (2022) conducted a study to establish criteria for recognizing different morphological types of Mg-clays and their paragenetic relationships with pre-salt carbonate reservoirs. Their analysis, based on petrographic data from six wells drilled in the Tupi Field, specifically focusing on the Barra Velha Formation, revealed that Mg-clays typically correspond to stevensite and kerolite, with sepiolite occurring in small quantities (up to 7% of the analyzed volume) and saponite being rare. Siliciclastic grains of muscovite, biotite, quartz, and feldspar are present in subordinate quantities, primarily associated with peloids, intraclasts, and magnesium silicate ooids, rarely exceeding 10% in volume. Mg-clays are observed in all facies associations, although their

proportions are significantly lower within facies associations related to moderate to high-energy environments (Faria et al., 2017; Artagão, 2018; Pedrinha et al., 2018; Gomes et al., 2020; Carramal et al., 2022; Pedrinha et al., 2024; Pedrinha and Artagão, 2024). Lima and De Ros (2019), Wright and Barnett (2019), and Carramal et al. (2022) suggest that Mg-clays may represent the background of lacustrine sedimentation within the Barra Velha Formation and that the dissolution of Mg-clays could be a primary mechanism for generating large volumes of secondary porosity. Particularly, Wright and Barnett (2019) argue that the removal of clay matrices through congruent dissolution is the most significant process for porosity generation, while Carramal et al. (2022) differentiate the types and intensities of diagenetic alteration for each structural setting, noting that dissolution is more pronounced in structural highs and preservation more prominent in structural lows.

Azerêdo et al. (2021) underscore the ongoing discussions within the scientific community regarding numerous aspects of Aptian pre-salt geoscience, including the genesis and significance of Mg-clays. These debates encompass: (i) the provenance of carbonate fabric, questioning whether it can be categorized as biotic, biotic-induced, biochemical, or abiotic/chemical; (ii) the understanding of lake settings and their evolutionary trajectories; (iii) the terminology and classification of carbonate rocks; and (iv) the origin and significance of not only Mg-clays but also spherulites. Pedrinha and Artagão (2024) note that Mg-clays can appear as massive or laminated aggregates and are

predominantly associated with calcitic spherulites and commonly linked with detrital siliciclastic components. The precise mechanisms and processes responsible for the formation, preservation, and deposition of these Mg-clay minerals remain highly debated. Some researchers, such as Sartorato (2018), Artagão (2018), and Faria et al. (2017), suggest that these deposits are linked to flooding events involving the influx of siliciclastic material and/or the precipitation of dolomite crystals at the air-water interface. Furthermore, the association of Mg-clays with biofilms and microbial carbonates, as indicated by Bontognali et al. (2010) and Perri et al. (2017), suggests that microbial activity might also play a role in their precipitation (Gomes et al., 2020). In contrast, Tosca and Wright (2015) argue that the primary clay minerals in the Barra Velha Formation are aluminum-free magnesium silicates, reasoning that aluminum is insoluble under the chemical conditions of most natural surface waters. Their laboratory experiments established a kinetic limit for the precipitation of these minerals in the absence of bacterial activity, a notion corroborated by subsequent studies (Wright and Barnett, 2015; Herlinger et al., 2017; Lima and De Ros, 2019; Carramal et al., 2022).

Despite the inherent challenges tied to the origin and litho-seismostratigraphic characterization of the Barra Velha Formation carbonate reservoirs, we have seen significant advancements in this field. This progress has resulted in the accumulation of substantial knowledge that has shed light on the complexities of these geological assemblies. According to Pietzsch et al. (2018),

these pre-salt carbonates in the Santos Basin were deposited in a vast lacustrine setting, surpassing the area of Lake Tanganyika, which is currently considered the world's largest rift lake. As suggested by Minzoni et al. (2021), such extensive lacustrine systems generally exhibit a sequence-stratigraphic architecture like marine environments but with potential variations in carbonate components and elements of high-frequency sequence stratigraphy. The importance of these high-frequency sequence stratigraphy elements in understanding reservoir quality and distribution has been emphasized by Magalhães et al. (2020). Amidst this complex geological backdrop, the challenging endeavor of distinguishing among reservoir, non-reservoir, and transitional rock domains directly mirrors the facies heterogeneity and petrogeophysical complexity of the pre-salt carbonate rocks.

Bringing our examination of the Barra Velha Formation geological, stratigraphic, and petrogeophysical aspects to a close, we once more utilize the example of Mg-clays to stress the inherent geological and petrophysics complexity of the study area. These clay minerals demonstrate petrological characteristics that significantly differ from weathering-derived terrigenous clays and authigenic clays typically found in clastic reservoir environments (Herlinger et al., 2020). Interestingly, both high-porosity carbonate reservoir intervals and non-reservoir intervals rich in clay minerals exhibit similar acoustic impedance responses (Johann and Monteiro, 2016; Teixeira et al., 2017; Castro, 2019; Vasquez et al., 2019; Penna et al., 2019; Castro

and Lupinacci, 2022; Mello and Lupinacci, 2022). However, the analysis of nuclear magnetic resonance (NMR) porosity logs (Coates et al., 1999) enables us to discriminate, at least at the well-scale, intervals with high clay mineral content. Among the petrophysical characteristics of these clay-rich carbonates, noticeable features include extremely low permeability (< 0.3 mD), free fluid porosity (Φ_{iFF}) values frequently below 2%, effective porosity (Φ_{iE}) typically below 6%, and high total porosity (Φ_{iT}), all indicating a microporosity setting (Ellis and Singer, 2007; Teixeira et al., 2017; Artagão, 2018; Castro, 2019; Vasquez et al., 2019; Herlinger et al., 2020; Mello, 2020; Castro and Lupinacci, 2022; Mello and Lupinacci, 2022). We plan to delve deeper into the seismic attributes, providing a more extensive geophysical characterization of the Barra Velha Formation at the relevant intersection.

Study Area and Datasets

This study required the integration of well data (including logs and rock samples), seismic data, and occasionally, drill stem test evaluations, along with production and injection histories. All these data are accessible through the collections of the Brazilian National Agency of Petroleum, Natural Gas and Biofuels (Agência Nacional do Petróleo, Gás Natural e Biocombustíveis; ANP).

The Tupi Field

Located atop the External High of the Santos Basin, approximately 280 km off the coast of Rio de Janeiro city, the Tupi Field was discovered in mid-2006 (Machado, 2018), with estimated reserves of six to eight billion barrels of oil

equivalent (Artagão, 2018; Pedrinha et al., 2018). Its first oil production commenced in April 2009 with an Extended Well Test (EWT) in the well 3-BRSA-496-RJS, located in the southern portion of the Area of Geological Interest (AGI). In October 2010, the Cidade de Angra dos Reis, the field's first floating production storage and offloading unit, began operations in the Tupi Pilot production module (Cruz et al., 2021b). Over the next decade, Tupi rapidly became Brazil's largest oil producer, currently responsible for about 30% of the country's production (boe/d; ANP, 2024). Today, the field features over 100 drilled wells and provides a dynamic dataset from 15 years of production and injection, representing the largest reservoir database for Brazil's pre-salt section (Pedrinha et al., 2024; Artagão and Pedrinha, 2024).

Structurally, the topography at the top of the Barra Velha Formation reflects most of the depositional landscape, influencing the distribution of reservoir facies (Gomes et al., 2020; Faria et al., 2017; Cruz et al., 2021b; Pedrinha et al., 2024). Information from 3D and 4D seismic data, combined with extensive drilling data, supports those higher structural areas favored the deposition of lithologies associated with moderate to high-energy environments, which exhibit good porosities. However, reservoir quality degrades from the flanks toward the structural lows, where Mg-clays and general low-energy facies dominate (Artagão et al., 2018; Pedrinha et al., 2018; Cruz et al., 2021b; Carramal et al., 2022). Petrographic studies reveal that Mg-clay minerals – whether preserved, modified, or

dissolved – make up a significant volume of the rock. These minerals are well-preserved in wells drilled in lower structural positions and significantly affected by diagenesis in structural highs, where dissolution is a major porosity generator (Carramal et al., 2022).

The reservoirs of the Tupi Field are primarily the carbonates of the uppermost intervals of the Barra Velha Formation, specifically zones BVE100 (main) and BVE200 (secondary), known for their optimal porosities and permeabilities (Pedrinha et al., 2018; Cruz et al., 2021b; Pedrinha et al., 2024; Pedrinha and Artagão, 2024). Notably, in-situ shrobs and reworked carbonates with dissolution features are the facies with the most favorable reservoir characteristics (Pedrinha et al., 2018; Artagão, 2019; Magalhães et al., 2020; Cruz et al., 2021b; Pedrinha et al., 2024).

In terms of geological-geophysical complexity and economic significance, the Tupi Field is exemplary within the Brazilian and global oil and gas industries. It showcases substantial heterogeneity and complex structures arising from a variety of depositional and diagenetic processes. These characteristics are crucial for developing and applying advanced interpretation and characterization methodologies in facies, petrogeophysical, and seismostratigraphic studies. Such methodologies enhance understanding of the spatial distribution of the main pre-salt reservoir rock types, providing invaluable input for building predictive reservoir models and devising projects with reduced risks, thus enabling more effective decision-making in project development.

Well Data Catalog

We selected 51 wells from the main area of the Tupi Field for this study (Figure 5). The selection process was based on several criteria:

a) Geographical placement and area coverage, aiming to represent adequately the variety of topographic and sedimentary environments of interest. This included wells situated in the Regional and Relative Structural Lows, Main and Secondary Structural Highs, their slopes, and the Eastern and Western Edges (Figure 5).

b) Accessibility of rock data, such as sidewall samples and cores, accompanied by multi-scale description reports, drilling reports, sedimentological logs, and basic petrophysical lab tests, including laboratory measurements of porosity and permeability.

c) Availability of logs, especially borehole image logs (preferably acoustic), nuclear magnetic resonance (NMR), and spectral gamma-ray (GRT) logs, among other conventional logs such as density and sonic (preferably dipolar).

A full suite of conventional wireline logs is present in the vast majority of the wells, including total gamma-ray (GRT) logs, spectral gamma-ray (SGR) logs, resistivity logs ranging from shallowest to deepest curves (RES1 to RES5; RES shallow/deep), density (RHOB/DEN), neutrons (NPHI/NEU), compressional sonic (DT/DTCO), shear sonic (DTS/DSI), caliper (CL), and nuclear magnetic resonance (NMR). Additional borehole image (BHI) logs, either acoustic (in most cases) or resistive (only in two wells), are available for 44 wells. Besides the information derived from the

more conventional wireline and BHI logs, eight wells have cores (totaling 557 m) with core gamma-ray logs (measured directly on the rock core sample), and 34 wells have rock sidewall samples. Additionally, ^{40}Ar - ^{39}Ar dating information is available for the igneous rocks. When necessary, various quality controls were applied to the input well data, including depth adjustments of cores and sidewall samples by comparing wireline gamma-ray logs with core gamma-ray logs.

Description of Available Seismic Data

The study area is covered by high-quality 3D narrow-azimuth towed-streamer seismic data, encompassing both pre- and post-stack migrated data, full and partial angle stacks, sourced from the high-definition seismic survey titled HD Tupi-Iracema (0302_TUPI_IRACEMA). This seismic survey was conducted by PGS in 2008 and 2009 (Penna et al., 2013). According to these authors, towed cables with a length of 8 km and processing cells of 12.5 m by 6.25 m were used to enable reservoir-scale studies, resulting in a seismic trace density of approximately 1,395,200 traces per km². The main seismic amplitude volume resulted from advanced seismic processing executed by CGG, with the assistance of Petrobras. The seismic processing workflow included anisotropic velocity modeling (TTI – Tilted Transverse Isotropy), pre-stack depth migration using the Kirchhoff algorithm (TTI KPSDM), and Internal Multiples Attenuation – IMA (Griffiths et al., 2011; Cruz, 2019). The seismic amplitude interval extends up to 8 seconds sampled at 4

ms, or 10 km sampled at 5 m. The seismic data polarity indicates a positive or peak amplitude reflection as an increase in acoustic impedance at the interface of two geological layers.

Numerous pre- and post-stack imaging enhancement techniques were employed to minimize various types of noise, particularly those associated with the overlying salt package (for instance, internal multiples). Pre-stack processing steps prominently feature the application of 3D Surface Related Multiple Elimination (SRME) and high-resolution Radon for multiple attenuation (Herrmann et al., 2000; Schonewille et al., 2007). Post-stack processes include resolution enhancement through the Q-Inverse filter, with a Q factor of 140 applied in depth, and spectral "whitening" achieved via spectral balancing (Yilmaz, 2001; Wang, 2008; Braga and Moraes, 2013; Lupinacci et al., 2017; Dias, 2020). To further reduce processing residual multiples noise, we also applied the Curvelet Transform (Oliveira et al., 2012) over the full-stack data.

For high-resolution seismostratigraphic and structural mapping, investigating the vertical resolution capability of seismic amplitude data is imperative. The minimum thickness that seismic data can resolve, aiding in the accurate definition of layer thickness by delineating a reflection at its top and another at its base, is a function of the data's frequency content, the compressional velocity of the medium, and the associated waveform (Kallweit & Wood, 1982). Any layer thinner than the minimum vertical resolution may appear with distorted amplitude in seismic data due to constructive and

destructive interference between adjacent seismic reflectors and the wavelet's side lobes.

In the pre-salt section, within the 4,400-5,000 ms window, the post-stack seismic volume exhibits a global frequency content ranging from approximately 6 Hz to 65 Hz, with a plateau around 35 Hz. The peak frequency is approximately 32 Hz, and the dominant frequency is about 42 Hz. Assuming a velocity of around 4,892 m/s, the average compressional velocity of the porous carbonates within the study area (reservoir intervals, measured from sonic logs), and using the one-quarter wavelength criterion (Kallweit & Wood, 1982), we estimate the vertical resolution of the available seismic data to be approximately 30 meters.

Step-by-Step Methodology and Foundational Outputs

We executed several macro-activities to fulfill the objectives of this study. These are broadly outlined in Figure 6 and will be elaborated upon at the appropriate juncture. The primary activities included conducting petrogeophysical studies, which involve the integration of geological, petrophysical, and seismic data, to individualize the Barra Velha Formation and characterize the stratigraphic intervals BVE100 and BVE200. This focus included identifying seismic attributes that could facilitate a comprehensive seismostratigraphic interpretation of the entire pre-salt section, highlighting stratigraphic intervals and geographic domains where carbonates with clay minerals and carbonates with dissolution

features predominate. Additionally, we undertook elastic seismic inversion based on the constrained sparse-spike methodology (Pendrel, 2001) and calculated supplementary seismic attributes to aid in mapping seismic horizons and geological faults, as well as recognizing depositional and/or diagenetic features and textures, such as those identified by the Sobel Filter (Chopra and Marfurt, 2007; Oliveira et al., 2019) and Iterdec (Cunha et al., 2019). Selecting and mapping the main seismic horizons and geological faults with a proper well-seismic tie to interpreted well markers (stratigraphic zone tops/limits) was also a crucial part of this process.

In the context of the petrogeophysical studies, we highlight several sub-steps. First, a step-by-step explanation of the criteria used to differentiate the Barra Velha Formation from the pre-Alagoas section, including the seismostratigraphic characterization of Pre-Salt, Intra-Alagoas, and Pre-Alagoas unconformities. Second, interpreting facies associations in wells using rock samples, BHI, NMR and other logs. Third, conducting a combined analysis of distinct log trends (e.g., gamma-ray logs, DT, NPHI, RHOB) and facies associations. Additionally, implementing seismostratigraphic zoning of the Barra Velha Formation considering rock-logs-seismic correlations. Executing well-log to seismic ties for mapping seismic horizons and rock to well-log to seismic feasibility correlations also played a critical role in identifying seismic attributes capable of aiding in the litho-

seismostratigraphic interpretation and characterization of the Barra Velha Formation.

The following sections provide a detailed description and illustration of the step-by-step methodology employed and the key studies conducted, divided into main stages. Throughout these stages, we will introduce a few debates to leverage key foundational outputs and address upcoming challenges. These intermediate outputs at the end of each stage guide, or even dictate, the implementation of the next workflow stage.

Petrogeophysical Studies

In this phase, the main objectives include detailed differentiation and characterization of the stratigraphic intervals BVE100 and BVE200. To achieve a detailed understanding of these intervals within the Barra Velha Formation, it is necessary to first identify and individualize the larger stratigraphic packages. Concurrently, it is essential to identify and understand which seismic attributes can aid in qualitative and/or quantitative analyses of reservoir properties, including the distribution of facies associations and the porosity and permeability characteristics. Numerous factors influence the elastic properties of rocks, including variations in fluid saturation and type, porosity, pore shape, clay content, mineralogy, and pressure (Eberli et al., 2003; Mavko et al., 2009; Xu and Payne, 2009; Silva et al., 2020; Cruz et al., 2021b). Modifications in the elastic properties of rocks can be converted into variations of the seismic signal once seismic acquisition and processing effects have been compensated

(Sheriff, 1975; Cruz et al., 2021b). This transformation, linking elastic properties to reservoir characteristics, is made possible through Rock Physics (Mukerji et al., 1988; Avseth et al., 2005; Dvorkin et al., 2014) and petrogeophysical studies, in which well data (logs and rock samples), laboratory tests, and seismic data (amplitude and its derived attributes) are collectively analyzed at various scales.

At the rock scale, we reviewed, organized, and classified information from sidewall and core sample descriptions and porosity and permeability measurements. At the well-log scale, we interpreted BHI logs and a series of more conventional wireline logs to extrapolate discrete point-based rock information and generate continuous, or nearly-continuous, vertical profiles of depositional/diagenetic facies associations. In a subsequent step, wireline and interpreted facies association logs supported the seismostratigraphic zoning approach of the Barra Velha Formation and the delineation between the BVE100, BVE200, and BVE300 intervals. With representative geological markers at the upper limits of each stratigraphic zone/unit, stratigraphic correlations, synthetic seismograms, and crossplot diagrams, we identified the well logs and rock information that could be spatially distributed at the regional seismic scale (from kilometers and/or spanning between oil fields) to the reservoir scale (tens of meters).

Seismostratigraphic Individualization of the Barra Velha Formation

To differentiate the Barra Velha Formation from the pre-Alagoas section and the Ariri Formation, and with the goal of determining geological markers, such as the tops of zones or the limits of stratigraphic intervals of interest, we opted to interpret geological sections and regional unconformities from the newest to the most ancient deposits. The aim was to first establish a low to medium resolution seismostratigraphic framework, which would later be refined into a high-resolution one. The process began with identifying the unconformity, often referred to as the Base of Salt or Pre-Salt Unconformity, which separates the pre-salt section from the saline evaporites of the Ariri Formation. Upon completing this task, we advanced to the characterization of the Pre-Alagoas Unconformity (PAU). Subsequently, we effectively differentiated the igneous deposits of the Camboriú Formation.

The geological marker, commonly referred to as the Base of Salt – alluding to the Pre-Salt Unconformity – was designed to represent, both in wells and seismic data, the interface between the base of the saline evaporite sequences of the Ariri Formation and the top of the carbonate reservoirs. However, we observed that in most wells, it is only possible to link the Base of Salt seismic event to the top of the last basal anhydrite within the saline evaporite package. This is because the density and sonic velocity contrast between anhydrite and the other types of salts exceeds the contrasts between basal anhydrite and the pre-salt carbonates, combined with the fact that the thickness of the basal anhydrite, on average, does not exceed

12 meters. The seismic amplitude cannot adequately differentiate the top and base of the basal anhydrite interval due to its limited thickness relative to the vertical resolution of the seismic data, which is approximately 30 meters.

Notably, Teixeira et al. (2020) studied a subset of the seismic and well data from the present study (Tupi Field) and reached similar conclusions regarding the vertical resolution of the seismic amplitude in the saline evaporite section: between 25 and 30 meters. In reviewing seismic inversion and facies classification studies within the saline evaporite package, these authors also note that even after acoustic seismic inversion, the vertical seismic resolution would be around 15 meters, still larger than the average 12 meters previously mentioned.

As a complicating factor, the interpretation of the Base of Salt geological marker is often hampered due to the drilling strategy of the well itself, in which the basal portion of the Ariri Formation and/or the first five to ten meters of the Barra Velha Formation are not wireline logged or do not have reliable logs, due to the setting of the support borehole shoe case (cement) and the change in the well's drilling phase (diameter change). On various occasions, there is an intercalation between anhydrite salts and carbonates at the base of the Ariri Formation, resulting in greater uncertainty in the geological marking. To circumvent these situations, whenever possible, we correlated logging while drilling (LWD) data and cutting samples acquired in the salt interval with wireline logs run in the pre-salt interval.

In terms of well-seismic tie, correlating the basal anhydrite – approximately the Base of Salt marker – with its corresponding seismic interface posed a significant challenge. Among the wells in our dataset, only three – namely well N2, the water-alternating-gas injection well number 1 (WAG1), and the gas injection well number 4 (IG4) – contain wireline sonic logs within the salt section, which would have enabled a more detailed characterization of the basal anhydrite/carbonate interface. In the wells where logging was not compromised, i.e., instances where LWD and/or wireline logs were in good condition, the basal anhydrite and the Base of Salt geological marker were interpreted based on these available logs. Specifically, gamma-ray logs, density, and sonic logs were employed, with the basal anhydrite signature being easily recognized: density around 2.98 g/cm³ and a null or extremely low radioactivity response (Serra, 1990).

Additionally, we utilized drilling geological monitoring reports when available. These reports often contain descriptions of the primary lithologies identified during well drilling, along with descriptions of cutting samples and information on the variation of the drilling rate of penetration (ROP), which is typically higher in anhydrites due to their high densities. Bearing in mind the inherent uncertainties and adopting a practical approach, the seismic horizon that best represents the top of the basal anhydrite - Base of Salt geological marker is a positive and continuous seismic reflector (amplitude peak). This seismic horizon is also pragmatically referred to as the Base of Salt. Its mapping is

supported by the synthetic seismograms computed for the three wells that have wireline sonic logs obtained in the salt evaporite interval, as exemplified in a seismic amplitude section across well N2 (Figure 7).

Continuing to the next task, the methodology for seismostratigraphic distinction of the Barra Velha Formation from the other underlying strata of the pre-Alagoas section, namely, the Itapema, Piçarras, and Camboriú formations, is not well defined in the existing literature. There are few examples, especially concerning the seismic response at the Alagoas–pre-Alagoas transition. Despite varying tectono-stratigraphic interpretations for the pre-salt section in the Santos Basin, there is a consensus that the entry of bioclastic carbonates (coquinas), the identification of an unconformity (termed Pre-Alagoas) of an angular and/or erosive nature, and the surge in rift-related tectonic deformation, indicated by the development of thickening sedimentary sequences, mark the transition from the younger Barra Velha Formation to the older deposits of the Itapema Formation (Moreira et al., 2007; Carminatti et al., 2009; Pietzsch et al., 2018; Barnett et al., 2021; Oliveira et al., 2021). In this study, we adopted these three criteria and supplemented them by evaluating the local variation patterns in total and spectral gamma-ray logs, as observed through stratigraphic correlation sections among several wells, together with their relation to seismic interfaces.

In wells where a thickness of sediments is attributed to the Itapema Formation, that is, where the formation has not been completely

eroded or bypassed by sediment on structural crests, the upper limit of this interval is referred to here as the top/onset of the stratigraphic zone/interval ITP100 (without any further subdivisions like BVE200-300). However, it is important to clarify that since the separation between the Barra Velha and Itapema formations is primarily based on the identification of an erosive and/or angular unconformity, it is challenging to assert that the interface always pertains to the very top or upper limit of the older underlying formation in a chronostratigraphic sense. Occasional younger igneous rock intrusions might be present. Given tilted and/or eroded sediment packages in a particular drilled well, the PAU might indicate the upper limit or the middle of the once wholly deposited Itapema Formation. Alternatively, it might denote the base or a partially eroded top of igneous rocks of different ages in another well. In certain cases, the PAU geological boundary and its corresponding seismic interface could coincide with multiple unconformities at the same time, particularly in stratigraphic pinch-out situations. Oliveira et al. (2021) further highlighted that the elastic properties of the overlying packages (Barra Velha Formation) and the underlying ones (Itapema Formation) relative to the Pre-Alagoas Unconformity (PAU) can vary. For example, lateral changes might occur in the content of fine sediments in relation to more proximal and distal positions of the local structural highs, resulting in varying contrasts of acoustic impedance and subsequent fluctuation of the amplitude of the seismic surface representing the PAU.

Particularly for the study area and following multi-scale descriptions of rock samples from the pre-Alagoas section, the structurally lower portions typically comprise mudstones and dark shales rich in organic matter. These rock types exhibit specific gamma-ray logs signatures, represented by high peaks, usually embedded within a trend of relatively lower values. The coquina reservoirs are not particularly large and are substantially discontinuous, predominantly observed in wells drilled on structural highs and upper flanks of the economic basement (Camboriú Formation). In these situations, a pattern of lower gamma-ray logs values is seen at the interface between the Alagoas and pre-Alagoas sections, although isolated log spikes may still be present.

Figure 8 illustrates the variation in gamma-ray logs signatures observed for the pre-Alagoas section in the I10, WAG2, and P1 wells. It also demonstrates the variation in seismic signatures (synthetic seismograms and compressional sonic logs), along with changes in the attitude (configuration, inclination, and dip) of the strata in the Itapema Formation relative to the overlying strata in the Barra Velha Formation. Emphasized in well P1 is the interpretation of the bedding planes' azimuths and a sample of the coquina reservoir collected at the onset of the pre-Alagoas section within the upper part of the Itapema Formation. The clear flexion in the cumulative dip curve (shown in red) signifies an unconformity. All bedding directions, inclinations, and dips were interpreted from the available BHI logs, following methodologies proposed and

discussed by Lagraba et al. (2010); Pöppelreiter et al. (2010); Kingdon et al. (2016); Fatah et al. (2019); and Fatah (2020). The PAU is seismically represented in most wells by a positive reflection, as illustrated in the synthetic seismograms. Figure 8 displays photo examples from sidewall rock samples of bioaccumulated carbonates (coquinas) that aid in defining the boundaries of the Alagoas and pre-Alagoas sections. By scrutinizing these characteristics - variations in dip poles, logs signatures, and the types of rocks described - it was possible to distinguish the Barra Velha Formation in all the wells. Stratigraphic correlation sections, such as the one depicted in Figure 8, were utilized to note lateral variations in gamma-ray logs signatures and to aid in marking the PAU/pre-Alagoas section in wells that lack BHI logs and/or rock data.

At the Tupi Field, particularly in areas of structural highs and flanks, it is common to find the rocks of the Barra Velha Formation directly overlying the igneous rocks of the Camboriú Formation, as illustrated by well P11 (Figure 8). In these instances, the Itapema and Piçarras formations have either undergone erosion or were never deposited, especially on the upper structural crests. In our dataset, none of the wells shows a direct transition from the sediments of the Barra Velha Formation to those of the Piçarras Formation. Furthermore, in all the studied wells, the rocks from the Piçarras Formation are described as clayey and/or shale-rich in organic matter, lacking reservoir potential, and exhibiting anomalously low acoustic impedance values (as shown in

Figure 9). Consequently, the Pre-Jiquiá Unconformity (PJU), typically associated with the transition from the deposits of the Itapema Formation to those of the Piçarras Formation, has not been extensively mapped in this study. However, it can be identified in some wells as a distinct negative amplitude trough (refer to Figure 9).

The top of the Camboriú Formation is marked by the onset of igneous rocks, predominantly basalts, which present distinct log signatures. It is relatively straightforward to identify these rocks by their high-density values, sometimes reaching saturation at a local scale, as well as increased concentrations of potassium (K), thorium (Th), and uranium (U) in spectral gamma-ray logs. Generally, the Camboriú Formation is considered the base of the reservoirs within the study area (economic basement of the deposit). Wells P1, P11, and N2 exemplify the typical gamma-ray logs signatures of its igneous rocks (Figures 8, 9, 10, and 11). In 12 wells, a more recent magmatic event, dated at 119-120 Ma using ^{40}Ar - ^{39}Ar , has been interpreted and named in this study as the Tupi Magmatic Event (or simply Tupi Event). This event is represented by igneous rocks of various compositions and textures, including volcanoclastic intervals (e.g., pyroclastic/ignimbrite rocks) with reservoir potential, indicated by porosity and traces of oil. In well N2, as in other wells, these igneous rocks from the Tupi Magmatic Event are interbedded with the clayey/shale sediments of the Piçarras Formation (Figures 9 and 10). However, these igneous rocks may

occasionally intercalate not only with the K36 (Piçarras), but also with K38 (Itapema) sequence, as pointed out by Moreira et al. (2007), although they do not use our specific terminology. Regardless, no systematic occurrence of igneous rocks intercalated with the Barra Velha and Itapema formations was observed in the study area, even though such a configuration is typical in the Mero Field (Penna et al., 2019).

The seismic sections in Figures 7, 9, 10, and 11 summarize and schematically present the seismic signatures of the main unconformities recognized for the Alagoas and pre-Alagoas sections. These figures illustrate how these unconformities were interpreted in the study area, and they showcase the distinction of the Barra Velha Formation based on well data and seismic amplitude interpretation. Seismic and well cross-correlation sections were assessed to confirm and/or fine-tune the geological markers/unconformities mapped in the wells. Exemplifying, in wells N2 and P6 (Figure 10), the angular contact represented by the change in inclination of the strata's cumulative dip curve (CDV) is evident. This characteristic of the Pre-Alagoas Unconformity (PAU) is corroborated by the altitude of the seismic reflectors, which are significantly more tilted in the pre-Alagoas section than in the Alagoas section, especially around P6 (Figure 11) – a characteristic particularly helpful to extent interpretation far from drilled wells. The observed seismic geometries in the deposits of the Itapema and Piçarras formations, conditioned by syn-depositional tectonic activity resulting in

substantial sediment section growth (thickness variations), are mostly wedge-shaped. These generally alternate between bright positive and negative seismic reflections that thin out and pinch-out (terminate) against the structural highs of the economic basement (Camboriú Formation igneous rocks) (Figures 10 and 11). As previously noted, the PAU is mostly mapped upon a positive seismic reflector, as signaled by the wells synthetics and recognized in the seismic sections, notably in wells N2 and P6 (Figures 7 and 10). Nevertheless, lateral variations in amplitude/impedance contrasts occur at this interface, as also demonstrated in the wells' correlation section in Figure 8, in the vicinity of well N2 (Figure 10; blue arrow), and the seismic section passing through well WAG1 (Figure 11). Therefore, the methodology we adopted for seismostratigraphic mapping accommodates the variation in the reflection polarity along the PAU instead of simplifying its seismic response as a peak or a trough. In the stratigraphic wells' correlation section displayed in Figure 8 and at the location of well I10, the PAU is represented as a zero crossing in the synthetic seismic amplitude.

The Tupi Magmatic Event was predominantly interpreted as being intercalated with the clayey sediments of the Piçarras Formation, overlying the basalt flows of the Camboriú Formation. As exemplified in well N2 (Figures 7, 9, and 10), the top of the Tupi Magmatic Event is represented by a high-amplitude positive reflector. Its base often corresponds to a level of clayey sediments from the Piçarras Formation, which can be recognized as a strong negative reflection, a

seismic trough right atop the Economic Basement positive reflection (e.g., well N2 surroundings, Figures 9 and 10). In the seismic sections presented in Figures 7 and 10, the economic basement can be identified by the absence of strong amplitude/impedance contrasts and by a relatively rough seismic texture along with a more homogeneous seismic facies pattern. However, in some areas, the characteristic seismic facies of the Camboriú magmatism are internal planar-parallel reflections that are tilted and angular relative to the Tupi Magmatic Event or the overlying sedimentary sequences. In these instances, the alternation of reflections within the economic basement has a higher frequency pattern when compared to other stratigraphic intervals, and the seismic reflectors representing the different lava flows are identifiable by their high structural dip towards the continent (Figures 10 and 11).

Interpretation of depositional/diagenetic facies associations profiles within the Barra Velha Formation

To compile a continuous vertical log of facies associations for the Barra Velha Formation in the study area, we thoroughly analyzed descriptions of rock sidewall samples and cores available for 34 wells. We employed a facies classification approach that considered genetic and environmental implications and observed porosity and permeability characteristics, building on the approach, and nomenclature, adopted by Pedrinha et al. (2018; 2024) and Pedrinha and Artagão (2024). These characteristics were deduced from the

assimilation of laboratory petrophysical measurement results. Table 1 showcases the adopted terminology of facies/facies associations, their corresponding average porosity and median permeability values. Median values were calculated from laboratory measurements on rock-sidewall samples and plugs. Considering the high standard deviations inherent in the permeability data, medians might better represent the reservoir's varying responses to fluid flow. This data underscores the inherent heterogeneity of these complex carbonate facies associations.

We identified seven facies or facies associations: **1.** Carbonates with dissolution features, related to subaerial exposure, meteoric fluid percolation, or the action of ascending hydrothermal fluids; **2.** Carbonates with well-developed shrubs (in-situ shrubs) associated with a moderate to high-energy depositional environment; **3.** Carbonates with incipient development of shrubs (in-situ incipient), connected to a moderate-energy depositional environment; **4.** Reworked carbonates, tied to a moderate to high-energy depositional environment; **5.** Reworked carbonates with siliciclastic content, related to a high to moderate-energy depositional environment; **6.** Lithologies linked to low-energy depositional environments (low-energy facies in general including thin siliciclastic particles); and **7.** Carbonates with clay minerals, in which porosities and permeabilities are drastically reduced by a significant amount of Mg-clay minerals – in association with other clayey and thin siliciclastic particles – filling the rock pores.

The rock sample photographs in Table 1 are representative of the 34 wells with core and rock samples analyzed. Based on the average porosity and permeability values, the highest effective porosities are linked to reworked carbonates and carbonates with dissolution features, while the highest permeabilities are observed in in-situ shrubs and carbonates with dissolution features. Following the organization and classification of rock data, we calibrated this information against log depth for subsequent comparisons between rock samples, BHI logs, and other wireline logs. For rock cores, a visual comparison between core gamma-ray logs and the reference gamma-ray logs for each well proved sufficient. For sidewall rock samples, we identified the circular cavities in the BHI logs where the samples were extracted, allowing for residual depth adjustment in aligning rock samples vertically with the image logs. In the absence of BHI logs or where cavity identification was uncertain, we used laboratory measurements of effective porosity and effective porosity logs (from NMR) for reliable depth positioning. These rock data adjustment procedures are standard in the oil and gas industry and have been described in other works focused on the Brazilian pre-salt carbonates (Artagão, 2018; Sartorato, 2018; Carmo, 2021). Once appropriately depth-positioned, the rock sample information supported well logs interpretations, enabling us to extrapolate point-based facies interpretations/classifications across the entire logged interval of the Barra Velha Formation.

In the acoustic image logs depicted in Figure 12, we assigned reworked facies to intervals displaying smoother, more uniform textures. In the static acoustic image, we observed a distinct contrast between the upper portion, featuring various facies, and the lower part of the image, predominantly displaying reworked facies. We differentiated reworked facies with siliciclastic content from other carbonate reworked facies by their higher levels of potassium (K) in the gamma-ray logs (GRK), typically exceeding 10° API, and their lower effective and free fluid porosities. Compared with adjacent intervals in cores and image logs, low-energy facies exhibited more laminated (laminites) or crinkled/crenulated patterns (spherulitic) and elevated gamma-ray log values. The upper portions of the cores were slightly darker and browner due to elevated oil impregnation. In-situ facies presented arborescent structures and organized geometries. We interpreted dissolved/karstified facies as irregular, distorted dark features, sometimes forming "holes" in the image. These features allowed us to qualitatively infer the degree of dissolution within the interval relative to neighboring ones or even interpret the presence of large vugs or caverns, where such features may extend vertically for 1-3 meters (Figure 13). In these circumstances, we supplemented the BHI logs with drilling reports (data on intervals with high loss of drilling fluid circulation), production data (injectivity/production tests), and other available logs (e.g., sonic, neutron, density, and caliper) to interpret karstification more reliably and extrapolate to intervals without rock sampling. For instance, in well P23 (Figure 13), the tested

interval containing the karstified section experienced significant fluid loss during drilling and presented an injectivity index (II) of 415 (m^3/D) (Kg/cm^2), approximately 15 times higher than the II observed in the upper interval dominated by reworked facies without noticeable dissolution, which was 26 (m^3/D) (Kg/cm^2). The formation damage ratios (DR) were similar: 6 in the interval without drilling fluid loss and 7 in the interval with drilling fluid loss, dissolution/karstification, and interpreted caverns. We also observed relatively larger borehole enlargements (caliper log) and anomalously low density and high sonic slowness ("amplitude bright spot" on the sonic log), highlighting the interval with maximum dissolution where a cavern is interpreted. The highest porosities and permeabilities were detected within this interval. Despite the relatively more noticeable caliper, the log readings were deemed reasonably reliable – the high transit time pattern, for example, was consistent among wells drilled through a similar stratigraphic level and correlated with seismic data. We duly corrected spurious spikes resulting from the borehole's general enlargement (abnormally high caliper values) in all logs.

As previously stated, the approach adopted for securing continuous facies association logs for non-clayey intervals involved a collective interpretation of BHI logs, other available logs, and rock sample data. We dismissed the extrapolation of facies associations through automated facies clustering and/or electrofacies classifications. This decision was underpinned

by feasibility studies revealing considerable overlap in the facies associations clusters displayed in analyzed petrogeophysical crossplots, such as those presented in Figure 14. Constructed using data from 44 wells with BHI logs and without upscaling, these graphs underscore the interpretative difficulties encountered when attempting to recognize these facies associations in wells lacking image logs and in intervals without rock sampling guidance. For instance, although we observed a predominance of reworked carbonate facies with higher siliciclastic content for spectral gamma-ray log values, specifically potassium (GRK) above 10° API, there was substantial overlap of this facies cluster with others within the 10 to 20° API range. To ensure greater reliability and predictability, we performed facies analysis on a well-by-well basis, considering neighboring wells, and recommend this approach for future studies. For the reworked carbonates with siliciclastic content facies, this analysis should commence following the identification of sediment reworking characteristics in rock samples, supported by the geoscientist's background knowledge and experience.

It is essential to mention that the in-situ shubs, in-situ incipient, and reworked carbonates facies did not present any specific clustering in the analyzed crossplots, forming a single colorful cloud of points. Low-energy facies were typically associated with peaks of higher values in gamma-ray logs within the cluster of total gamma-ray (GRT) values above 30 - 40° API. However, the interpretation of BHI logs or the

availability of rock samples for a more reliable separation was still required, given the recurring observed facies clusters overlapping (Figure 14). The same was true for the carbonates with dissolution features facies. Although this facies association predominantly had density values up to 2.3 g/cm^3 , it still significantly competed with reworked and in-situ shubs facies.

Next, we address the interpretation methodology for carbonates with clay minerals. These correspond to clayey carbonate rocks with a significant content of preserved Mg-clay minerals, though other types of clays and fine sediments, including detrital and siliciclastic materials, might also be present in association. Although carbonates with clay minerals can be categorized as low-energy facies, they were separated into their own class due to their distinct petrophysical characteristics. These clayey intervals range from the description of 'massive clay' to low-energy facies associations with a high content of clay minerals. For example, spherulitic rocks rich in clay minerals, in-situ facies, reworked carbonates, and other facies associations of any type, with a high content of clay minerals obliterating the pore space, although this latter case (reworked carbonates) is less common.

According to Ramnani et al. (2021), even the presence of over 5% of Mg-clay minerals in the pre-salt rocks can significantly alter their permeability, classifying them as a non-reservoir. The authors' mineralogical analyses, employing techniques such as X-ray diffraction (XRD) and scanning electron microscopy (SEM), revealed that the intervals considered

clayey non-reservoirs had, on average, a 15% content of Mg-clay that not often exceeds 50% of the total rock mineralogy. Additionally, petrographic studies specific to the wells in the Tupi Field, conducted by Carramal et al. (2022), indicated a high proportion of preserved syngenetic Mg-clay matrix in clayey-fine sediments non-reservoir intervals. Carvalho et al. (2022) presented an even more quantitative approach, drawing on a dataset of petrographic, mineralogical, and geochemical data from 21 wells in the Tupi Field, focusing on the Barra Velha Formation. According to these authors, the "Mg-claystones with few spherulites" facies exhibited a preserved syngenetic Mg-clay matrix content that averaged 14% but could reach as high as 83% in certain intervals.

Given this context, we conducted a comprehensive analysis of available logs for the carbonates with clay minerals facies association. We focused particularly on NMR responses while also considering resistivity, compressional and shear sonic, and density logs, along with derived logs of acoustic impedance and Vp/Vs ratio. We corroborated these log readings with rock data, sedimentological, and petrographic reports, and supported them with stratigraphic correlation sections. While BHI logs are valuable tools, we exercised extra caution when interpreting carbonates with clay minerals, as these facies can be misinterpreted as any other facies if they do not exhibit a massive clay pack aspect. Conversely, intervals with a high content of preserved Mg-clay minerals often exhibit more distinct petrogeophysical characteristics,

forming a reasonably distinguishable data cloud despite some overlap with other facies. We highlighted the carbonates with clay mineral clusters in red in all the evaluated crossplots (Figure 14). In our well-by-well interpreter analysis, we found that free fluid porosity values frequently less than 2% and effective porosities less than 6%, in a context of higher total porosities, stood out as the most notable discerning characteristics. Leveraging this trait, we calculated a log indicative of clay content (clay percentage/"volume"- V_{clay}) from the NMR log (Figure 15), using the equation: $V_{clay} = (\Phi_{IT} - \Phi_{IE}) / \Phi_{IT}$ (Ehigie, 2010; Castro and Lupinacci, 2022).

In general, besides the aforementioned petrogeophysical characteristics, the carbonates with clay minerals intervals neither produce nor inject, showed no evidence of oil, and lacked apparent porosity, thus considered clayey non-reservoir. These intervals could sometimes be partially dolomitized (photo in Figure 15). After analyzing all the intervals and assigning them a set of facies, we found that the vast majority of intervals that do not produce, do not inject, and present no oil indications exhibited effective porosity values below 6% (Figures 14 and 15). Accordingly, we determined it was reasonable to adopt this effective porosity value as a cutoff for distinguishing between reservoir and non-reservoir intervals, regardless of the facies (clayey, low-energy facies, highly cemented, and/or dolomitized intervals).

To assess the feasibility of interpreting seismic and/or structural sections and maps, or even for

a future three-dimensional volumetric separation of the described facies associations supported by seismic attributes, especially those derived from seismic elastic inversion, we constructed diagnostic tables and additional crossplot graphs (Figures 16 and 17). These graphics illustrate the relationships between acoustic impedance (I_p), shear impedance (I_s), and V_p/V_s ratio, considering facies associations and PhiE classes. By analyzing the average I_p , I_s , and V_p/V_s values for each facies association and assessing the general behavior of the facies points distribution in the graphs, we noted a tendency for low-energy facies association sample points to increase with higher I_p and I_s values. Conversely, we observed a relative increase in in-situ shubs, reworked carbonates, and carbonates with dissolution features sample points for the respective lower values of I_p and I_s .

Additionally, we examined the average effective porosity values per facies association (Figure 16; compiled from basic petrophysical measurements). Lower averages were related to low-energy facies and carbonates with clay minerals, while higher averages were linked to in-situ shubs, reworked carbonates, and carbonates with dissolution features. To facilitate subsequent mapping of seismic features and underpin future seismic facies classification, we then performed an additional separation of porosity classes, establishing continuous porosity classes logs per well. These continuous logs, qualitatively, and considering geographical and/or seismostratigraphic positioning can be

associated with the predominance of reservoir and/or non-reservoir depositional and/or diagenetic facies associations (Figure 17). In this manner, above 6% effective porosity, the Reservoir Facies porosity class is delineated (Figure 17; blue shading), where in-situ shubs, reworked carbonates, and carbonates with dissolution features prevail. Below 6% PhiE and for higher shear or acoustic impedance values (Figure 17; green shading), the Tight Non-Reservoir Facies porosity class is distinguished, where there is a significant increase in general low-energy facies and, a little behind, in-situ incipient carbonates. Carbonates with clay minerals are labeled as Clayey Non-Reservoir Facies regardless of the associated effective porosity value. However, clayey facies are predominantly related to values below 6% PhiE and high V_p/V_s ratio values (Figure 17; red shading), with only a few spurious samples deviating from this trend.

Table 2 summarizes the relationships among predominant facies associations (depositional and diagenetic), the effective porosity classes suggested in this work, and the average trends of seismic attributes. These relationships were instrumental in our detailed seismostratigraphic reservoir zonation to follow. It is crucial to emphasize that while in-situ shubs, reworked carbonates, and carbonates with dissolution features were primarily associated with the Reservoir Facies porosity class, smaller proportions of in-situ incipient, reworked carbonates with siliciclastic content, and, occasionally, low-energy facies can also be found within the Reservoir Facies porosity

class. Similarly, although low-energy facies are predominant within the Tight Non-Reservoir Facies porosity class, in-situ incipient facies can be present in significant proportions, and other non-clayey facies can appear in minor proportions.

High-Frequency Seismostratigraphic Zoning of the Barra Velha Formation

The stratigraphic zoning approach we utilized builds on the sequential stratigraphic analysis suggested by Pedrinha et al. (2018), and further expanded in Pedrinha et al. (2024) and Pedrinha and Artagão (2024), with a heightened emphasis on distinguishing the characteristic seismic responses for each interval/zone. This methodology led us to divide the Barra Velha Formation into three seismically mappable intervals: BVE300, BVE200, and BVE100. We focused particularly on the BVE200 and BVE100, as these represent the primary hydrocarbon reservoir zones within the Tupi Field. The BVE100 interval is further subdivided into three subintervals or subzones, specifically BVE130, BVE120, and BVE110, from the oldest to the youngest, with the latter also recognized as "Marco Lula" or "Lula's Fingers" (Wright and Barnett, 2017a, 2017b; Machado, 2018; Neves et al., 2019).

Sequential stratigraphic analysis primarily focuses on changes in the sedimentary facies stacking pattern, driven by variations in accommodation space and sediment supply rates over time. These changes culminate in the formation of stratigraphic surfaces, indicating significant shifts in the sedimentation regime,

both at the local scale of the oil field and at the regional scale of the sedimentary basin. Identifying these bounding stratigraphic surfaces, such as the maximum lake retraction surface, is crucial for establishing robust stratigraphic correlations, predicting intervals likely to harbor better reservoir facies, and understanding the sedimentary evolution of the study area. In essence, a sedimentary sequence can be characterized as a succession of strata exhibiting a complete cycle of variation in their facies stacking pattern, bounded at the top and base by stratigraphic surfaces (Catuneanu, 2006; Catuneanu & Zecchin, 2013; Artagão, 2018; Pedrinha et al., 2018; Pedrinha et al., 2024).

In the Tupi Field, the tops of the expanding and retracting lake facies tracts represent the boundaries of the stratigraphic sequences. The primary medium-scale genetic sequences identified align with the field's stratigraphic zones. Notable characteristics defining the tops of the retracting lake facies tracts include a higher proportion of in-situ shrubs facies associations and lower gamma-ray logs readings (Artagão, 2018; Pedrinha et al., 2018; Magalhães et al., 2020; Pedrinha et al., 2024; Pedrinha and Artagão, 2024) (Figure 4). In this study, we did not argue a direct relationship between the implemented stratigraphic zoning and second or third-order tracts due to the lack of extensive and robust chronostratigraphic dating to accurately establish the hierarchy of the recognized depositional tracts. Our methodological solution adopted the terms "medium-scale sequence" and "large-scale

sequence" to refer typically to decameter packages (less seismically mappable) and hundreds of meters packages (seismically mappable), respectively. Nonetheless, according to Magalhães et al. (2020), medium-scale sequences that can be mapped throughout the entire oil field could potentially be associated with a third-order system tract.

In this context and taking into consideration the subset of wells selected, we interpreted and considered a combination of aspects for the identification, definition, and potential adjustment of geological markers (the tops or bases of the stratigraphic intervals) and the ensuing seismostratigraphic zoning of the Barra Velha Formation. These aspects include:

- **Local and Known Regional Variations in Log Patterns:** We analyzed the variations in the patterns (shapes, trends/signatures, and values) of the available logs, particularly those of gamma-ray logs (total spectrum and elements) and compressional sonic logs.
- **Cycle-Stratigraphy Elements:** We considered cycle-stratigraphy elements such as depositional cycles within lake expansion and retraction regimes, recurrence of strata stacking patterns and trends, identification of genetic sequences, and the hierarchization of sequences at different scales. We also performed stratigraphic correlations of patterns between wells and assessed the mapability of bounding surfaces/sequence boundaries

(Artagão, 2018; Pedrinha et al., 2018; Neves et al., 2019; Magalhães et al., 2020; Pedrinha et al., 2024; Pedrinha and Artagão, 2024).

- **Recurring Facies Patterns:** We evaluated the recurring predominance of depositional and/or diagenetic facies in specific portions of the stratigraphic section and potential allogenic controls (e.g., tectonics, climate).
- **Seismic Signatures:** We examined seismic signatures in time or depth amplitude reference well sections.

In most of the wells, unlike what is observed for the PAU, we do not observe significant flexion in the cumulative dip curve at the top of the BVE300 stratigraphic interval. Consequently, this criterion of substantial variation in the dip of the layers, indicating an angular unconformity, was not broadly incorporated into the reservoir zoning methodology of the Barra Velha Formation. We detected only minor changes in the dip angles and bedding directions as interpreted from the BHI logs, which, at times, resulted in the corresponding seismic surface being mapped in correlative conformity with the other strata/reflectors. However, in a distinct and localized manner, inflections in the cumulative dip curves were utilized for a subset of wells drilled on the Eastern Edge (Figure 18). These inflections aid in marking the top of the BVE300 zone and the tops of the BVE130 and BVE200 intervals (Figure 18). Therefore, only in these sections of the Eastern Edge does the mapping methodology include the use of inflection curves of cumulative dip as interpreted

in the wells. Nevertheless, across the entire study area, the top of the BVE300 zone is interpreted as the end of a more tectonically active period, during which significant growths of the sedimentary section related to fault throws are still evident, especially towards the Regional Structural Lows. Consequently, the BVE300 mapped packages may appear slightly wedge-shaped when compared to the strata mapped in the pre-Alagoas section, ITP100 interval.

Regarding the facies stacking pattern, higher proportions of carbonates with clay minerals are anticipated towards the top of the BVE300 stratigraphic zone (Figure 4). However, this increased presence of clay minerals is not observed on structural highs and upper flanks, particularly not in the upper structural flanks of the Eastern Edge of the Tupi Field, where reworked carbonates, in-situ shubs facies, and carbonates with dissolution features are more common. Specifically, mound-type seismic features are observed in wells where in-situ shubs facies dominate, and these can be interpreted from the seismic amplitude data (Figure 18). Conversely, within the Eastern Edge, dome features are also identified in association with the upper intervals (BVE200 and BVE100) and in-situ shubs. However, as we move towards the dipping edge, the dome features tend to acquire a more sigmoidal shape, and reworked carbonates tend to prevail.

The typical total gamma-ray log signature for the BVE300 is illustrated in Figure 19. Elevated gamma-ray values or peaks are observed

around the top and base of this interval in most wells studied in structural lows and the flanks of the Western Edge and the Secondary Structural High, such as wells N2 and P2 (Figure 19). These patterns suggest that this stratigraphic interval has been completely logged with no apparent sequence erosion within the western lower flanks and saddles. In addition to the gamma-ray logs signature, total and components, higher density values and relatively lower transit times (compressional sonic log) are noted when compared to the upper stratigraphic interval (BVE200). Conversely, in structurally elevated and thinner to pinching parts, lower total gamma-ray values might indicate only a partial representation of the typical BVE300 signature. This suggests that the profiling of the stratigraphic interval may be incomplete due to erosion or the non-deposition of part of the BVE300. When positioning the BVE300 between the IAU and the PAU, it aligns with the description by Moreira et al. (2007) of an interval in the lower Barra Velha Formation that tends to thin out and disappear towards structural highs (Figure 1). In cases where a significant angular and/or erosional unconformity is observed in the seismic data, particularly at the Eastern Edge, where the most significant changes in dip angles occur, the cumulative dip curve helps delineate the entire BVE200 interval, thereby simplifying the identification of the upper limit of the BVE300 zone, mostly marked in consonance with the IAU (Figure 18).

Applying a comprehensive methodology, which involves the joint analysis of well logs

signatures, facies stacking patterns, cumulative dip curves, and inter-well stratigraphic correlations, augmented with time and depth reference seismic section interpretations, facilitates accurate differentiation of the BVE300 stratigraphic interval (refer to Figures 7, 10, 18, and 19 for the illustrated process). It is important to note that lateral variations in the seismic response at the interface pertaining to the onset or upper preserved limit of the BVE300 zone and IAU, like those noted for the PAU, can occur, depending on the velocity and density attributes of the surrounding sediment packages. Despite this, in the western portion – particularly within the Regional Structural Lows, the Western Edge, and the flanks of the Secondary Structural High – the onset of the BVE300 is often represented by a positive seismic reflector of medium to high amplitude (Figures 7 and 10). This reflector usually terminates in a pinch-out manner against the economic basement highs and/or the structural highs associated with the Tupi Magmatic Event and/or the PAU/ITP100 stratigraphic interval (Figure 10). In these structural highs, similar to what occurs with the sediments of the pre-Alagoas section, the packages of the BVE300 have been either eroded or not deposited at all. On the Eastern Edge, a reversal of the associated seismic signal polarity occurs, and the seismic surface that best represents the top of the BVE300 interval is a negative reflector of medium to low intensity (Figure 18).

The BVE200 stratigraphic interval is generally characterized by relatively higher readings on the total (GRT) and potassium spectral element

(GRK) gamma-ray logs, lower density values, and higher transit times (sonic log) when compared to the upper stratigraphic interval, BVE100 (Figures 19 and 20). On the Eastern Edge, the lower GRT and density values are associated with highly porous carbonates, predominantly reworked carbonates, and those featuring dissolution and/or karstification, typically concentrated in the central portion of the BVE200 interval (Figure 4). In the Regional or Relative Structural Lows, the lower density values are associated with carbonates with clay minerals, as highlighted in the vertical facies proportion curves for the BVE200 interval (Figure 4). In wells where carbonates with clay minerals dominate the entire Barra Velha Formation, there are less significant vertical amplitude variation in the synthetic seismic response (e.g., well W2; Figure 20).

Moving from the upper limit of the BVE200 geological marker towards the lower intervals, we observe a notable increase in siliciclastic sediment content amidst the reworked facies. This increase in siliciclastic sediments drives the rising trend in the spectral gamma-ray curve for the potassium element (Figure 4), a trend particularly noticeable in the basal portion of the BVE200 interval in wells P21 and W3 (Figures 18 and 20). Seismically, the top of the BVE200 is typically represented by a reflector with a negative amplitude, largely due to the combination of vertical seismic resolution and the increase in total porosity related to clayey facies (Figures 7, 10, 15, and 20). This feature becomes particularly pronounced towards the Regional Structural Lows, owing to an

increased proportion of carbonates with clay minerals around the onset of this interval (wells N2, W2, W3, and I5; Figures 7, 10, and 20). However, as with other interfaces, seismic responses may exhibit lateral variations due to contrasts in acoustic impedance with adjacent strata. We considered these variations during seismic mapping. In the upper flanks and structural highs, where the BVE200 displays superior porosity and permeability properties and its top does not correspond with layers rich in dissolution features, we applied a reversal in the seismic polarity of the representative reflector (Well P21; Figure 18 and Well P4; Figure 21).

Regarding its external geometry and tectonic context, the BVE200 (or BVE-II) interval presents moderate thickness variations (Figures 10 and 20) compared to the BVE300 (BVE-III; upper rift) and BVE100 (BVE-I; sag) intervals. We interpreted this interval as having been deposited in a mixed tectonic setting, where thermal and mechanical subsidence processes occurred simultaneously at the transition between the rift and sag stages (as pointed out in Figure 1 and illustrated in Figures 10 and 20). Consequently, especially towards the Main Structural High, the strata of the BVE200 zone exhibit slight section thinning and occasional pinch-outs. Nonetheless, the internal reflectors tend to conform and show fewer lateral and vertical amplitude contrasts compared to those of the BVE300. The tops of the BVE200 and BVE300 intervals correspond to the upper limits of medium-scale genetic sequences of a retracting lake regime (Figures

4 and 20). Yet, when analyzing large-scale sequences, the significant trend of increasing in-situ facies, particularly in-situ shrubs, is more pronounced at the onsets of the BVE200 (Figure 4) and BVE120 (e.g., Well W3; Figure 20) intervals. The BVE100 interval will undergo further detailed mapping explanations next.

We interpret the stratigraphic interval BVE100 (or BVE-I, as shown in Figure 1) as having the most notable characteristics of a sag-type tectonic context, characterized by predominantly tabular strata and limited significant sedimentary thickenings. These characteristics facilitated our tracking of seismic facies and features, log behaviors, and facies stacking patterns over extended distances and across several wells (Figures 7, 10, 19 and 20). Within this interval, gamma-ray logs reveal an upward and downward trend of increasing average values, forming a crescent moon-shaped pattern (Figure 19). Particularly for the BVE100, recognizing zones BVE110, BVE120, and BVE130 greatly aids in interpreting and understanding the entire interval.

The BVE130 zone exhibits a clear trend of decreasing gamma-ray values towards the top; however, the general pattern of average gamma-ray values within this interval is higher compared to the BVE120. This trend can be observed in wells W3 and I5 (Figure 20). The density log signature is relatively higher, and sonic log transit times are relatively lower (Figure 19). In this zone, representing the base of the BVE100 interval, significant proportions of low-energy facies are typically anticipated, with

spherulites being particularly notable (Figures 4 and 20). Transitioning to the BVE120 zone, the usual pattern of gamma-ray values undergoes a drastic change. In the BVE120 zone, high proportions of in-situ shrubs facies are expected, leading to lower gamma-ray values (Figures 4, 19, and 20). The high average GRT values observed within the BVE130 zone gradually decrease towards the top of the BVE120 zone. The top of the BVE120 zone coincides with the surface of maximum lake retraction for a large-scale sequence (Figures 4 and 20).

At the onset of the pre-salt section, zone BVE110 is typically characterized by a distinct “serrated” pattern of high values – averaging nine peaks or “fingers” – in gamma-ray logs, known as “Marco Lula” or “Lula's Fingers” (Wright and Barnett, 2017a, 2017b; Machado, 2018; Neves et al., 2019). Unlike the tops of other stratigraphic zones, which are interpreted as consistent with the boundaries of retracting lake facies tracts, the top of the BVE110 interval is identified, in most of the studied wells, as being adjacent to a lake expansion sequence boundary (Figures 4 and 20). As previously noted during the definition and analysis of the geological marker Base of Salt, there is frequently a recurrent absence of wireline logs in the first few meters of the BVE100/110 interval, and its upper limit is then simplistically equivalent to the seismic surface interpreted as the Base of Salt. For instance, in wells W3 and I5 (Figure 20), the absence and/or poor quality of logs in the

initial meters of the BVE100 zone can be observed, along with anomalous caliper values (spikes in the blue line, first tracks). Given the sag-type behavior of the BVE100, facies can be inferred from stratigraphic correlations with neighboring wells, supported by rock data. The increase in low-energy carbonate facies, especially laminites associated with fine siliciclastic sediments, and the reduction of in-situ shrub facies indicate a period of lake expansion. In such a period, the center of the water body is distant from its margins, but at this point in the lake's evolution, the depth of the lake's center is not deep. We interpret this as a very shallow, expanded lake. Pedrinha and Artagão (2024) explain that extremely reduced water depths, which prevent the development of fascicular forms, account for the relative increase in in-situ incipient facies compared to in-situ shrubs. Additionally, they suggest that more diluted, less alkaline lake waters, represented by a lower proportion of well-developed shrubs and the transition to the Ariri Formation saline evaporates at the top of BVE100/110, may indicate a marine influence during this period of lake evolution. Regardless of the possibility of a marine influence, we interpreted the top of the BVE100/110 as coinciding with a lake expansion surface, marking its top in coincidence with an increase in low-energy facies and higher gamma-ray values.

The thickness of these BVE100 subzones – BVE110, BVE120, and BVE130 – ranges between 10 and 40 meters. Typically, their

tops are not seismically mappable due to the coincidence of more than one geological marker for the same seismic reflector. This can be observed around well P21 (Figure 18), where the top of the BVE130 zone, zero crossing at well P20, laterally wind-up coinciding with the top of the BVE200 zone (positive peak). However, in certain seismic sections traversed by wells displaying high contrasts between the observed porosities and acoustic impedances for these intervals, or in rare cases where there is a considerable increase in thickness within the BVE100 zone (e.g., well P20; Figure 18), the top of the BVE130 can be mostly correlated with a positive seismic reflector of medium to high amplitude (e.g., wells N2, W2 and I5; Figures 7, 10 and 20). Therefore, despite the associated uncertainty and the significant discontinuity of this seismic horizon, the areal occurrence of this subzone can be locally estimated through detailed seismic mapping (Figures 7, 10, 18 and 20).

Results and Discussion

This section aims to consolidate the results while providing a comprehensive analysis and discussion of our key findings. Through the combined interpretation, at different scales, of sidewall rock samples and cores, well logs (including BHI logs), historical production data, and seismic volumes, we determined continuous facies association profiles and performed a sequential stratigraphic analysis of the facies stacking pattern. This approach allowed us to establish the reservoir zoning and seismostratigraphic framework of the Barra

Velha Formation within the Tupi Field. Detailed interpretations, extending from the Economic Basement to the BVE100 interval, were successfully carried out, bolstered by maps and sections of geometric, acoustic, and elastic seismic attributes. Additionally, our analysis accounted for the vertical resolutions and meanings of these seismic data, ensuring a more accurate definition of the most common seismic responses at each stratigraphic boundary.

The Camboriú Formation, characterized by igneous rocks, predominantly basalts, was identified as the economic basement of the AGI's reservoirs. The Tupi Magmatic Event, comprising igneous rocks of various compositions and textures, including volcanoclastic intervals with reservoir potential, was differentiated from the surrounding shaly sediments of the Piçarras Formation. In numerous wells within the study area, the crest of the Tupi Magmatic Event forms the base of the carbonate reservoirs, while the PJU, although identifiable as a negative amplitude trough indicating the emergence of the Piçarras Formation shaly sediments, is discontinuous and interpretable only in the deepest and most thickened sections west of the Main Structural High. In elevated structural flanks and peaks, a single seismic surface can correspond to the top of the Camboriú Formation, the top of the Tupi Magmatic Event, the upper limit of the Piçarras Formation, the PAU, or the IAU, in cases where sedimentary sections are absent due to erosion, non-deposition, or crosscutting uplift of igneous

rocks (e.g., well P11; Figure 21; schematic chart; Figure 22).

The seismostratigraphic distinction between the sediments of the Itapema Formation and the deposits of the Barra Velha Formation considered the presence of bioclastic carbonates (coquinas), the identification of the PAU as a predominantly angular (and sometimes erosive) unconformity, increased tectonic deformation associated with the lower rift context, and the local pattern of gamma-ray logs variations. Within the AGI, the PAU was frequently mapped seismically as a positive amplitude peak, primarily representing the transition from the commonly clayey basal sediments of the BVE300 to the relatively unexpressive moderate to high acoustic impedance reservoirs of the Itapema Formation. It is essential to note that the PAU also marks the lower limit of the Barra Velha Formation, even in elevated areas where the Itapema Formation sediments might have been completely eroded, resulting in the coincidence of PAU, PJU, and the Tupi Magmatic Event (T.M.E) within the same seismic horizon (Figure 22). Buckley et al. (2015) also seismically identified the PAU as mostly a positive amplitude peak. However, this contrasts with other regions of the Santos Pre-salt, such as the Mero Field, where coquina reservoirs are more substantial and permeate most of the field, and the PAU is frequently recognized as a negative amplitude peak: in structural highs, usually signaling the emergence of more voluminous permo-porous reservoirs, and in structural lows, commonly indicating the emergence of shaly

and silty deposits. Despite this, it is noteworthy that Oliveira et al. (2021) also indicate variability in the seismic signal of the PAU due to the presence of conformable to crosscutting igneous rocks, highly porous coquinas, and/or the volume of low-energy facies associated with the transition between the Alagoas and pre-Alagoas sections.

For the Barra Velha Formation, our analysis yielded high-resolution seismostratigraphic mapping, delineating the BVE300, BVE200, and BVE100 stratigraphic intervals throughout the study area. We also achieved partial tracking of the BVE130 subzone, which is contained within the main interest interval and constrained by favorable preserved sediment thickness and seismic resolution. Notably, intervals with average thicknesses under 15 meters remain uninterpretable, even with the use of Iterdec and/or acoustic impedance attributes. Figures 21 to 25 summarize the main tectonic-sedimentary, paleoenvironmental, and petrogeophysical observations made from the studied wells and amplitude seismic data (refer to the derived synthetic seismograms). The top of the BVE300, as interpreted from the wells and substantiated by seismic data, closely corresponds to the IAU. In this way, we can associate the BVE300 with sequence K44 from Moreira et al. (2007). Still, it is important to emphasize that this study does not include a comprehensive interpretation of biostratigraphic and chronostratigraphic data, and since the basal sediments of the BVE200 frequently overlie the BVE300 sediments in a conformable manner, it is plausible not to consider this

association perfect or exact. Hence, we use the concomitant terminology of BVE-I, BVE-II, and BVE-III to highlight that some level of misalignment between what we call, for instance, BVE300 and the rock package between the IAU and the PAU described in Moreira et al. (2007) may exist. Nonetheless, we have assigned the BVE300 interval to an upper (or late) rift tectonic context. The top of the BVE300 stratigraphic interval is often seismically identified as a positive amplitude peak, signifying the departure from the frequent basal clayey sediments of the BVE200 interval. This seismic polarity interpretation aligns with findings by Buckley et al. (2015) and Brazil et al. (2022) for the Pão de Açúcar, Tupi, and Búzios Fields.

Although we navigated through the lower (pre-Alagoas) and upper (BVE300) rift sections to comprehensively explain the individualization of the upper portion of the Barra Velha Formation, our primary focus remains on the BVE200 and BVE100 stratigraphic intervals. We interpreted that the BVE200 facies associations were deposited in a mixed tectonic setting, transitioning from an upper rift to a sag stage. This interpretation is based on the thickness variations observed in the wells and their relation to the mapped seismic thickness, faults, and gaps. The interpreted syndepositional sediment accommodation space, although not as extensive as that of the lower and upper rift portions, was considerably larger than the space available to the BVE100. These variations in thickness are represented in the stratigraphic correlation section depicted in

Figure 21 and in the seismostratigraphic interpretation maps of Figure 25.

At the base of the BVE200 and towards the depocenters inherited from early rift tectonics, carbonates with clay minerals predominate and are closely associated with thin siliciclastic material (see wells W2, P4, and P6; Figure 21). Given the diminished proportions of in-situ shrubs, the abundance of siliciclastic sediments, and the higher preservation of clayey facies observed from mid-BVE200 (especially BVE230 as displayed in Figures 4 and 24) and in the BVE300 zone (such as in wells P4 and W2; Figure 21), we settle that the early depositional paleoenvironment of the Barra Velha Formation was indeed more humid, less saline, and exhibited lower depositional energy in general (Figures 4 and 24). In the study area's Regional and Relative Structural Lows, a combination of larger accommodation space and a more protected environment from climatic influences (denoting a relatively lower energy environment) led to a greater accumulation (and/or preservation) of carbonates with clay minerals. In these areas, the BVE200 is mainly non-reservoir, with its top aligning with a negative (trough) seismic amplitude reflector (Figures 20 and 21). Despite these characteristics, a progressive shallowing of the lake is interpretable during the entire deposition of the BVE200 interval. This regressive depositional trend, characterized by the progressive filling of the sediment accommodation space, is noticeable (Figures 21 and 24). Moreover, moving towards the Eastern Edge, a gradual decline in preserved

clayey facies is accompanied by a relative increase in in-situ shubs facies associations. The heightened energy and wave influence along the eastern margin of the lake lead to a significant increase in reworked carbonates as well. As we approach the dipping margin, the degree of sediment reworking intensifies. These highly porous in-situ shubs and reworked carbonates display seismically discernible dissolution features all the way along the eastern margin (e.g., W5; Figure 23).

Lateral variations in the dominance of reworked facies associations suggest a rise in environmental energy towards the Eastern Edge of the Tupi Field. In the wells within this margin region, facies associated with moderate to high-energy environments are found at substantially deeper levels compared to those observed in wells drilled at the Western Edge (Figure 23). The sediment reworking combined with dissolution processes makes their original textures and depositional vertical stacking patterns less discernible, and we assume that the sedimentary zone boundaries may be more uncertain in this locality. From a seismic perspective, the lateral transition in facies dominance can be inferred from the shift in the amplitude signal at the top of the BVE200. This shift is marked by a negative (trough) amplitude reflection in the thickened structural low non-reservoir portion (well W2; Figures 21 and 23), transitioning to a positive amplitude peak in a significant portion of the reservoir section (well P4; Figure 21). At the Eastern Edge, where concentrations of dissolution features coincide with the top of the BVE200, this sequence

boundary can be associated with either a zero-crossing or a negative seismic amplitude reflection, the latter being more common. This association is always dependent on the contrast with the reservoirs of the BVE100 (well W5; Figure 22). Despite the lateral thickness variations (occasionally featuring pinch-outs) and changes in depositional and diagenetic facies, the BVE200 stratigraphic interval can be seismically mapped across the study area. The exception is the highest structural positions of the Main Structural High, where the interval is either eroded or not deposited at all (steep areas). It is also worth noting that despite the high effective porosities observed in the wells drilled in the structural highs and at the Eastern Edge, the majority of the BVE200 (including its areal extent) is filled with carbonates with clay minerals (wells W2, W3, I5, P4, and P6; Figures 21 and 23).

As we approach the Pre-salt Unconformity – Base of Salt/top of basal anhydrite geological marker and seismic horizon – and transition into a more "traditional" sag tectonic setting, we encounter the sediments of the BVE100. Examination of the wells shows that the BVE100 package exhibits minor variation in the sediment accommodation space (Figure 21). At its base, the BVE130 subzone typically comprises high proportions of overall lower energy facies, transitioning from in-situ incipient facies on the upper structural flanks to low-energy facies associations on the lower structural flanks and finally to carbonates with clay minerals in the Regional and Relative Structural Lows (Figures 21 and 23). With a

progressive increase in aridity and salinity, the BVE120 subzone accumulates the highest proportions of in-situ shubs towards the top of the sequence, particularly in the structural highs and upper flanks, especially around the Secondary Structural High (wells P4 and W4; Figures 21 and 23). In the crest positions, however, the proportions of reworked carbonates increase. On the Eastern Edge, the quantity of reworked carbonates typically surpasses that of in-situ shubs, and the occurrence of carbonates with dissolution features is significantly larger, paralleling observations made for the BVE200 interval.

In the depositional context of the BVE110 subzone, where the lake would have been relatively shallow but in a more humid environment, there is a broad occurrence of laminites (smooth or crenulated). Additionally, it is common to find tabular silica levels, ranging from decimetric to centimetric thicknesses, as well as fine sands and other silt-sized siliciclastic sediments. The tabular silica levels may indicate a syngenetic precipitation process, as suggested by their tabular shape. Coupled with the presence of fine siliciclastic material and the scarcity of well-developed shubs, these features may indicate a scenario of lake water dilution during wetter periods, as proposed by Artagão (2018). The influx of meteoric water during rainy periods could reduce the lake's pH, promoting the precipitation of dissolved silica during periods of elevated alkalinity, as observed by Wright & Barnett (2015) and Artagão (2018).

The BVE100 interval can be seismically mapped with no occurrences of pinch-outs. The BVE120 and BVE130 subzones are only locally seismically individualized. Furthermore, it is worth noting that the western portion of the Regional Structural Lows, a geographical environment represented by well W2, is seismically characterized by notably low amplitude values and modest reflector contrasts. Observe the amplitudes of the reflectors in the synthetic seismogram and the color pattern of the sonic log of well W2 in Figures 21 and 23. This observation aligns with the interpretation that in well W2, a considerable portion of the Barra Velha Formation, including BVE100 and BVE200 intervals, is densely filled with carbonates with clay minerals.

Importantly, the relative proportions of facies associations tied to environments of lower or higher energy and dissolution features interpreted for the entire Tupi Field (Figure 4) are consistently observed in the subset of wells we examined (Figure 24). Notably, there is a relative increase in reworked facies and in-situ shubs towards the tops of the BVE220 to BVE120 subzones boundaries, along with a significant rise in carbonates with clay minerals and reworked carbonates containing siliciclastic material within the BVE200 interval. The vertical facies stacking patterns reveal a regressive depositional trend, characterized by the progressive infill of accommodation space up to the top of the BVE120 subzone, which is interpreted as the surface of maximum lake retraction. Consequently, the most advantageous reservoirs are typically located

towards the tops of the stratigraphic intervals, particularly within the BVE120, in terms of porosity and permeability classes. Dissolution features are frequently associated with these superior reservoir facies, facilitating enhanced fluid percolation and flow. The processes of dissolution and karstification further enhance the primary porosity and permeability characteristics that distinguish these reservoirs.

Transitioning to the consolidation and discussion of the detailed seismostratigraphic and structural mapping results, Figures 25 to 35 provide additional information about the tectono-sedimentary context of the Barra Velha Formation. This compendium of knowledge assists in extrapolating paleoenvironmental inferences and the areal and vertical distributions of facies associations, interpreted from the wells. We achieved a concise delineation of the base of the BVE200 stratigraphic interval through detailed seismic interpretation. This process involved rock-log-seismic correlations and subsequent seismic mapping conducted from the Camboriú Formation up to the upper seismic limit of the Barra Velha Formation (i.e., the Base of Salt). Significant variations in seismic thicknesses were identified from the Economic Basement seismic horizon to the PAU, associated with the throw of the interpreted geological faults and intense tectonic activity. These seismic thicknesses align with the thickness variations we observed in the wells. In the structural crests, the pre-Alagoas strata were either eroded or not deposited at all, and the rocks of the BVE200 reside directly atop the igneous

rocks of the Camboriú Formation and/or Tupi Magmatic Event (Figures 22, 23, and 25). Conversely, in the Regional Structural Lows, the thicknesses of pre-Alagoas sediments – measured from the top of the igneous rocks of the Tupi Magmatic Event to the PAU – exceed 1,000 meters (Figure 25). Fault throws that typically exceed 100 meters at the PAU level were verified, and the vertical displacements of the Tupi Magmatic Event packages surpassed 500 meters. Consequently, in the acoustic impedance sections (see section displayed in Figure 26), abrupt lateral changes in the patterns of acoustic impedance values are emphasized. There is a predominance of high acoustic impedance values associated with the basaltic flows of the Camboriú Formation, and lower acoustic impedance values are linked to the early rift sedimentary depocenters filled with high proportions of thinner facies, clayey carbonates, and shales. These characteristics affirm a classic rift context, in which sediment deposition occurred amid forceful tectonic activity, as proposed by Moreira et al. (2007), among others (revisit Figure 1).

The Barra Velha Formation reaches thicknesses of up to 600 meters within the primary depocenters or the Regional Structural Lows (Figure 25b). Notably, between the PAU and the IAU (Figure 25c) within the BVE300 interval, permitting a small misalignment, we observed significant seismic thickness variations. These variations correspond with the thickness variations recorded in the wells but do not exceed 300 meters. Much of the BVE300 stratigraphic interval reflects structural

geometries inherited from the early rift phase and possible fault reactivations. However, a significant portion of the BVE300 interval is either eroded (predominantly) or non-deposited, as depicted by the substantial zero-thickness area emphasized in dark red tones in the map of Figure 25(c). The IAU is therefore primarily interpreted as erosive, in accordance with the illustrations of Moreira et al. (2007). During the deposition of sediments in the BVE300, the dominant topography, paired with a relatively more humid climate, led to a significant influx of sediments from the emergent structural highs. This steep relief did not favor sediment accumulation on the crests inherited from the basement but instead promoted their erosion. This is further evidenced by the significant contribution of siliciclastic sedimentary material, including clasts from the igneous rocks of the Camboriú Formation and the Tupi Magmatic Event, as observed in the facies stacking pattern of the lower zones of the Barra Velha Formation (Figures 4 and 24). Even so, most interpreted faults cut across the IAU, and the geological fault throws are clearly discernible in the structural maps. Accordingly, it is worth noting that although the attributes of the BVE300 stratigraphic interval do not entirely align with the classic early rift tectonic context, they also do not fit within a sag context. To preserve this distinction, we have adopted the term "upper rift," as previously suggested by Castro (2019) (Figure 1).

Figure 25(e) displays the seismic thicknesses derived from the seismostratigraphic interpretation of the BVE200. As in the BVE300,

we observed thickness variations of up to 300 meters. However, the eroded or non-deposited area is confined to the uppermost parts of the Main Structural High (continuous red shaded crest areas). It is also noteworthy that even within the elevated structures of the Tupi Area, the structural top map of the BVE200 demonstrates that the thickness variations are closely tied to the throws of the interpreted geological faults. This suggests that many of these geological faults either remained active or were reactivated during the deposition of the BVE200 interval, consequently influencing the availability of sediment accommodation space. Such characteristics contradict a classic sag context, thereby reinforcing the narrative of a mixed or transitional tectonic context for the BVE200 interval (BVE-II; Figure 1) in which both thermal and mechanical subsidence processes contribute to providing sediment accommodation space (Silva et al., 2021). Furthermore, although other studies have not categorically suggested a mixed tectonic context for the deposition of the upper Barra Velha Formation's sedimentary packages, the recurrence of geological faults influencing these strata's configuration and potentially interfering with fluid flow within reservoir intervals is undeniable (Karner and Gambôa, 2007; Buckley et al., 2015; Thompson et al., 2015; Faria et al., 2017; Oliveira et al., 2019; Cruz et al., 2021a; Cruz et al., 2021b). For instance, Karner and Gambôa (2007) reported that extensional faults extend up to the base of the Ariri Formation's saline evaporites, indicating active extensional deformation until the Late Aptian.

Mapping the top of the BVE200 stratigraphic interval has proven crucial for understanding the tectono-stratigraphic context and enhancing reservoir characterization. The relative increase in sediment accommodation space – compared to the overlying BVE100 interval – is accompanied by a significant increase in non-reservoir facies. High proportions of Non-Reservoir Clayey Facies tend to be deposited (and/or preserved) in the thicker sections of the Regional and Relative Structural Lows. In seismic sections, similar to observations from various well logs, the dominance of carbonates with clay minerals is marked by low amplitude and acoustic impedance values (wells W2 and I5; Figures 23 and 26). Spatially, the prevalence of carbonates with clay minerals in the BVE200 can be better delineated using an average map of the seismic attribute Vp/Vs ratio (Figure 27). A strong correlation exists between the highest average Vp/Vs values, the thickened structural lows and adjacent structural flanks, and increased proportions of carbonates with clay minerals (Figure 27). High proportions of reworked carbonates with siliciclastic content can be linked to the fault displacements of the Main Structural High and the Eastern Edge (well I7, Figure 26), particularly in the basal portions of the BVE200 stratigraphic interval. The increase in siliciclastic content is reasonably well represented in the acoustic impedance sections (slightly more positive values, in shades of greenish-blue, Figure 26).

To further the seismostratigraphic analysis of the Barra Velha Formation, Figures 25f and 28 showcase structural and seismic thickness

maps. These maps are calculated from interpreting seismic horizons and geological faults within the BVE100 stratigraphic interval. The structural top of the BVE130 subzone mapped across areas within thicker structural lows is represented in Figure 28. For mapping structural flanks and highs, seismic sections of the acoustic impedance and Iiterdec attributes, known for their superior vertical seismic resolutions, proved particularly useful. The high proportions of low-energy facies, characteristic of the BVE130, are well indicated by the relative increase in acoustic impedance values, and a resulting positive amplitude peak could be traced throughout the Iiterdec volume (Figures 28 and 29). From a reservoir characterization perspective, delineating the BVE130 subzone in areas of Regional Structural Lows and the Western Edge assists in identifying the increase in Tight Non-Reservoir Facies and potential intercalations with carbonates with clay minerals, as exemplified in well I5 (Figure 23). Within the BVE100, carbonates with clay minerals are more prevalent in the basal sections (BVE130 subzone) and geographically in the Regional and Relative Structural Lows. In terms of seismic analysis and in line with the interpretation of the BVE200 interval, areas with a higher concentration of Non-Reservoir Clayey Facies can be estimated through an average map of the seismic attribute Vp/Vs ratio (Figure 27). It is relevant to point out that in the BVE100 zone, the amplitude of variations in the average values of the Vp/Vs ratio attribute is smaller, and the Western Edge is less affected by the presence of carbonates with clay minerals (wells I5 and W3; Figure 27).

A meticulous structural analysis of the BVE130 subzone revealed that many geological faults traversing the BVE100 interval are confined mainly to its basal portion. However, a substantial number of geological faults distinctly reach and displace the Base of Salt seismic horizon, with fault displacements ranging from tens of meters - typically less than 50 meters - to sub-seismic values. Utilizing maps and volumes of geometric seismic attributes as guides, 54 geological faults extending from the Economic Basement seismic horizon to the Base of Salt seismic horizon were mapped for the Tupi Area, totaling 99 geological faults. Specifically, within the study area, there are 36 geological faults intersecting the Base of Salt seismic horizon (Figure 5). Most mapped geological faults are extensional, normal to oblique-slip faults, predominantly oriented NE-SW. Minor structural inversions related to accommodating transcurrent forces of NW-SE direction - the dominant structuring of the Iracema Area (Figure 5) - are particularly prevalent in the northern and northeastern regions of the Tupi Area. Here, NNE-SSW, N-S, and NW-SE oriented faults are also frequently mapped. Importantly, regardless of the associated direction, the displacements of the mapped faults considerably decrease towards the younger strata and are substantially diminished in the BVE100 interval compared to fault displacements observed in the lower intervals (from the Economic Basement to the top of the BVE200). Consequently, as evidenced in the wells, only subtle seismic thickness variations are apparent in the BVE100 interval, while syn-rift thickness variations are

more pronounced (Figure 25). There is also good lateral continuity of seismic reflectors linked to the BVE100. These are typically plane-parallel to tabular, locally convex in regions of carbonate mounds, or slightly concave in areas of the Relative Structural Lows. Therefore, subtle structural alterations are consistent with a significant tectonic quiescence period. The sediments of the BVE100 interval cover and fill the pre-existing topography.

When examining the seismic thicknesses of the BVE100 and BVE200 stratigraphic intervals together (Figure 25d), the structural configuration of the BVE200 strata prevails, presenting greater variability in the seismic thicknesses. The summed intervals roughly correspond to the K46-K48 sequence of Moreira et al. (2007). In general, the most significant thicknesses of the 'BVE100 and BVE200' set occur in regions influenced by plane-parallel seismic facies and onlaps that fill the Regional Structural Lows and the basal portions of the Western Edge, such as the regions of wells W2 and W3 (Figures 30 and 31), as well as sigmoid seismic features observed on the Eastern Edge, for instance, those sampled by wells P16 and W5 (Figures 26, 29, 30, and 31). The thickening of sediments and the corresponding seismic features are associated with low to moderate seismic amplitude, acoustic impedance values, and high total porosity values. In the Regional Structural Lows (well W2), carbonates with clay minerals (Non-Reservoir Clayey Facies; Table 2) predominate, while on the Eastern Edge (wells P16 and W5) reworked carbonates lead, followed by in-situ shrubs, carbonates with

dissolution features, and reworked carbonates with siliciclastic content. Thus, there is a clear preponderance of Reservoir Facies (Table 2) within sigmoid features, although other facies associations may be present in smaller proportions. In wells W5 and P16, the relatively higher acoustic impedance values observed in the basal portion of the BVE200 stratigraphic interval were associated with an increase in reworked carbonates with siliciclastic content (Figures 26 and 31). On the other hand, the lower acoustic impedance values observed in these wells' locations, situated in the central portion of the sigmoid seismic feature crossed by these wells, were related to relatively larger proportions of carbonates with dissolution features (Figures 26 and 31).

Carbonates with dissolution features are present in the BVE100 and BVE200 intervals, associated with the maximum lake retraction (dry) surfaces and subaerial exposures, but they predominantly stratify near or within the central portion of the BVE200 interval (often BVE220 zone; Figures 23, 24 and 31), and geographically, within the sigmoid features of the thickened Eastern Edge, mainly associated with reworked carbonates and in-situ shrubs. The concentration of dissolution and karstification on the Eastern Edge (wells P23, P16 and W5; Figures 13, 26, 31 and 32) suggests additional paleoenvironmental differentiation of this margin. In addition to the higher-energy environment associated with wells with a high proportion of reworked carbonates, the more significant presence of high porosity and permeability facies within the

BVE200 stratigraphic interval, located near the interpreted oil-water contact, could have facilitated greater circulation and concentration of fluids, such as a higher percolation of meteoric waters. This scenario would be conducive to the development of an epigenic karst system. Nevertheless, considering that the Eastern Edge is highly structured and faulted, the formation of a hypogenic karst system generated by the upward flow of subsurface fluids through faults and fractures cannot be ruled out. Despite this, it is worth noting that the dissolution observed in the wells is more concentrated in a specific stratigraphic interval and not along specific geological faults. In addition, lithologies typical of environments under hydrothermal action, such as tufas and travertines (Renaut et al., 2013; Mancini et al., 2019; Vital et al., 2023), have not been identified in the wells of the Eastern Edge or the other wells in the study area. As previously emphasized, on the Western Edge, the BVE200 stratigraphic interval is largely filled with carbonates with clay minerals, which are not potential reservoirs.

In the horizon slices and average maps of the seismic geometric attribute Sobel Filter for the BVE100 and BVE200 (Figures 32 and 33), a high concentration of dissolution features can be interpreted, represented by an accumulation of discontinuities, and distorted to chaotic seismic features. These features are observed at the locations of producing wells W5 to P21 (wells drilled along the Eastern Edge). Additionally, there is a perceivable relative increase in these discontinuities, shown in

darker tones, on the Sobel Filter average map for the BVE200 interval (Figure 32c). The BVE200 shows an increase in the concentrations of carbonates with dissolution features and a higher incidence of cave interpretations made upon borehole image logs. After analyzing the interpretations of dissolution features in the wells and correlating them with the generated maps and sections of seismic attributes (amplitude, impedance, and Sobel Filter), it can be inferred that the BVE100 exhibits more diffuse karst features, disseminated vuggy porosity, or small concentrations of carbonates with dissolution features. Conversely, in the BVE200, there is a predominance of caves and concentrations of dissolution features that can be better detected seismically (well W5; Figures 23 and 31). In the BHI logs of wells P15, P16, P19, and P23, some of these cave interpretations for the BVE200 are exemplified (in dark brown tones; Figure 32c). The 3D visualization of the Sobel Filter seismic attribute reinforces the interpretation of the Eastern Edge as a high-energy, steep, reworked structural edge with a strong influence of percolation and fluid circulation, especially along the Reservoir Facies located there, near the estimated paleo-free water level/oil-water contact (Figure 32). In detail, the accumulation of seismic discontinuities is manifested as a series of "rough" or "dendritic" seismic features, tubular, circular to pseudo-circular, primarily distributed around the estimated oil-water contact for the Eastern Edge. Supported by borehole image logs, these seismic features have been further interpreted as irregularly contoured depressions (uvalas), conduits,

sinkholes, concretions, and/or dolines, typical of a karst system (Figures 32 and 33). The previously mentioned "dendritic" appearance refers to the tree-branch-like grooves that may have been formed by water slowly percolating throughout the porous rock. The karst system of Minerve (located in France), illustrated in the photo of Figure 32, can be seen as an analog for the physiography and seismic relief of the Eastern Edge. Various authors link these same types of seismic features to diverse diagenetic elements and paleo-karst systems (Oliveira et al., 2019; Van Tuyl et al., 2019; Makhankova et al., 2020; Hendry et al., 2021).

Lastly, to summarize our joint analysis of the "BVE100 and BVE200" set regarding seismic features and variations in sediment thickness, moderate sediment thickenings have been associated with the Relative Structural Lows (mainly), and mild to moderate sediment thickenings have been connected to the carbonate mounds (Figures 31, 34, and 35). These observations follow the more significant sediment thickenings detected in regions influenced by plane-parallel and onlap seismic facies (Regional Structural Lows; the domain of carbonates with clay minerals) and sigmoid features with associated dissolution (Eastern Edge; domain of reworked carbonates) (Figures 26, 30, 31, 34, and 35). Apart from the seismic facies common to the BVE100 and BVE200 intervals together, a unique seismic feature, named Feature X, was recognized (Figures 3, 26, 30, 34, and 35). This feature contributes to the seismostratigraphic differentiation of the BVE100 interval, with its base, or the top of the

BVE200 interval, coinciding with the base of Feature X (Figure 34).

Feature X gets its name from its resemblance to the letter X and is characterized by high acoustic impedance values, often delineating the interface between the plane-parallel and onlap termination seismic facies and the convex geometries of the carbonate mounds (Figures 3, 34, and 35). Feature X is also visible in the Relative Structural Lows and at the vertices of sigmoid features on the Eastern Edge. We observed that Feature X is present only in the BVE100, accompanying wells that sampled high proportions of low-energy and/or in-situ incipient facies with occasional intercalated levels of carbonates with clay minerals, which places it within the domain of the Tight Non-Reservoir Facies and presenting a baffle for fluid flow (wells I5 and W3; Figures 25, 31, and 35; along with the area between wells WAG2 and P3; Figure 3). Due to its importance as a marker for reservoir quality degradation and/or reduced permo-porous thickness, as evidenced in the Tupi Nodes Pilot through dynamic historical data and 4D seismic (Figure 3), the identification and interpretation of Feature X aid in the strategic drilling of injection and production wells in structural flank positions. Structurally above Feature X, it is expected that wells will traverse the BVE100 (primarily) and BVE200 intervals filled with high proportions of Reservoir Facies (e.g., well W4; Figure 35). Wells positioned at the core of Feature X or its adjacent areas are expected to encounter higher relative proportions of Tight Non-Reservoir Facies within BVE100 (e.g., wells W3

and I5; Figure 35; and the area in-between wells WAG2 and P3; Figure 3) and carbonates with clay minerals in the underlying BVE200 (e.g., well I5; Figure 35). Wells located structurally downdip to Feature X tend to have high proportions of carbonates with clay minerals in both the BVE100 and BVE200 intervals, posing a potential risk of these wells being non-viable for drainage networks (e.g., well W2; Figure 35). Therefore, since water-alternating-gas (WAG) wells, as well as exclusive water injection (IW) and gas injection (IG) wells, tend to be strategically positioned on the structural flanks within the perimeter of reservoir areas suitable for injection, Feature X may represent the structural descent limit of a fluid injection line, aimed at maintaining production and/or enhancing oil sweep efficiency.

CONCLUSIONS

This study underscored the importance of conducting detailed seismic and geological interpretations at different scales – rock, logs, and seismic – and successfully applied a comprehensive methodology that proved effective in interpreting facies associations from well logs. We established and described objective criteria, emphasizing reservoir characterization, to achieve reliable seismostratigraphic reservoir zoning and robust differentiation of the Barra Velha Formation deposits from the pre-Alagoas section. Furthermore, we performed a meticulous petrogeophysical characterization of the Barra Velha Formation within the study area, focusing on the separation and analysis of BVE100 and BVE200 intervals. The tectonic contexts of

these deposits were also analyzed and discussed with the support of high-resolution seismic interpretation and rock data.

In the petrogeophysical study phase, integrated interpretation across various scales of rock data, conventional electric logs, borehole image logs, historical production data, and seismic data facilitated the conception of continuous to nearly continuous facies association profiles for the wells. It also enabled the discrimination of effective porosity classes significant for seismic reservoir quality prediction extrapolations. It was concluded that although a direct relationship between a range of specific seismic attribute values and a single facies association cannot be established, effective porosity classes can be linked with the prevalence of certain groups of facies associations and depositional and/or diagenetic elements. Above 6% effective porosity, the Reservoir Facies porosity class was successfully delineated, characterized by high proportions of in-situ shubs facies, reworked carbonates, and carbonates with dissolution features. The Tight Non-Reservoir Facies porosity class was identified below 6% effective porosity and for the highest acoustic impedance values, signifying an increase in low-energy facies closely associated with in-situ incipient facies. Carbonates with clay minerals were classified as Clayey Non-Reservoir Facies, irrespective of the associated effective porosity value, although they are primarily associated with values below 6% and high V_p/V_s ratios.

The methodology adopted for the seismostratigraphic zoning of the Barra Velha

Formation – which accounted for variations in well logs patterns, several cycle-stratigraphy elements, the recurrent predominance of depositional and/or diagenetic facies in certain portions of the stratigraphic section or geography of the study area, potential allogenic controls, and seismic signatures in both time and depth amplitude reference sections – proved efficient in identifying the most promising intervals and areas for superior reservoir occurrence. This methodology resulted in a robust subdivision of the Barra Velha Formation into three seismically mappable intervals: BVE300, BVE200, and BVE100, including subzones. This partition provides numerous benefits for understanding the study area and the pre-salt section of the Santos Basin as a whole. It is essential to underline that many publications regarding the Brazilian pre-salt do not offer this level of petrophysical, stratigraphic, and seismic interpretation detail. The thoroughness and step-by-step methodological description presented here are invaluable for the study and training of new geoscientists focused on the Brazilian pre-salt carbonates.

Apart from the upper limits of BVE100 and BVE110, the tops of the reservoir zones were interpreted in line with the boundaries of retracting lake facies tracts signifying an increase in in-situ shubs facies and permeability. The top of the BVE120 subzone was recognized as the maximum lake retraction surface with enormous potential for great reservoir quality. The stratigraphic sequences detailed in this work exert control over the

petrophysical characteristics of intervals considered as reservoir and non-reservoir. Lake expansion periods are associated with an increase in the proportion of thinner, low-energy facies with lower porosities, along with higher preservation of clayey sediments. In contrast, dissolution features are often associated with facies of superior permo-porous quality, such as in-situ shrubs and reworked carbonates, related to moderate to high-energy environments. We found that structural positioning greatly affects the vertical and areal distributions of facies associations as well as their seismic responses. Geographically, the thickest package of rock with Reservoir Facies is located on the Eastern Edge. At the same time, the most significant assemblages of Clayey Non-Reservoir Facies are placed within the Regional Structural Lows.

The detailed seismostratigraphic and structural understanding was achieved from the Camboriú Formation to the Barra Velha Formation, aided by maps and sections of geometric, acoustic, and elastic seismic attributes. The Tupi Magmatic Event, including porous volcanoclastic intervals, was correctly distinguished from the shaly sediments of the Piçarras Formation. The differentiation between the sediments of the Itapema and Barra Velha formations considered the presence of bioclastic carbonates, identification and meticulous description of the PAU as an angular and/or erosive unconformity, including how PAU marks an increase in rift-related tectonic deformation. In the Barra Velha Formation, the seismostratigraphic framework accomplished a high-resolution facet by separating and analyzing not only BVE300,

BVE200, and BVE100 across the entire study area but also depicting the key petrogeophysical characteristics of the BVE130 subzone.

Based on the results, the detailed seismostratigraphic and structural segmenting and analysis of the Barra Velha Formation, considering the intervals BVE300, BVE200, and BVE100, offers several benefits. From a tectonic viewpoint, the characteristics of the BVE300 do not fit neatly into a classic rift context, nor are they compatible with a sag setting. The characteristics of the BVE200 conflict with a classic sag context, suggesting a mixed or transitional tectonic background. Only the BVE100 stratigraphic interval clearly shows sag-type tectonic context features. Regarding reservoir characterization, the individual analysis of the BVE300, BVE200, and BVE100 zones provided vital information to understand the distribution of depositional and diagenetic elements. We stated that BVE100 presents more diffuse karst features, while BVE200 displays extra caves and higher concentrations of dissolution features, which are more easily seismically detected. In summary, the methodology we employed for the thorough seismostratigraphic and structural subdivision and examination of the Barra Velha Formation and its tectonic characteristics and facies/seismofacies distributions provided a more in-depth understanding of the Tupi Field. The analogies adopted can be undoubtedly extrapolated to other areas of the pre-salt section. This approach also enables the easy identification of the main stratigraphic zones

and a perception of their petrogeophysical relationships in the context of hydrocarbon carbonate reservoir exploration and development.

Sediment thickening variations also play a role in reservoir quality prediction. Moderate sediment thickenings in the BVE100 and BVE200 intervals have been associated with the Relative Structural Lows, containing increased amounts of Tight and Clayey Non-Reservoir Facies. Minor to moderate sediment thickenings have been linked to carbonate mounds and in-situ shrubs facies. Regions influenced by plane-parallel and onlap seismic facies within the Regional Structural Lows – Clayey Non-Reservoir Facies domain – and sigmoid features on the Eastern Edge – related to reworked carbonates and dissolution – showed more significant sediment thickenings. Additionally, the recognition of Feature X, characterized by high acoustic impedance values, has been crucial. This feature aids in the seismostratigraphic differentiation of the BVE100 interval, marking the transition from the BVE200. The presence of Feature X in wells indicates higher proportions of low-energy facies and serves as a marker for reservoir

quality degradation and reduced permo-porous thickness, abetting in the strategic drilling of injection and production wells and representing a limit for fluid injection lines, enhancing production and oil sweep efficiency.

To summarize, this study offers a detailed compendium of vital petrogeophysical aspects, enabling a deep understanding of the geological and seismic attributes of the upper Aptian reservoirs within the Brazilian pre-salt. This extensive knowledge substantially enhances exploration and exploitation strategies in the Tupi Field and can be extended to similar pre-salt regions, improving hydrocarbon recovery and reservoir management.

ACKNOWLEDGMENTS

The authors extend their gratitude to Petrobras and its coventurers, Shell and Petrogal, as well as all the geoscientists and reservoir engineers involved in the Tupi projects. We express our special thanks to Luciana Santos, Flávio Cruz, Victor Hugo Proença, Saulo Pedrinha, Victor Artagão, Bibiana Santos, Camila Ramnani, Nivea Carramal, Rejhane Cunha, Carlos Cunha, Tatiana Oliveira, Mario Paes, and Danielle Marques for their invaluable technical contributions throughout this work.

REFERENCES

- ANP, 2024. Boletim Mensal da Produção de Petróleo e Gás Natural - Abril de 2024, Agência Nacional do Petróleo, Gás Natural e Biocombustíveis. Accessed in June 2024: <http://www.gov.br/anp/pt-br/assuntos/dados-estatisticos/boletins-anp>.
- Artagão, V.M., 2018. Análise estratigráfica de alta resolução aplicada aos depósitos da Formação Barra Velha, Bacia de Santos: identificação, correlação e mecanismos de controle de ciclos sedimentares, Master Dissertation, Faculdade de Geologia, Universidade do Estado do Rio de Janeiro, Rio de Janeiro, Brazil, 174 pp.

- Artagão, V.M., 2019. Geological Characterization and Modelling of a Unique Carbonate Reservoir, OTC Special Session Presentation, Lula Complex: 10 years and 1 million barrels per day, Rio de Janeiro, Brazil.
- Avseth, P., Mukerji, T., Mavko, G., 2005. Quantitative seismic interpretation: Applying rock physics tools to reduce interpretation risk, Cambridge University Press, ISBN: 0521816017. DOI: 10.1017/CBO9780511600074.
- Azerêdo, A.C., Duarte, L.V., Silva, A.P., 2021. The challenging carbonates from the Pre-Salt reservoirs offshore Brazil: Facies, palaeoenvironment and diagenesis, *Journal of South American Earth Sciences*, 108, 103202. DOI: 10.1016/j.jsames.2021.103202.
- Barnett, A.J., Fu, L., Rapasi, T., Scotellaro, C., Guha, J., Cabolova, A., Domingues, A.L., 2021. Seismic characterization and origin of clinoforms in lacustrine depositional environments: a case study from the Cretaceous of the South Atlantic, Geological Society, London, Special Publications, 509, 127-145. DOI: 10.1144/sp509-2019-148.
- Bergamaschi, G.S., 2021. Relationship between porosity type and petroelastic properties for a complex carbonate reservoir, Master of Science in Petroleum Engineering, Politecnico di Torino, Italy, 85 pp.
- Bontognali, T.R.R., Vasconcelos, C., Warthmann, R.J., Bernasconi, S.M., Dupraz, C., Strohmenger, C.J., McKenzie, J.A., 2010. Dolomite formation within microbial mats in the coastal sabkha of Abu Dhabi (United Arab Emirates), *Sedimentology* 57 (3), 824–844. DOI: 10.1111/j.1365-3091.2009.01121.x.
- Braga, I.L.S., Moraes, F.S., 2013. High-resolution gathers by inverse Q filtering in the wavelet domain, *Geophysics*, 78(2), V53–V61. DOI: 10.1190/geo2011-0508.1.
- Brazil, F., Guerrero, J.C., Carvalho, R.K., Silva, C.M.D.A., Moliterno, A.M.C., Araújo, C.H.V., Barbosa, G.F., Yamato, A.A., Cacela, A.S.M., Leite, C.D.O.N., Rocha, N.P., Oliveira, V.C.B.D., Campos, M.T.R., Rocha e Silva, V.G.M.D., Natori, H.O.H., Lima, F.P., Oliveira, D.L.D., Queiroz, L.E.S., Souza, L.B.D., 2022. Búzios Field, Offshore Brazil: The Journey from Reservoir Characterization to Production Development. Fourth HGS/EAGE Conference on Latin America, 2022, 1-5. DOI: 10.3997/2214-4609.202282024.
- Buckley, J. D., Bosence, D.W., Elders, C.F., 2015. Tectonic setting and stratigraphic architecture of an Early Cretaceous lacustrine carbonate platform, Sugar Loaf High, Santos Basin, Brazil: Geological Society, Special Publications 418, 1–17. DOI: 10.1144/SP418.13.
- Cainelli, C., Mohriak, W.U., 1999. Some remarks on the evolution of sedimentary basins along the Eastern Brazilian continental margin, *Episodes*, 22(3), 206–216.
- Calvo, J.P., Blanc-Valleron, M.M., Rodríguez-Arandía, J.P., Rouchy, J.M., Sanz, M.E., 1995. Authigenic Clay Minerals in Continental Evaporitic Environments, *The International Association of Sedimentologists, Special Publications*, 27, 129–151. DOI: 10.1002/9781444304190.ch5.
- Carminatti, M., Wolff, B., Gambôa, L., 2008. New Exploratory Frontiers in Brazil, 19th World Petroleum Congress, Madrid, Spain.

- Carminatti, M., Dias, J., Wolff, B., 2009. From Turbidites to Carbonates: Breaking Paradigms in Deep Waters, Offshore Technology Conference, Houston, Texas.
- Carmo, M.C., 2021. Reconhecimento de Eletrofacies Carbonáticas e Interpretação Depositional e Diagenética, com base em dois poços do Pré-Sal da Bacia de Santos, Master Dissertation, Instituto de Geociências, Universidade Federal Fluminense, Rio de Janeiro, Brazil, 186 pp.
- Carramal, N.G., Oliveira, D.M., Cacela, A.S.M., Cuglieri, M.A.A., Rocha, N.P., Viana, S.M., Toledo, S., Pedrinha, S., De Ros, L.F., 2022. Paleoenvironmental insights from the deposition and diagenesis of Aptian pre-salt magnesium silicates from the Lula Field, Santos Basin, Brazil, *Journal of Sedimentary Research*, 92(1), 12-31. DOI: 10.2110/jsr.2020.139.
- Carvalho, A.M.A, Hamon, Y., de Souza Jr, G.O., Carramal, N.G., Collard, N., 2022. Facies and diagenesis distribution in an Aptian pre-salt carbonate reservoir of the Santos Basin, offshore Brazil: A comprehensive quantitative approach, *Marine and Petroleum Geology*, 141, 105708. DOI: 10.1016/j.marpetgeo.2022.105708.
- Castro, T.M., 2019. Avaliação dos Reservatórios Carbonáticos do Pré-Sal no Campo De Búzios, Bacia De Santos, Master Dissertation, Instituto de Geociências, Universidade Federal Fluminense, Rio de Janeiro, Brazil, 168 pp.
- Castro, T.M., Lupinacci, W.M., 2022. Comparison between conventional and NMR approaches for formation evaluation of presalt interval in the Buzios Field, Santos Basin, Brazil, *Journal of Petroleum Science and Engineering*, 208, 109679. DOI: 10.1016/j.petrol.2021.109679.
- Catuneanu, O., 2006. Principles of sequence stratigraphy, Heidelberg: Elsevier, 375 pp.
- Catuneanu, O., Zecchin, M., 2013. High-resolution sequence stratigraphy of clastic shelves II: controls on sequence development, *Marine and Petroleum Geology*, 39(1), 26-38. DOI: 10.1016/j.marpetgeo.2012.08.010.
- Ceraldi, T.S., Green, D., 2016. Evolution of the South Atlantic lacustrine deposits in response to Early Cretaceous rifting, subsidence and lake hydrology, *Geological Society, London, Special Publications*, 438(1), p 77–98. DOI: 10.1144/SP438.10.
- Chang, H.K., Assine, M.L., Corrêa, F.S., Tinen, J.S., Vidal, A.C.; Koike, L., 2008. Sistemas petrolíferos e modelos de acumulação de hidrocarbonetos na Bacia de Santos, *Revista Brasileira de Geociências*, São Paulo, Brazil, 38 (2), 29-46. DOI: 10.25249/0375-7536.2008382S2946.
- Chopra, S., Marfurt, K.J., 2007. Seismic Attributes for Prospect Identification and Reservoir Characterization, *Society of Exploration Geophysicists*, 481 pp. DOI: 10.1190/1.9781560801900.
- Coates, G.R., Xiao, L.Z., Prammer, M.G., 1999. NMR Logging Principles and Applications, Halliburton Energy Services, Houston: Gulf Publishing Company, 234 pp.
- Cruz, N.M., 2019. Geophysical Characterization and Monitoring, OTC Special Session Presentation, Lula Complex: 10 years and 1 million barrels per day, Rio de Janeiro, Brazil.

- Cruz, N.M., 2023. Mapeamento de elementos deposicionais e diagenéticos: impactos nos modelos de reservatório e nas estratégias de desenvolvimento de campos do Pré-sal, Master Dissertation, Universidade Federal Fluminense, Brazil, 313 pp.
- Cruz, N.M., Cruz, J.M., Costa, M.M., Urasaki, E.N., Teixeira, L.M., Santos, M.S., Grochau, M.H., 2021a. First 4D Seismic Results for Tupi Field, Santos Basin, XVII Congresso Internacional da Sociedade Brasileira de Geofísica, Rio de Janeiro, Brazil.
- Cruz, N.M., Cruz, J.M., Teixeira, L.M., Costa, M.M., Oliveira, L.B., Urasaki, E.N., Bispo, T.P., Jardim, M.S., Grochau, M.H., Maul, A.R., 2021b. Tupi Nodes pilot: A successful 4D seismic case for Brazilian presalt reservoirs, *The Leading Edge*, 40, 886–896. DOI: 10.1190/tle40120886.1.
- Cunha, C.A., Damasceno, A., Teixeira, L., Pimentel, A., Cruz, N.M.S.M., Oliveira, T.A., 2019. High Resolution Impedance Inversion, *Brazilian Journal of Geophysics*, 37(4), 461–469. DOI: 10.22564/rbgf.v37i4.2022.
- Day, P.I., 1997. The Fischer diagram in the depth domain; a tool for sequence stratigraphy, *Journal of Sedimentary Research*, 67(5), 982–984. DOI: 10.2110/jsr.67.982.
- Demicco, R.V., & Hardie, L.A., 1994. Sedimentary Structures and Early Diagenetic Features of Shallow Marine Carbonate Deposits, *SEPM Atlas Series*, No. 1. DOI: 10.2110/sepmatl.01.
- Deutsch, C.V., Journel A.G., 1998. *GSLib: geostatistical software library and user's guide*, 2nd ed., Oxford University Press, New York, 369 pp.
- Dias, J.L., 2005. Tectonics, stratigraphy and sedimentation during the Aptian along the Brazilian eastern margin, *Boletim de Geociências Petrobras*, 13, 7–25.
- Dias, R.M., 2020. Aumento de resolução através do uso do filtro Q inverso e da inversão acústica em reservatórios carbonáticos do Pré-sal da Bacia de Santos, Master Dissertation, Universidade Federal Fluminense, Brazil, 107 pp.
- Dias, R.M., Castro, T.M., Santos, M.A.C., Lupinacci, W.M., 2019. Understanding the Relationship between Acoustic Impedance and Porosity in the Presalt of the Buzios Field, Santos Basin, Conference Proceedings, First EAGE Workshop on Pre-Salt Reservoir: from Exploration to Production, European Association of Geoscientists & Engineers, Rio de Janeiro, Brazil. DOI: 10.3997/2214-4609.201982009.
- Doligez, B., Hamon, Y., Barbier, M., Nader, F., Lerat, O., Beucher, H., 2011. Advanced Workflows for Joint Modelling of Sedimentary Facies and Diagenetic Overprint, Impact on Reservoir Quality, Paper presented at the SPE Annual Technical Conference and Exhibition, Denver, Colorado, USA. DOI: doi.org/10.2118/146621-MS.
- Dunham, R.J., 1962. Classification of Carbonate Rocks According to Depositional Texture. In: Ham, W.E., Ed., *Classification of Carbonate Rocks*, AAPG, Tulsa, 108-121.
- Dupraz, C., Reid, R.P., Braissant, O., Decho, A.W., Norman, R.S., & Visscher, P.T., 2009. Processes of carbonate precipitation in modern microbial mats, *Earth-Science Reviews*, 96(3), 141-162. DOI: 10.1016/j.earscirev.2008.10.005.

- Dvorkin, J., Gutierrez, M.A., & Grana, D., 2014. *Seismic Reflections of Rock Properties*, Cambridge University Press, 387 pp. DOI: 10.1017/CBO9780511843655.
- Eberli, G.P., Baechle, G.T., Anselmetti, F.S., Incze, M.L., 2003. Factors controlling elastic properties in carbonate sediments and rocks, *The Leading Edge*, 22 (7), 654–660. DOI: 10.1190/1.1599691.
- Ehigie, S.O., 2010. NMR - Openhole Log Integration: Making the Most of NMR Data Deliverables, Nigeria Annual International Conference and Exhibition, Society of Petroleum Engineers. DOI: doi.org/10.2118/136971-MS.
- Ellis, D., Singer, J., 2007. *Well logging for earth scientists*, Springer Dordrecht, 708 pp. DOI: 10.2118/136964-MS.
- Faria, D., Reis, A.D., Souza Jr., O., 2017. Three-dimensional stratigraphic-sedimentological forward modelling of an Aptian carbonate reservoir deposited during the sag stage in the Santos basin, Brazil, *Marine Petroleum Geology*, 88, 676–695. DOI: 10.1016/j.marpetgeo.2017.09.013.
- Fatah, T.Y.A., 2020. Análise de zonas de fraturas através de perfis de imagem em poços do Pré-sal da Bacia de Santos, Master Dissertation, Universidade Federal Fluminense, Brazil, 113 pp.
- Fatah, T.Y.A., Lupinacci, W.M., Freire, A.F.M, Gambôa, L.A.P, 2019. Borehole image analyses at presalt carbonate reservoirs of the Mero Field, Santos Basin, 16th International Congress of the Brazilian Geophysical Society, Rio de Janeiro, Brazil. DOI: 10.22564/16cisbgf2019.075.
- Ferreira, D.J.A., Lupinacci, W.A., Neves, I.A., Zambrini, J.P.R., Ferrari A.L., Gambôa, L.A.P., Azul, M.O., 2019. Unsupervised seismic facies classification applied to a presalt carbonate reservoir, Santos Basin, offshore Brazil, *AAPG Bulletin*, 103, 997–1012. DOI: 10.1306/10261818055.
- Fischer, A.G., 1964. Lofer cyclothems of the Alpine Triassic. In *Symposium on Cyclic Sedimentation*, Kans. Geol. Surv. Bull., 167, 107–149.
- Formigli, J.F., 2007. Pre-salt reservoirs offshore Brazil: perspectives and challenges. In: *Bank of America Energy Conference*.
- Formigli, J.F., 2008. Santos Basin Pre-Salt Cluster: How to Make Production Development Technical and Economically Feasible, Rio Oil & Gas Conference Presentation, Rio de Janeiro, Brazil.
- Formigli, J.M., Pinto, A.C.C., Almeida, A.S., 2009. Santos Basin's Pre-Salt Reservoirs Development – The Way Ahead, OTC Presentation, Houston, Texas. DOI: 10.4043/19953-MS.
- Gambôa, L.P., Machado, M., da Silveira, D., de Freitas, J., da Silva, S., 2009. Evaporitos estratificados no Atlântico Sul: interpretação sísmica e controle tectono-estratigráfico na Bacia de Santos, *Sal: Geologia e Tectônica, Exemplos nas Bacias Brasileiras*, Editora Beca, pp. 342-361.
- Gomes, J.P., Bunevich, R.B., Tedeschi, L.R., Tucker, M.E., Whitaker, F.F., 2020. Facies classification and patterns of lacustrine carbonate deposition of the Barra Velha Formation, Santos Basin, Brazilian Pre-salt, *Marine and Petroleum Geology*, 113, 104176. DOI: 10.1016/j.marpetgeo.2019.104176.
- Griffiths, M., Hembd J., Prigent H., 2011. Application of interbed multiple attenuation, *The Leading Edge*, 30(8): 906-912. DOI:10.1190/1.3626498.

- Hendry, J., Burgess, P., Hunt, D., Janson, X., Zampetti, V., 2021. Seismic characterization of carbonate platforms and reservoirs: an introduction and review, Geological Society of London, Special Publications, 509, 1-28. DOI: 10.1144/SP509-2021-51.
- Herlinger, R., 2016. Controles deposicionais e diagenéticos das propriedades petrofísicas dos reservatórios Aptianos/Barremianos do Grupo Lagoa Feia no norte da Bacia de Campos, Master Dissertation, Universidade Federal do Rio Grande do Sul, Porto Alegre, RS, Brazil, 124 pp.
- Herlinger, R., Freitas, G., Ramnani, C., De Ros, L., 2020. Petrological and Petrophysical Implications of Magnesian Clays in Brazilian Pre-Salt Deposits, SPWLA 61st Annual Symposium.
- Herlinger, R., Zambonato, E.E., De Ros, L.F., 2017. Influence of diagenesis on the quality of Lower Cretaceous pre-salt lacustrine carbonate reservoirs from northern Campos Basin, offshore Brazil. *Journal of Sedimentary Research*, 87(12), 1285-1313. DOI: 10.2110/jsr.2017.70.
- Herrmann, P., Mojesky, T., Magesan, M., Hugonnet, P., 2000. De-aliased, high-resolution Radon transforms: 70th Annual International Meeting, SEG, Expanded Abstracts, 1953–1956. DOI: 10.1190/1.1815818.
- Johann, P.R.S., Monteiro, R.C., 2016. Geophysical Reservoir Characterization and Monitoring at Brazilian Pre-Salt Oil Fields, Offshore Technology Conference, Houston, Texas. DOI: 10.4043/27246-MS.
- Kallweit, R., Wood, L., 1982. The limits of resolution of zero-phase wavelets, *Geophysics*, 47 (7), 1035–1046. DOI: 10.1190/1.1441367.
- Karagodin, Y.N., 1975. Mutual relationships between sedimentary cyclic complexes in sections of oil and gas bearing basins, *Doklady Akademii Nauk SSSR*, 220, 1414–1416.
- Karner, G.D., Gambôa, L.A.P., 2007. Timing and origin of the South Atlantic pre-salt sag basins and their capping evaporites, Geological Society, London, Special Publications, 285, 15–35. DOI: 10.1144/SP285.2.
- Kingdon, A., Fellgett, M.W., Williams, J., 2016. Use of borehole imaging to improve understanding of the in-situ stress orientation of Central and Northern England and its implications for unconventional hydrocarbon resources, *Marine and Petroleum Geology*, 73, 1-20. DOI: 10.1016/j.marpetgeo.2016.02.012.
- Kneller, E., Teixeira, L., Hak, B., Cruz, N.M.S.M., Oliveira, T.A.S., Cruz, J.M.N., Cunha, R.S., 2019. Challenges and Solutions of Geostatistical Inversion for Reservoir Characterization of the Supergiant Lula Field, IV European Association Geophysicists & Engineers Conference on Petroleum Geostatistics. DOI: 10.3997/2214-4609.201902176.
- Labourdette, R., Hegre, J., Imbert, P., Insalaco, E., 2008. Reservoir-scale 3D sedimentary modelling: approaches to integrate sedimentology into a reservoir characterization workflow, The Geological Society, London, Special Publications, 309 (1), 75-85. DOI: 10.1144/SP309.6.

- Lagraba, J.O.P., Hansen, S.M., Spalburg, M., Helmy, M., 2010, Borehole image tool design, value of information, and tool selection, Dipmeter and borehole image log technology, AAPG Memoir 92, p. 15-38.
- Lebedev, S., Boonen, J., Trampert, J., 2009. Seismic structure of Precambrian lithosphere: New constraints from broadband surface-wave dispersion, *Lithos*, Special Issue "Continental Lithospheric Mantle: The Petro-Geophysical Approach", 109, 96-111. DOI: 10.1016/j.lithos.2008.06.010.
- Lima, B.E.M., De Ros, L. F., 2019. Deposition, diagenetic and hydrothermal process in the Aptian Pre-Salt lacustrine carbonate reservoirs of the northern Campos Basin, Offshore Brazil, *Sedimentary Geology*, 383, 55-81. DOI: 10.1016/j.sedgeo.2019.01.006.
- Lupinacci, W.M., Franco, A.P., Oliveira, S.A.M., Moraes, F.S., 2017. A combined time-frequency filtering strategy for Q-factor compensation of post-stack seismic data. *Geophysics*, 82, no. 1, V1–V6. DOI: 10.1190/geo2015-0470.1.
- Lupinacci, W., Fernandes, F.J.D., Oliveira Neto, E., Vizeu, F., Freire, A.F.M., 2023. The importance of a priori models in the Bayesian facies classification in carbonate reservoirs, 84th EAGE Annual Conference & Exhibition, Proceedings, 2023 (1), 1–5, European Association of Geoscientists & Engineers. DOI: 10.3997/2214-4609.202310767.
- Machado, M.A.P., 2018. Pré-Sal: A saga, A história de uma das maiores descobertas mundiais de petróleo, L&PM Editores, Rio de Janeiro, Brazil, 316 pp.
- Magalhães, A.J.C., Raja Gabaglia, G.P., Fragoso, D.G.C., Bento Freire E., Lykawka, R., Arregui, C.D., Silveira, M.M.L., Carpio, K.M.T., De Gasperi, A., Pedrinha, S., Artagão, V.M., Terra, G.J.S., Bunevich, R.B., Roemers-Oliveira, E., Gomes, J.P., Hernández, J.I., Hernández, R.M., Bruhn, C.H.L., 2020. High-resolution sequence stratigraphy applied to reservoir zonation and characterisation, and its impact on production performance - shallow marine, fluvial downstream, and lacustrine carbonate settings, *Earth-Science Reviews*, 210, 103325. DOI: 10.1016/j.earscirev.2020.103325.
- Makhankova, A., Sautter, B., Manoj, M., Menier, M., Poppelreiter, M., 2020. Seismic stratigraphy and sedimentology of a Miocene carbonate platform in Luconia, South China Sea, *Geological Journal*, 56, 1–17. DOI: 10.1002/gj.3942.
- Mancini, A., Capezzuoli, E., Erthal, M., Swennen, R., 2019. Hierarchical approach to define travertine depositional systems: 3D conceptual morphological model and possible applications, *Marine and Petroleum Geology*, 103, 549–563. DOI: 10.1016/j.marpetgeo.2019.02.021.
- Maul, A., Fonseca, J., Teixeira, L., Barros, P., Boechat, J.B., Nunes, J.P., Yamamoto, T., González, M., González, G., 2018. Modeling Intra-Salt Layers when Building Velocity Models for Depth Migration: Examples of the Santos Basins, Brazilian Offshore, SEG Technical Program Expanded Abstracts, pp. 3764-3767. DOI: 10.1190/segam2018-2996209.1.
- Mavko, G., Mukerji, T., Dvorkin, J., 2009. The rock physics handbook: Tools for seismic analysis in porous media, Cambridge University Press, 511 pp. DOI: 10.1017/CBO9780511626753.

- Mello, V.L., 2020. Classificação de rochas carbonáticas do Pré-Sal com relação à composição mineralógica a partir de parâmetros elásticos, Master Dissertation, Instituto de Geociências da Universidade Federal Fluminense, Brazil, 121 pp.
- Mello, V.L., Lupinacci, W.M., 2022. Mineralogy based classification of carbonate rocks using elastic parameters: A case study from Buzios Field, *Journal of Petroleum Science and Engineering*, v. 209, 109962. DOI: 10.1016/j.petrol.2021.109962.
- Milani, E.J., Rangel, H.D., Bueno, G.V., Stica, J.M., Winter, W.R., Caixeta, J.M., Pessoa Neto, O.C., 2007. Bacias Sedimentares Brasileiras – Cartas Estratigráficas: Introdução, *Boletim de Geociências da Petrobras*, 15 (2), 183–198, Rio de Janeiro, Brazil.
- Minzoni, M., Cantelli, A., Thornton, J., Wignall, B., 2021. Seismic-scale geometries and sequence-stratigraphic architecture of Early Cretaceous syn-post rift carbonate systems, Presalt Section, Brazil, *Geological Society, London, Special Publications*, 509, 105-126. DOI: 10.1144/SP509-2019-78.
- Mio, E., Chang, H.K., Corrêa, F.S., 2005. Integração de métodos geofísicos na modelagem crustal da Bacia de Santos, *Revista Brasileira de Geofísica*, 23(3), 275-284. DOI: 10.1590/S0102-261X2005000300006.
- Moreira, J.L.P., Madeira, C.V., Gil, J.A., Machado, M.A.P., 2007. Bacia de Santos, *Boletim de Geociências da Petrobras*, 15, 531-549, Rio de Janeiro, Brazil.
- Mukerji, T., Jørstad, A., Avseth, P., Mavko, G., Granli, J.R., 1988. Applying statistical rock physics and seismic inversions to map lithofacies and pore fluid probabilities in North Sea reservoir, *SEG Technical Program Expanded Abstracts*.
- Muniz, M.C., Bosence, D.W.J., 2015. Pre-salt microbialites from the Campos Basin (offshore Brazil): image log facies, facies model and cyclicity in lacustrine carbonates, *Geological Society, London, Special Publications*, 418, 221–242. DOI: 10.1144/SP418.10.
- Neves, I.A., Lupinacci, W.M., Ferreira, D.J.A., Zambrini, J.P.R., Oliveira, L.O.A., Azul, M.O., Ferrari, A.L., Gambôa, L.A.P., 2019. Presalt reservoirs of the Santos Basin: cyclicity, electrofacies and tectonic-sedimentary evolution, *Interpretation*, 7(4), SH33–SH43. DOI: 10.1190/INT-2018-0237.1.
- Normando, M., Nascimento, D., Souza, A.C., Oliveira, K., Nepomuceno, F., Barbosa, T.H., Salgueiro, A.R., Almeida, N.A., 2022. A proposal for reservoir geostatistical modeling and uncertainty analysis of the Curimã Field, Mundaú Sub-Basin, Ceará Basin, Brazil, *Journal of South American Earth Sciences*, 114, 103716. DOI: 10.1016/j.jsames.2022.103716.
- Ojeda, H.A.O., Cesero, P., 1973. Bacias de Santos e Pelotas - geologia e perspectivas petrolíferas, Rio de Janeiro, Petrobras, 50 pp.
- Oliveira, L., Pimentel, F., Peiro, M., Amaral, P., Christovan, J., 2018. A seismic reservoir characterization and porosity estimation workflow to support geological model update: pre-salt reservoir case study, Brazil, *First Break*, 36(9), 75-85. DOI: 10.3997/1365-2397.n0122.

- Oliveira, T., Cruz, N.M., Cruz, J.M., Cunha, R., Matos, M., 2019. Faults, Fractures and Karst Zones Characterization in a Pre-Salt Reservoir using Geometric Attributes, 16th International Congress of the Brazilian Geophysical Society, Rio de Janeiro, Brazil. DOI: 10.22564/16cisbgf2019.139.
- Oliveira, L.C., Rancan, C.C., Sartorato, A.C.L., Farias, F.A., Pereira, E., 2021. Drowning unconformities on presalt carbonate platforms – Examples from the Itapema Formation (Lower Cretaceous), Santos Basin, offshore Brazil, *Palaeogeography, Palaeoclimatology, Palaeoecology*, 577, 110570. DOI: 10.1016/j.palaeo.2021.110570.
- Oliveira, M.S., Henriques, M.V., Leite, F.E., Corso, G., Lucena, L.D., 2012. Seismic denoising using curvelet analysis, *Physica A-statistical Mechanics and Its Applications*, 391(5), 2106-2110. DOI: 10.1016/j.physa.2011.04.009.
- Papaterra, G.E.Z., 2010. Pré-sal: Conceituação Geológica sobre uma Nova Fronteira Exploratória no Brazil, Master Dissertation, Instituto de Geociências, Universidade Federal do Rio de Janeiro, Rio de Janeiro, Brazil.
- Pedrinha, S., Artagão, V.M., Moreira, T.P., Freitas, L.C., Richter, E., Santos, B.T., 2018. Reservoir Geology Aspects of Lula Supergiant Field, Santos Basin – Brazilian Pre-Salt Province, AAPG Annual Convention and Exhibition, Salt Lake City, Utah. DOI: 10.1144/SP548-2023-91.
- Pedrinha, S., Artagão, V.M., Moreira, T.P., Santos, B.T., Cruz, N.M.S. M, Cruz, J.M., Cortes, V.H., 2024, Capítulo 13: O Campo de Tupi, As grandes descobertas do Pré-sal no Atlântico Sul, Petrobras, 853-883.
- Pedrinha, S., Artagão, V.M., 2024, High-resolution stratigraphy and characterization of reservoir critical heterogeneities in the giant Tupi Field, pre-salt Santos Basin, Brazil, *Geological Society, London, Special Publications*, 548. DOI: 10.1144/SP548-2023-91.
- Pendrel, J., 2001. Seismic inversion - The best tool for reservoir characterization, *CSEG Recorder*, 26 (1), <http://csegrecorder.com/articles/view/seismic-inversion-the-best-tool-for-reservoir-characterization>.
- Penna, R., Camargo, G., Johann, P.R.S., Dias, R., 2013. Challenges in Seismic Imaging and Reservoir Characterization of Presalt Oilfields in Offshore Brazil, *Offshore Technology Conference*, Houston, Texas. DOI: 10.4043/24173-MS.
- Penna, R., Araujo, S., Geisslinger, A., Sansonowski, R., Oliveira, L., Rosseto, J., Matos, M., 2019. Carbonate and igneous rock characterization through reprocessing, FWI imaging and elastic inversion of a legacy seismic data set in Brazilian pre-salt province, *The Leading Edge*, 38 (1), 11–19. DOI: 10.1190/tle38010011.1.
- Penna, R., Lupinacci, W.M., 2021, 3D modelling of flow units and petrophysical properties in Brazilian presalt carbonate, *Marine and Petroleum Geology*, 124, 104829. DOI: 10.1016/j.marpetgeo.2020.104829.
- Pereira, M.J., Feijó, F.J., 1994, Bacia de Santos, *Boletim de Geociências da Petrobras*, 8, 219-234, Rio de Janeiro, Brazil.

- Perri, E., Tucker, M.E., Słowakiewicz, M., Whitaker, F., Bowen, L., Perrotta, I.D., 2017. Carbonate and silicate biomineralization in a hypersaline microbial mat (Mesaieed sabkha, Qatar): roles of bacteria, extracellular polymeric substances and viruses, *Sedimentology*, 65(4), 213–245. DOI: 10.1111/sed.12419.
- Pietzsch, R., Oliveira, D.M., Tedeschi, L.R., Queiroz Neto, J.V., Figueiredo, M., Vazquez, J.C., Souza, R.S., 2018. Palaeohydrology of the Lower Cretaceous pre-salt lacustrine system, from rift to post-rift phase, Santos Basin, Brazil, *Palaeogeography, Palaeoclimatology, Palaeoecology*, 507, 60–80. DOI: 10.1016/j.palaeo.2018.06.043.
- Ponte, F.C., Asmus, H.E., 1978, Geological framework of the Brazilian continental margin, *Geologische Rundschau*, 67, 235. DOI: 10.1007/BF01803262.
- Pöppelreiter, M., Garcia-Carballido, C., Kraaijveld, M., 2010. Borehole image log technology: application across the exploration and production life cycle, AAPG Memoir 92 2010. DOI: 10.1306/M921318.
- Ramnani, W.C., Santos, F.J., Parizek-Silva, Y., Madrucci, V., Araújo, C.C., Vasquez, F.G., Morschbacher, J.M., Bonzanini, F.A.L., Viana, M.S., Souza, S.R., Alves, B.D., Anjos, C.M. S, 2021. Magnesian Clay Minerals in Brazilian Pre-salt Province, International Meeting for Applied Geoscience and Energy.
- Ravenne, C., Galli, A., Doligez, B., Beucher, H., Eschard, R., 2002. Quantification of Facies Relationships Via Proportion Curves. In: Armstrong, M., Bettini, C., Champigny, N., Galli, A., Remacre, A. (eds) *Geostatistics Rio 2000. Quantitative Geology and Geostatistics*, vol 12, Springer, Dordrecht, DOI: 10.1007/978-94-017-1701-4_3.
- Renaut, R.W., Owen, R.B., Jones, B., Tiercelin, J.J., Tarits, C., Ego, J.K., Konhauser, K.O., 2013. Impact of lake-level changes on the formation of thermogene travertine in continental rifts: evidence from Lake Bogoria, Kenya Rift Valley, *Sedimentology*, 60, 428–468. DOI: 10.1111/j.1365-3091.2012.01347.x.
- Riccomini, C., Sant, L.G., Tassinari, C.C.G., 2012. Pré-sal: geologia e exploração, *Revista USP* (95), 33–42. DOI: 10.11606/issn.2316-9036.v0i95p33-42.
- Riding, R., 2000. Microbial carbonates: the geological record of calcified bacterial–algal mats and biofilms, *Sedimentology*, 47, 179–214. DOI: 10.1046/j.1365-3091.2000.00003.x.
- Rosa, A.L.R., 2010. *Análise do Sinal Sísmico*, Sociedade Brasileira de Geofísica, 367 pp.
- Rosa, A.L.R., 2018. *The Seismic Signal and Its Meaning*, Society of Exploration Geophysicists, 788 pp. DOI: 10.1190/1.9781560803348.
- Saller, A., Rushton, S., Buambua, L., Inman, K., McNeil, R., Dickson, J.A.D., 2016. Presalt stratigraphy and depositional systems in the Kwanza Basin, offshore Angola. *AAPG Bulletin*, 100, p 1135–1164, 2016. DOI: 10.1306/02111615216.
- Sartorato, A.C.L, 2018. *Caracterização faciológica, estratigráfica e diagenética dos reservatórios carbonáticos da Formação Barra Velha, Bacia de Santos*, Master Dissertation, Faculdade de Geologia, Universidade do Estado do Rio de Janeiro, Brazil, 277 pp.

- Serra, O., 1990. Element Mineral Rock Catalog, Schlumberger.
- Sheriff, R.E., 1975. Factors affecting seismic amplitudes, *Geophysical Prospecting*, 23, 1, 125–138. DOI: 10.1111/j.1365-2478.1975.tb00685.x.
- Schonewille, M.A., & Aaron, P., 2007. Applications of time-domain high-resolution Radon demultiple, *ASEG Extended Abstracts*, 2007(1), 1-5. DOI: 10.1071/ASEG2007ab003.
- Silva, E., Davólio, A., Santos, M., Schiozer, D., 2020. 4D petroelastic modeling based on a presalt well, *Interpretation*, 8, no. 3, T639–T649. DOI: 10.1190/INT-2019-0099.1.
- Silva, S.F.C.R, Figueiredo, J.J.P., Coelho, P.H., Borghi, L., 2021. Evolução Tectonoestratigráfica da Formação Barra Velha na Área dos Campos de Lapa e Sapinhoá, Bacia De Santos – Brazil, *Geociências*, 40(1), 55–69.
- Silva-Telles, A., Henz, G.I., and Arai, M., 1994. Evidências das primeiras ingressões marinhas na fase rifte da margem leste Brasileira, *Boletim de Geociências da Petrobras*, 8, 409–410, Rio de Janeiro, Brazil.
- Strasser, A., Pittet, B., Hillgartner, H., Pasquier, J.B., 1999. Depositional sequences in shallow carbonate-dominated sedimentary systems: concepts for a high-resolution analysis, *Sediment. Geol.*, 128, 201–221. DOI: 10.1016/S0037-0738(99)00070-6.
- Strasser, A., Hilgen, F., Heckel, P., 2006. Cyclostratigraphy - Concepts, definitions, and applications, *Newsl. Stratigr.*, 42, 75–114. DOI: 10.1127/0078-0421/2006/0042-0075.
- Szatmari, P., More De Lima, C., Fontaneta, G., De Melo Lima, N., Zambonato, E., Menezes, M.R., Bahniuk, J., Coelho, S.L., Figueiredo, M., Florencio, C.P., and Gontijo, R., 2021. Petrography, geochemistry and origin of South Atlantic evaporites: the Brazilian side, *Marine and Petroleum Geology*, 127, 1–31. DOI: 10.1016/j.marpetgeo.2020.104805.
- Teixeira, L., Cruz, N.M.S.M., Silvany, P., Fonseca, J., 2017. Quantitative seismic interpretation integrated with well-test analysis in turbidite and pre-salt reservoirs, *The Leading Edge*, 36(11), 931–937. DOI: 10.1190/tle36110931.1.
- Teixeira, L., Lupinacci, W.M., Maul, A., 2020. Quantitative seismic-stratigraphic interpretation of the evaporite sequence in the Santos Basin, *Marine and Petroleum Geology*, 122, 104690. DOI: 10.1016/j.marpetgeo.2020.104690.
- Terra, G.J.S., Spadini A.R., França, A.B., Sombra, C.L., Zambonato, E.E., Juschaks, L.C.S., Arienti, L.M., Erthal, M.M., Blauth, M., Pittella Franco, M., Matsuda, N.S., Silva, N.G.C., Moretti, P.A., D'Avila, R.S.F., Souza, R.S., Tonietto, S.N., Anjos, S.M.C., Campinho, V.S., Winter, W.R., 2010. Classificação de Rochas Carbonáticas Aplicável às Bacias Sedimentares Brasileiras, *Boletim de Geociências da Petrobras*, 18, 9-29, Rio de Janeiro, Brazil.
- Tedeschi, L.R., Jenkyns, H.C., Robinson, S.A., Sanjine´S, A.E.S., Viviers, M.C., Quintaes, C.M.S.P., and Vazquez, J.C., 2017. New age constraints on Aptian evaporites and carbonates from the South Atlantic: implications for Oceanic Anoxic Event 1a, *Geology*, 45, 543–546. DOI: 10.1130/G38886.1.

- Thiede, D.S., Vasconcelos, P.M., 2010. Paraná flood basalts: rapid extrusion hypothesis confirmed by new $^{40}\text{Ar}/^{39}\text{Ar}$ results, *Geology*, 38(8), 747-750. DOI: 10.1130/G30919.1.
- Thompson, D.L.; Stilwell, J.D.; Hall, M., 2015. Lacustrine carbonate reservoirs from Early Cretaceous rift lakes of Western Gondwana: pre-salt coquinas of Brazil and West Africa, *Gondwana Research*, 28, 26–51. DOI: 10.1016/j.gr.2014.12.005.
- Tosca, N.J., & Wright, V.P., 2015. Diagenetic pathways linked to labile Mg-clays in lacustrine carbonate reservoirs: a model for the origin of secondary porosity in the Cretaceous pre-salt Barra Velha Formation, offshore Brazil, *Geological Society, London, Special Publications*, 435(1), 1-14. DOI: 10.1144/SP435.1.
- Vasquez, G.F., Morschbacher, M.J., Anjos, C.W.D., Silva, Y.M.P., Madrucci, V., Justen, J.C.R., 2019. Petroacoustics and Composition of Presalt Rocks from Santos Basin, *The Leading Edge*, 38(5): 342-348. DOI: 10.1190/tle38050342.1.
- Vasquez, G.F., Morschbacher, M., Justen, J., Abreu, E., Ramnani, C., Madrucci, V., Silva, Y., Santos, J., Anjos, S., 2021. Yet More Insights on the Petrogeophysics of Pre-salt Rocks from Brazil, *Sociedade Brasileira de Geofísica*, Rio de Janeiro, Brazil.
- Van Tuyl, J., Alves, T., Cherns, L., Antonatos, G., Burgess, P., Masiero, I., 2019. Geomorphological evidence of carbonate build-up demise on equatorial margins: a case study from offshore northwest Australia, *Marine and Petroleum Geology*, 104, 125–149. DOI: 10.1016/j.marpetgeo.2019.03.006.
- Vital, J.C. S., Ade, M.V.B., Morelato, R., Lupinacci, W.M., 2023. Compartmentalization and stratigraphic-structural trapping in pre-salt carbonate reservoirs of the Santos Basin: A case study in the Iara complex. *Marine and Petroleum Geology*, 151, 106163. DOI: 10.1016/j.marpetgeo.2023.106163.
- Wang, Y., 2008. *Seismic inverse Q filtering*, Blackwell Publishing Ltd, 238 pp.
- Winter, W.R., Jahnert, R.J., França, A.B., 2007. Bacia de Campos, *Boletim de Geociências da Petrobras*, 15(2), 511-529, Rio de Janeiro, Brazil.
- Wyman, R. E., 1981. *Petrogeophysics: The Interrelationships of Petrophysics, Geology and Geophysics*, American Association of Petroleum Geologists, 90 pp.
- Wright, V.P., Barnett, A.J., 2015. An abiotic model for the development of textures in some South Atlantic early Cretaceous lacustrine carbonates, *Geological Society, London, Special Publications*, 418, 209–219. DOI: 10.1144/SP418.3.
- Wright, V.P., Barnett, A.J., 2017a. Classifying reservoir carbonates when the status quo simply does not work: A case study from the Cretaceous of the South Atlantic: AAPG Annual Conference and Exhibition, 108–121.
- Wright, V.P., Barnett, A.J., 2017b. Critically evaluating the current depositional models for the pre-salt Barra Velha Formation, Offshore Brazil: AAPG Annual Conference and Exhibition: Search and Discovery, 1–40.

- Wright, V.P., Barnett, A.J., 2019. The textural evolution and ghost matrices of the Cretaceous barra Velha Formation carbonates from the Santos Basin, offshore Brazil, *Facies*, v. 66, 18 pp. DOI: 0.1007/s10347-019-0591-2.
- Wright, V.P., Rodriguez K., 2018. Reinterpreting the South Atlantic pre-salt microbialite reservoirs: Petrographic, isotopic and seismic evidence for a shallow evaporitic lake depositional model: *First Break*, 36, 71–77. DOI: 0.3997/1365-2397.n0094.
- Xu, S., Payne, M., 2009. Modeling elastic properties in carbonate rocks, *The Leading Edge*, 28(1), 66–74. DOI: 10.1190/1.3064148.
- Yang, D., Huang, Y., Chen, Z., Huang, Q., Ren, Y., Wang, C., 2021. A python code for automatic construction of Fischer plots using proxy data, *Nature, Scientific Reports*, 11, 10518. DOI: 10.1038/s41598-021-90017-9.
- Yilmaz, O., 2001. *Seismic Data Analysis: Processing, Inversion, and Interpretation of Seismic Data*, Society of Exploration Geophysicists, Tulsa, OK, 1028 pp. DOI: 10.1190/1.9781560801580.

Cruz, N.M.S.M.: conceptualization (lead), formal analysis (lead), investigation (lead), methodology (lead), project administration (lead), software (lead), validation (lead), writing – original draft (lead); **Moreira, T.P.B.:** conceptualization (equal), formal analysis (equal), investigation (equal), methodology (equal), project administration (supporting), software (equal), validation (equal), writing – original draft (supporting); **Nascimento, A.:** conceptualization (supporting), formal analysis (equal), investigation (equal), methodology (supporting), project administration (supporting), software (equal), validation (equal), writing – original draft (supporting); **Teixeira, L.:** conceptualization (supporting), formal analysis (supporting), investigation (supporting), methodology (supporting), project administration (supporting), software (supporting), validation (equal), writing – original draft (supporting); **Cruz, J.M.:** conceptualization (supporting), formal analysis (supporting), investigation (supporting), methodology (supporting), project administration (supporting), software (supporting), validation (supporting), writing – original draft (supporting); **Maul, Alexandre:** conceptualization (equal), formal analysis (supporting), investigation (supporting), methodology (supporting), project administration (supporting), software (supporting), validation (equal), writing – original draft (equal); **Lupinacci, W.M.:** conceptualization (equal), formal analysis (supporting), investigation (supporting), methodology (supporting), project administration (supporting), software (supporting), validation (equal), writing – original draft (equal).



| Time (Ma) | Period | Epoch | Group | Ages | Local Stages | Unconformities | Formations | Reservoir Zones or Stratigraphic Intervals | Sequences | Tectonic Evolution - Interpretation Examples | | | | Intervals of Interest | Key Lithologies Facies Associations | Formations | | |
|-----------|------------|-------|-----------|-------------|--------------|------------------------------|------------------|--------------------------------------------|------------|----------------------------------------------|------|----------------|-------------------------|-------------------------|---------------------------------------------------------------------------------------------------------------------|--------------------|-------------|----------|
| 113 | Cretaceous | Lower | Guaratuba | Albian | | Pre-Salt | Guarujá Ariri | BVE100 | K46-K48 | Drift | | | Passive Margin or Drift | Passive Margin or Drift | Main Secondary Tertiary Necessary for the individualization of the Barra Velha Formation in the study area | Guarujá Ariri | | |
| 117 | | | | Aptian | Alagoas | Intra-Alagoas (IAU) | Barra Velha | BVE200 IAU | | Post-Rift | Sog | Sog | Sog | BVE-I Sog | | | Barra Velha | |
| 123.1 | | | | | Jiquilá | Pre-Alagoas (PAU) | | | BVE300 PAU | K44 | | Rift | | | | BVE-II: Upper Rift | | |
| 126.4 | | | | Barremian | Buracica | Pre-Jiquilá (PJU) | Itapema | | ITP100 PJU | K38 | Rift | Upper Syn-Rift | Lower Rift | Lower Rift | | | | Itapema |
| 136.4 | | | | Hauterivian | Aratu | | Piçarras | | | | | | | | | | | Piçarras |
| | | | | | | Onset of basaltic lava flows | Camboriú | | | | | | | | Camboriú | | | |

| | | | | | | | | |
|-------------------------------------|----------------------------------------------------------------------|-------------------------------------|-----------------------|-------------------------|-----------------------|---------------|-----------------------------------|-----------------------|
| Modified from Moreira et al. (2007) | Modified from Pedrinha et al. (2018) and Pedrinha and Artagão (2024) | Modified from Moreira et al. (2007) | Menezes et al. (2007) | Carnietti et al. (2009) | Buckley et al. (2015) | Castro (2019) | Silva et al. (2024) - This work - | Moreira et al. (2007) |
|-------------------------------------|----------------------------------------------------------------------|-------------------------------------|-----------------------|-------------------------|-----------------------|---------------|-----------------------------------|-----------------------|

| | | | | | | | | |
|-------------------|---------------------|----------------------------------------------------------------------------|--------------------------------------------|------------------------------------------|---------------------------------------------|----------------------------------------------------------------|------------------------------------------------|-----------------------------------------------------------------------------------------------------------|
| Saline evaporites | Basic igneous rocks | Basic, intermediate, acidic, volcanoclastic, and pyroclastic igneous rocks | Siliciclastic, moderate-high energy facies | Carbonates (reworked and in-situ facies) | Carbonates with mixed siliciclastic content | Carbonates with clay minerals and low-energy facies in general | Clayey, shaly and low-energy facies in general | Association of high-energy carbonate facies with the presence of bioclastic carbonate clasts and bivalves |
|-------------------|---------------------|----------------------------------------------------------------------------|--------------------------------------------|------------------------------------------|---------------------------------------------|----------------------------------------------------------------|------------------------------------------------|-----------------------------------------------------------------------------------------------------------|

Figure 1 – Distinct interpretations proposed for the tectono-stratigraphic evolution of the Santos Basin, with an emphasis on the Barra Velha Formation. The summary table, adapted from Castro (2019) and complemented by Mello (2020), integrates the interpretation used in this study, providing a simplified schematic depiction of the key lithology/facies associations identified within the study area.

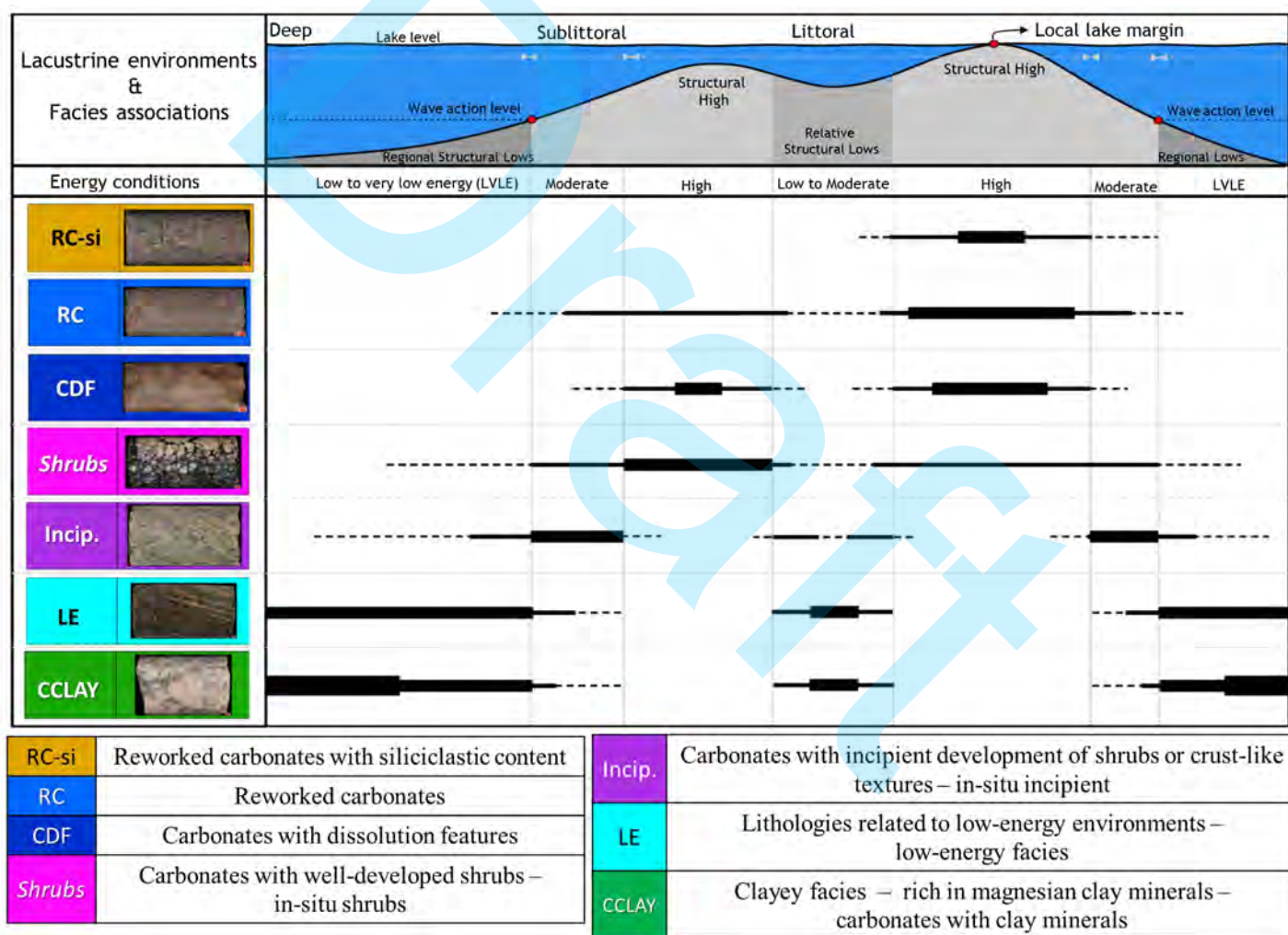


Figure 2 – Interpreted facies associations for the Tupi Field in relation to lake water depth, environmental energy of the lacustrine setting, and distance from the local lake margin. The depositional model underscores that reworked facies dominate in high-energy environments and the associated siliciclastic content increases towards the local lake margin. In-situ facies are abundantly observed under conditions of moderate to high-energy. Lithologies associated with low-energy facies in general, as well as clayey facies rich in preserved magnesian clay minerals, correlate more closely with deeper or energetically sheltered environments (Regional and Relative Structural Lows). After Pedrinha et al. (2018), Pedrinha et al. (2024), and Pedrinha and Artagão (2024).

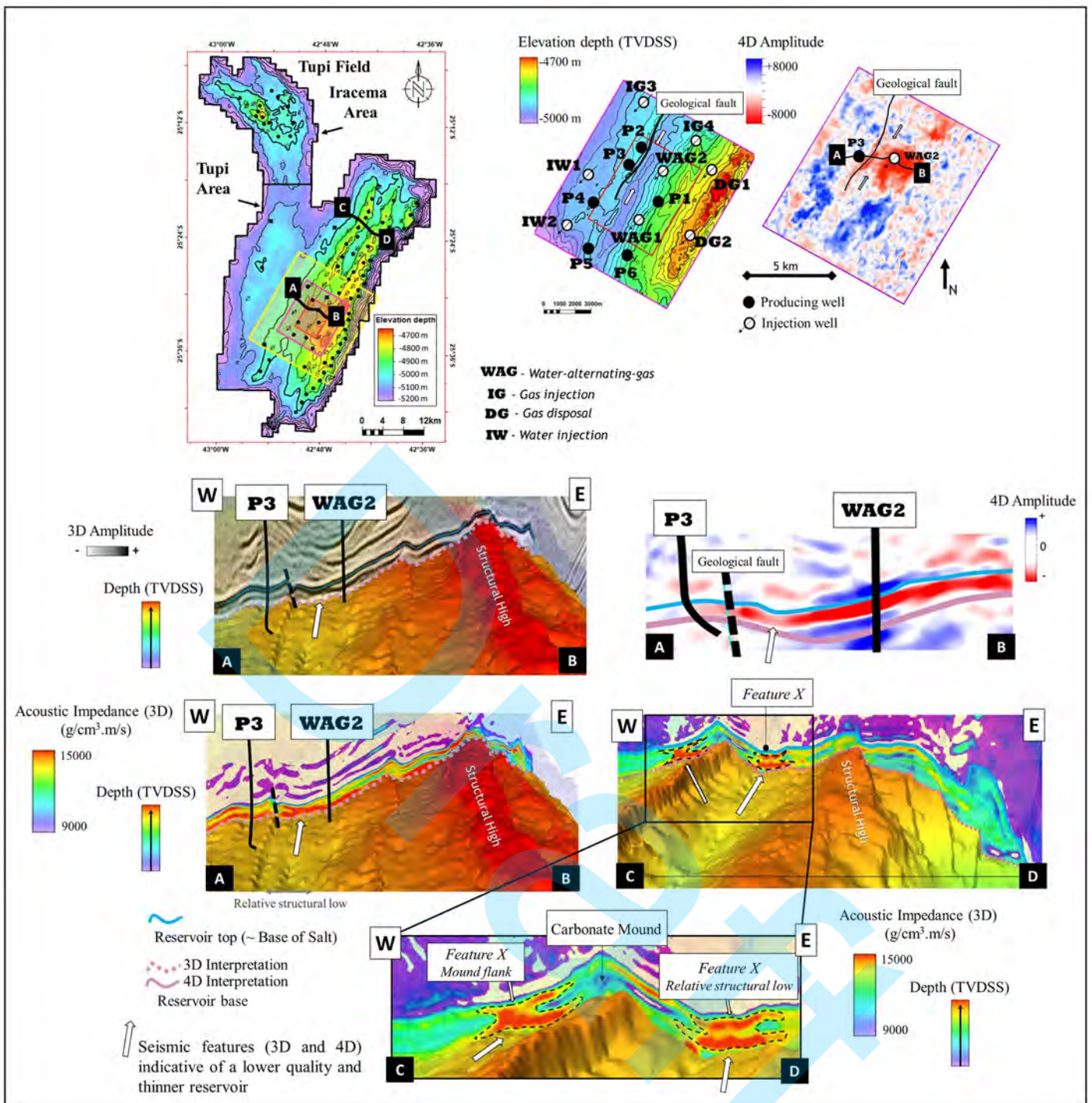


Figure 3 – Feature X, interpreted as a seismic feature indicative of reservoir quality degradation and/or reduction in permo-porous thickness towards structural lows, seen in the regions of the Tupi Nodes Pilot (seismic sections A-B) and the Tupi Northeast production module (seismic sections C-D), within the Tupi Field. Both the 4D seismic amplitude map for the reservoir interval and the 3D and 4D seismic amplitude sections reveal a fading seismic signal at the position of Feature X. Conversely, in the acoustic impedance sections, Feature X is highlighted by high values around 15000 g/cm³.m/s, displayed in shades of yellow and red. Its geometry is reminiscent of the letter X in the alphabet. The acoustic impedance section C-D shows Feature X in both a structural flank position (west mound flank) and a relative structural low position (east), with Feature X bordering a second seismic feature in both positions, interpreted as a carbonate mound. Adapted from Cruz et al. (2021a) and Cruz et al. (2021b).

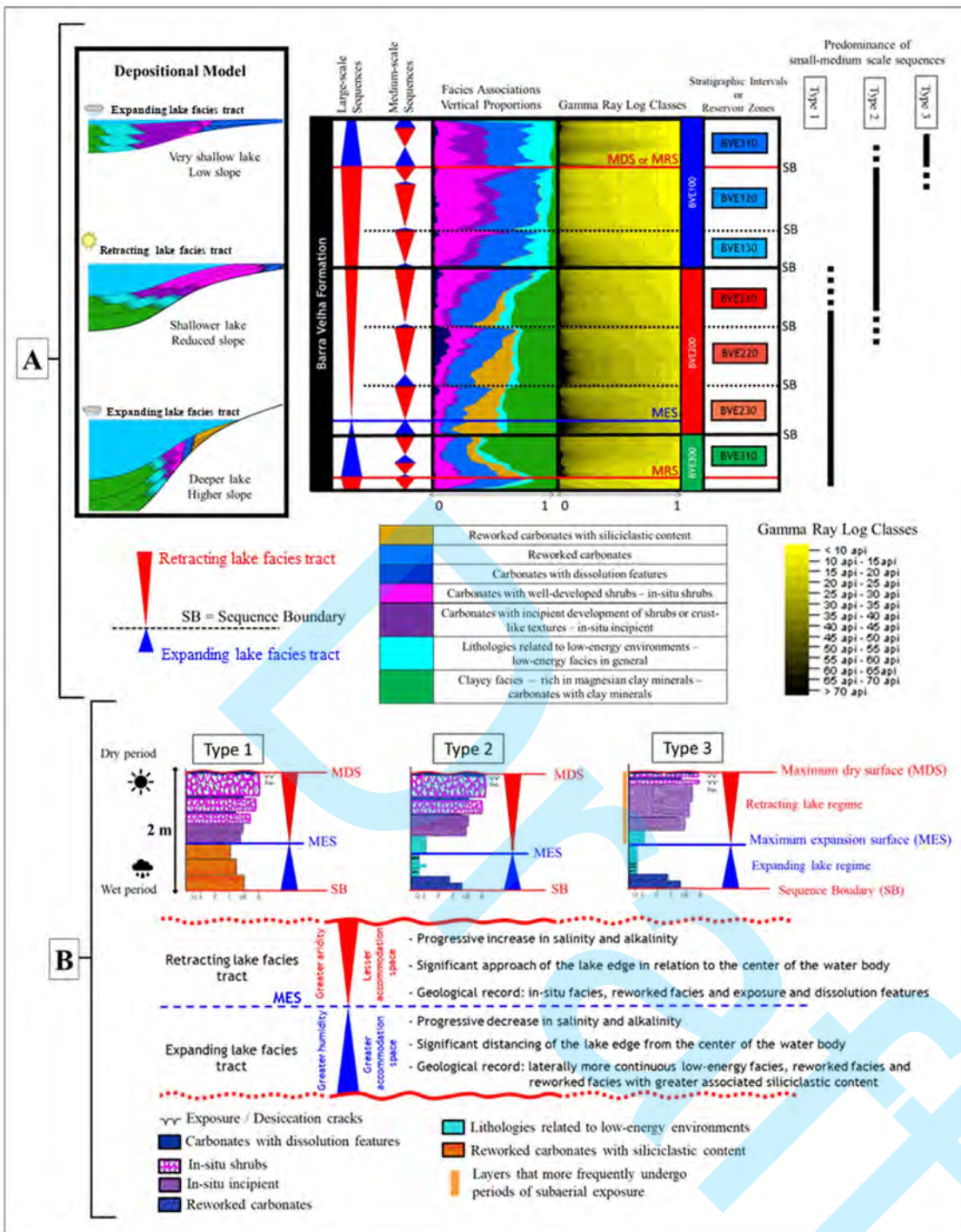


Figure 4 – [A] Schematic depiction of the depositional evolution of the Barra Velha Formation reservoirs within the Tupi Field, focusing on the BVE100 and BVE200 zones. Medium to large-scale stratigraphic sequences are associated with the paleotopography of the lake, a consequence of gradual changes in tectonic activity and climatic fluctuations. Distinct patterns of vertical facies stacking and variations in total gamma-ray log values and behaviors are related to reservoir zoning. The triangles represent Karagodin cycles (Karagodin, 1975), with lake expansion phases denoted by blue triangles and lake retraction phases represented by red triangles. Derived from Pedrinha et al. (2018), the vertical proportion curves for facies associations and total gamma-ray log classifications were calculated using data from all wells drilled up to 2018. **[B]** Schematic representations of the main types of elementary sequences identified. Adapted from Artagão (2018), Pedrinha et al. (2018), Magalhães et al. (2020), Pedrinha et al. (2024), and Pedrinha and Artagão (2024).

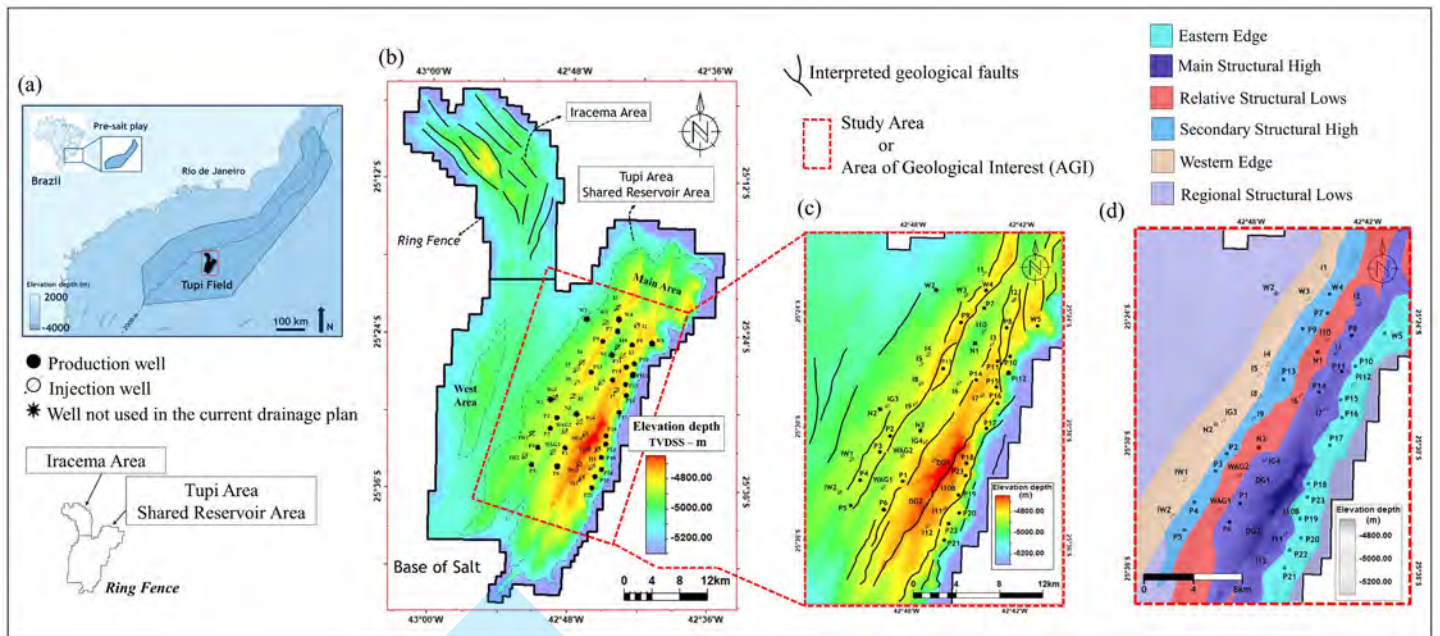


Figure 5 – Regional location of the Tupi Field within the Santos Basin pre-salt play (a), with detailed views of the Iracema (b) and Tupi [Shared Deposit; (b), (c) and (d)] areas. The Tupi Area can be further geographically subdivided into Western and Main areas [dashed black lines; (b)]. Highlighted within the Main area is the Area of Geological Interest (AGI) [dashed red rectangles; (b), (c) and (d)], which includes the selected wells and presents an overview of the geological faults [solid black lines; (c)] intersecting the Base of Salt seismic horizon, approximately corresponding to the top of the BVE100 stratigraphic interval. The principal structural orientation of the Iracema Area is NW-SE (b), while in the Tupi Area, including the AGI, it is NE-SW (c). To facilitate referencing the positioning of wells and interpretations throughout this paper, the AGI is further subdivided into six geographical environments (d). These are named the Eastern Edge (highlighted in cyan), Main Structural High (highlighted in dark blue), Relative Structural Lows (highlighted in salmon), Secondary Structural High (highlighted in light blue), Western Edge (highlighted in beige), and Regional Structural Lows (to the west and east; highlighted in purple).

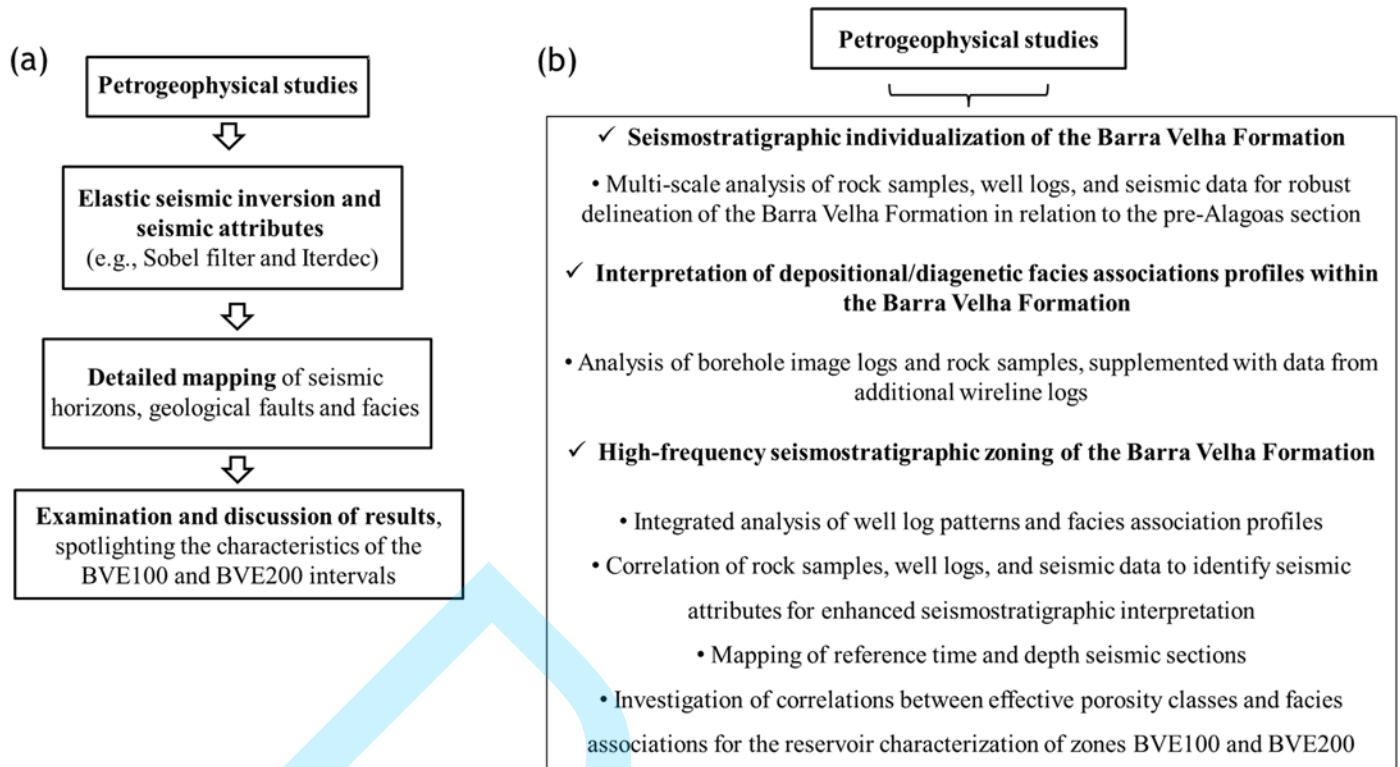


Figure 6 – (a) Step-by-step methodology schematic flowchart. (b) Petrogeophysical studies overview.

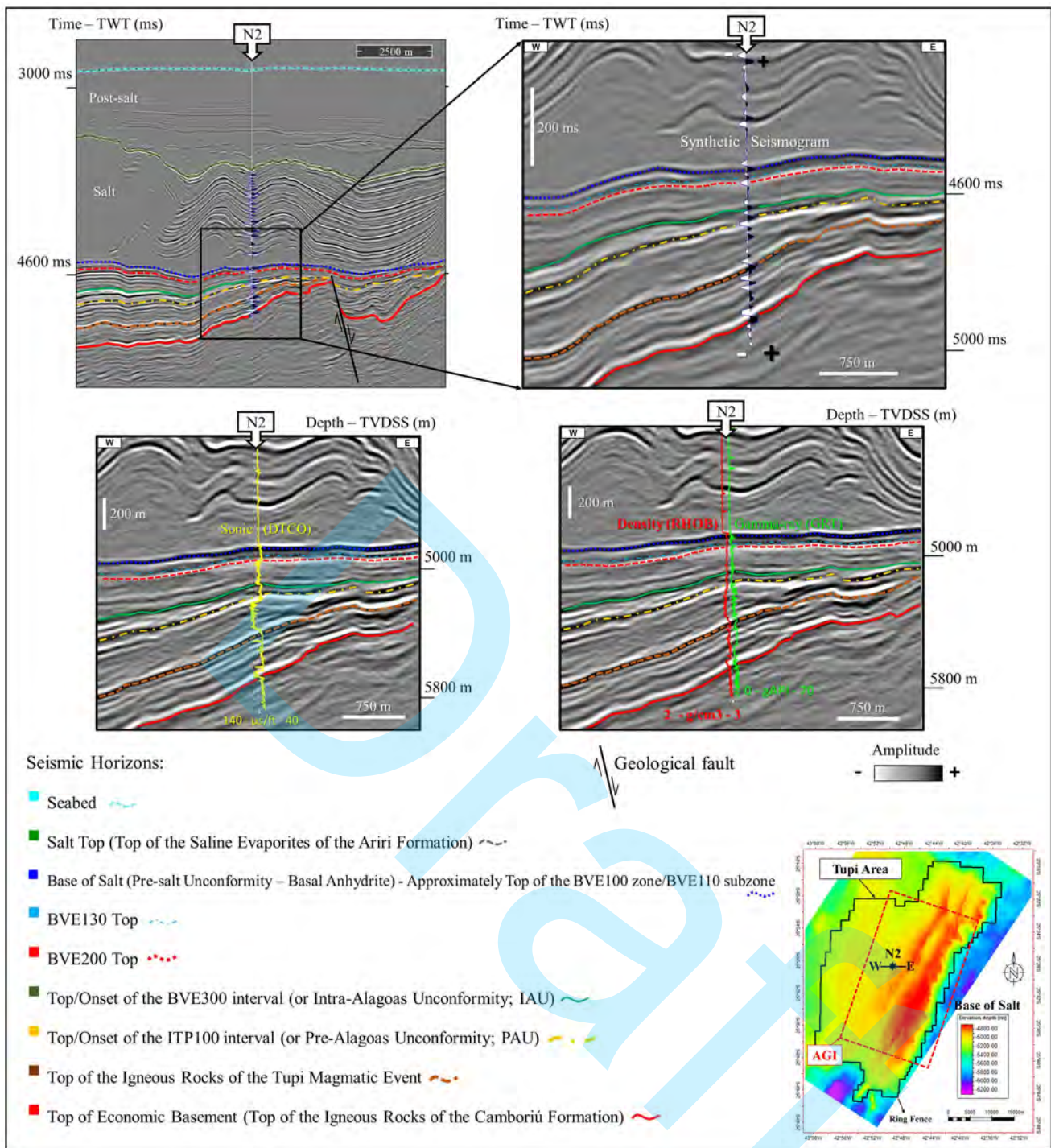


Figure 7 – Schematic view of the seismic interpretation in the vicinity of well N2 (Western Edge), including regional seismic horizons (Seabed and Salt Top), the main recognized unconformities for the Alagoas and pre-Alagoas sections (Pre-salt, IAU and PAU), and the stratigraphic zoning of the Barra Velha Formation within the study area, represented by the tops of the BVE100 (mappable Base of Salt), BVE130, BVE200, and BVE300 (approximately IAU) intervals. In the amplitude sections, it is possible to observe the relationship between the seismic reflectors and the responses of the compressional sonic (DTCO), total gamma-ray (GRT), and density (RHOB) logs for the interpreted seismic horizons. Geological markers were interpreted from the well logs, supported by rock data, and seismic amplitude sections in time (TWT; ms) and depth (TVDSS; m). Within the Ariri Formation (salt package), the acquired sonic log (shown in yellow) is of the logging-while-drilling (LWD) type. The location of the arbitrary seismic section is displayed on the Base of Salt structural map. West of the Main Structural High in the Tupi Area, the tops of the BVE100, BVE130, BVE300, and ITP100 (approximately

PAU) intervals are mostly represented by positive seismic reflectors, while the top of the BVE200 interval is usually represented by a negative reflection, indicative of an increase in carbonates with clay minerals.

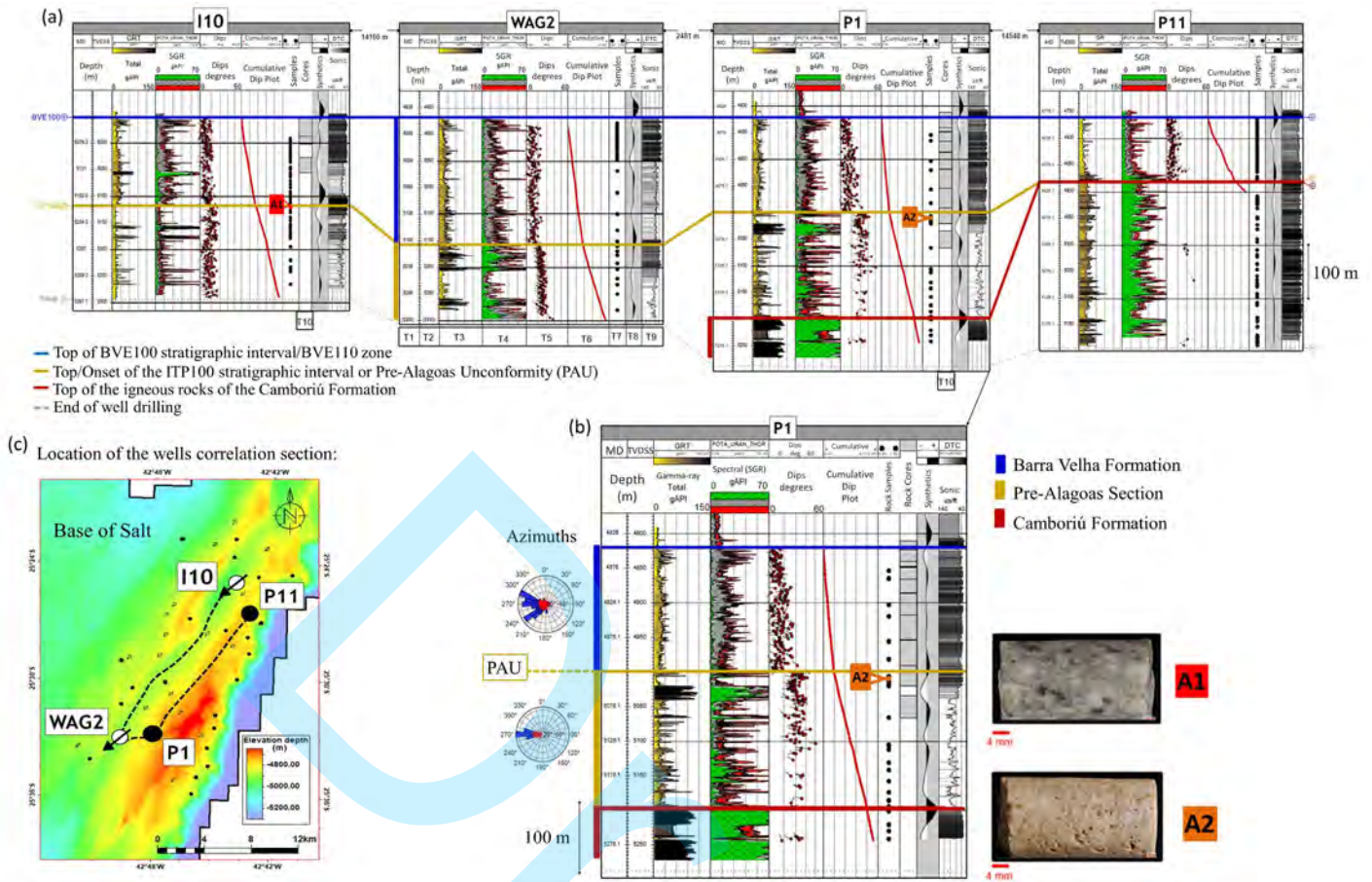


Figure 8 – (a) Interpretation of the Alagoas (Barra Velha Formation) and pre-Alagoas sections, and the tops/onsets of the BVE100 and ITP100 stratigraphic intervals in wells I10 and WAG2 (Relative Structural Lows), and P1 and P11 (Main Structural High). In wells P1 and P11, the igneous rocks of the Camboriú Formation can be distinctly identified. In structural highs, such as in well P11, the Itapema and Piçarras Formations were either eroded or not deposited. In most wells, the Pre-Alagoas Unconformity (PAU) is seismically represented by a positive reflection (refer to synthetic seismograms). Additionally, distinct patterns of total and spectral gamma-ray logs are observed for each interval. The displayed tracks include depths (T1 and T2), total and spectral gamma-ray logs (T2 and T3), interpreted borehole images (BHI) logs dip poles and cumulative dip plots/curves (T4 and T5), synthetic seismograms and compressional sonic log (T8 and T9). Sidewall rock samples (T7) and cores (T10), such as coquina samples A1 and A2, serve as guides for the markings; **(b)** This zoomed-in view highlights the interpretation in well P1. The PAU is indicated by the flexion in the cumulative dip plot, and different azimuth patterns of the bedding planes can be seen. In this well, the PAU corresponds with a positive seismic peak, as in most wells, but this signature can vary depending on the impedance contrast at the interface. Photos of rock samples illustrating the onset of the ITP100 zone in the wells are displayed; and **(c)** The wells correlation section is illustrated on the Base of Salt structural map.

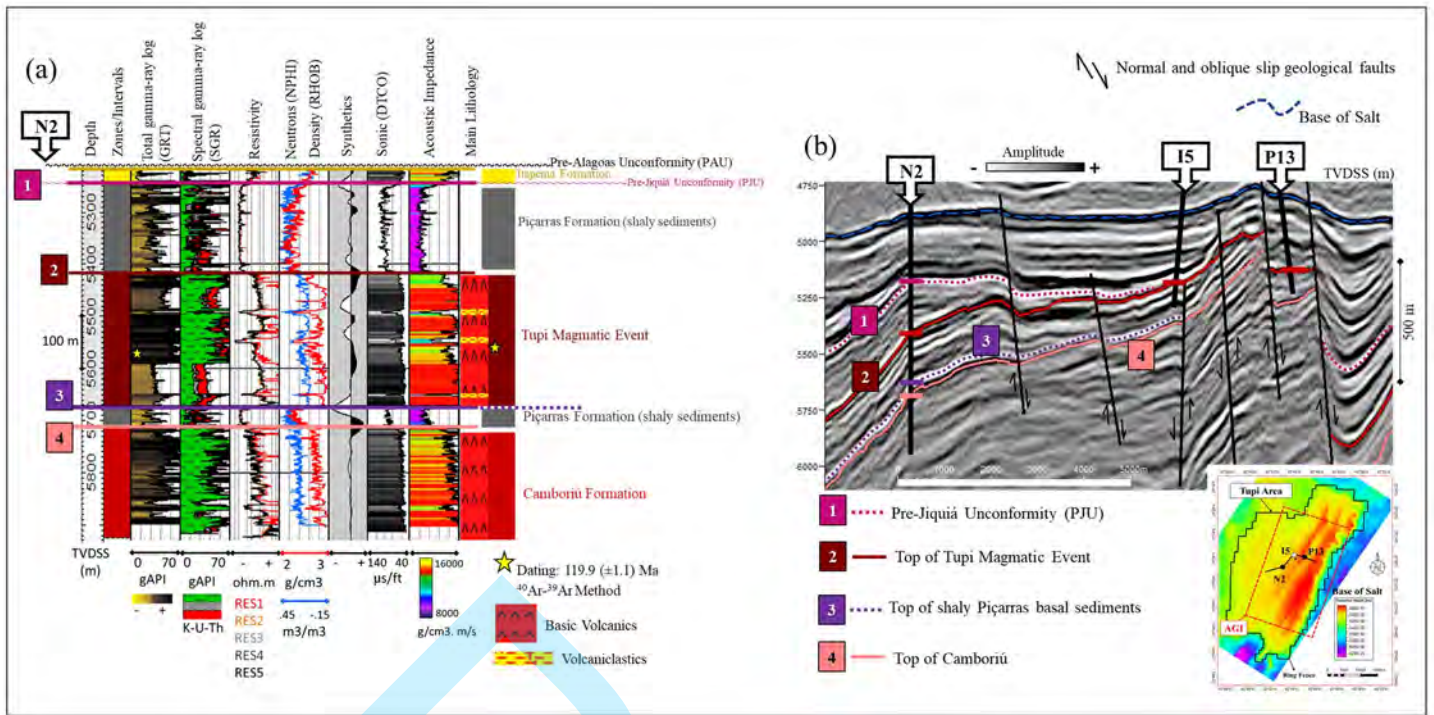


Figure 9 – A close-up view of the interpretation of the pre-Alagoas section in well N2 (Western Edge) emphasizing the distinct delineation of the Itapema, Piçarras, and Camboriú Formations (a). Additionally, a younger magmatic event, which was dated at 119 Ma using ^{40}Ar - ^{39}Ar dating, is identified, and termed the Tupi Magmatic Event (a). This event is situated within the shaly sediments of the Piçarras Formation (as illustrated by lower resistivities without curve separation) and comprises volcanoclastic rocks that occasionally exhibit reservoir potential. RES1 indicates the shallowest resistivity (10'), while RES5 represents the deepest resistivity (90'). For context, the drilling was carried out using synthetic oil-based mud fluid. Also, an arbitrary amplitude section presents the seismic interpretation of the Tupi Magmatic Event from N2 and across wells I5 and P13, accompanied by local identification and mapping of the Pre-Jiquiá Unconformity (PJU) around well N2 (b). The PJU correlates most closely with a discontinuous negative amplitude trough, marking the commencement of the predominantly shaly deposits of the Piçarras Formation (b). The location of the seismic section is depicted on the Base of Salt structural map (b).

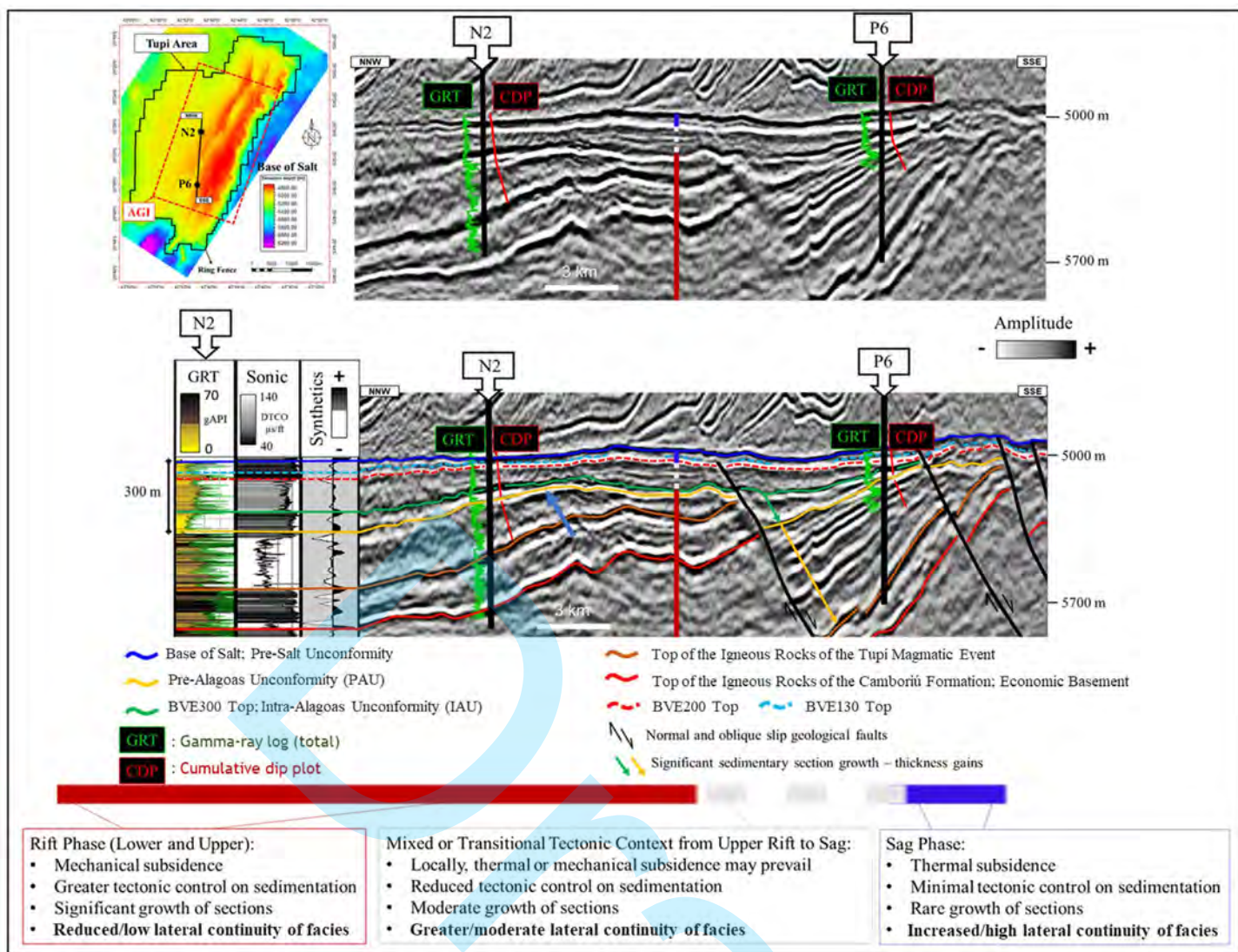


Figure 10 – Schematic view of seismic interpretation and tectonic context for the Alagoas and pre-Alagoas sections around wells N2 (Western Edge) and P6 (flank of the Main Structural High). The arbitrary seismic section location is shown on the Base of Salt structural map (black line N2-P6). Note the flexure and inclination change in the cumulative dip plot (CDP; red) and variations in total gamma-ray logs (GRT; green) around the Pre-Alagoas Unconformity (PAU; orange horizon). The seismic reflectors are more tilted in the pre-Alagoas section, especially near P6. The PAU is typically mapped over a positive seismic reflector (wells N2 and P6), with variations such as a negative reflector near well N2 (blue arrow). Near P6 within the BVE300 interval, observe the erosional to moderately wedge-shaped geometry of sedimentary strata. Significant thickness variations, characteristic of a rift context, are mapped from the Economic Basement to the Intra-Alagoas Unconformity (IAU; green horizon). Between the BVE200 top and the Base of Salt, within the BVE100 zone, thickness variation is minimal, reflecting characteristics of a sag phase. The BVE200 zone represents a transition between the rift and sag phases (mixed tectonic context).

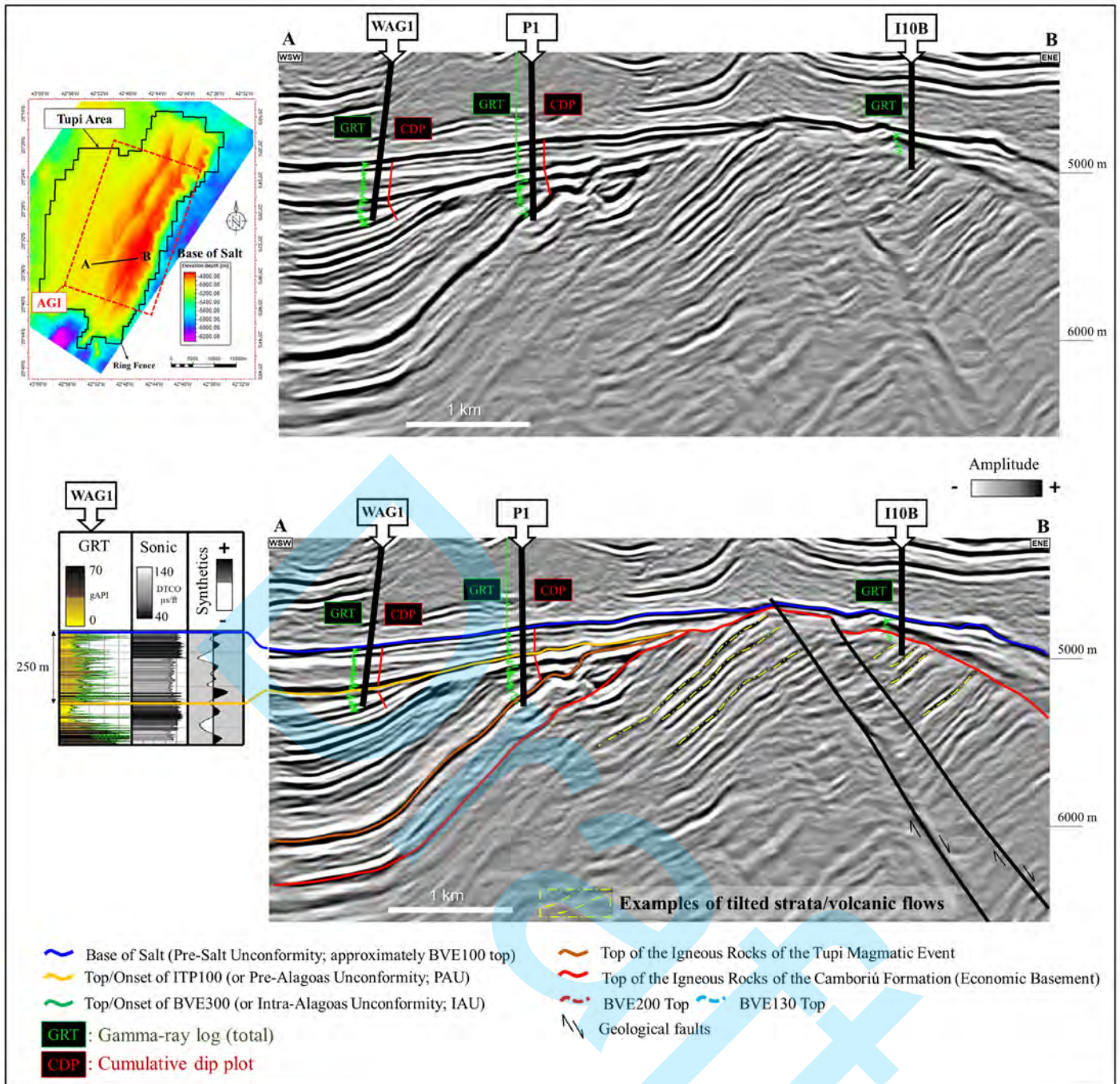


Figure 11 – Schematic view of the seismostratigraphic interpretation of the Alagoas and pre-Alagoas sections around wells WAG1 (Relative Structural Low), P1 (Main Structural High), and I10B (Eastern Edge). At the representative surface of the Pre-Alagoas Unconformity (PAU), take note of the change in slope of the cumulative dip plot (CDP; depicted in red), coupled with alterations in the patterns of the total gamma-ray (GRT; shown in green) log. In the seismic amplitude section, within the pre-Alagoas interval, observe how the strata pinch-out against the high of the Economic Basement seismic horizon. Within the Camboriú Formation, pay attention to the lateral and vertical variations in amplitudes and seismic facies. The strong tilted reflections, corresponding to a variety of basaltic flows, progressively lose amplitude contrast with increasing depth. The location of the arbitrary seismic section is marked on the Base of Salt structural map (black line A-B).

| Facies | Facies Associations | Macroscopic Aspects & General Descriptions | | Processes & Environments | Lithologies | Average Porosity (%) and Standard Deviation | | Permeability (mD) Median |
|--------|------------------------------------------------------------------------------------------------------|--------------------------------------------|-----------------------------------------------------------------------------------------------------------------------------------------------------------------------------------------------------------------------------------------------------------------------------------------------------------------------------------------------------------------------|---------------------------------------------------------------------------------------------------------------------------------------------------------------------------------------------------------------------------------------------------------------------------------------------------------------------------------------------------------------------------------------------------|------------------------------------------------------------------------------------------------------------------------------------------------|---------------------------------------------|-----|--------------------------|
| | | | | | | | | |
| 1 | Carbonates with dissolution features/ karstified | | Primary depositional texture intensely modified by dissolution processes. Vugular porosity observed. | Dissolution associated with subaerial exposure and/or the action of rising fluids, resulting in features indicative of both meteoric and hypogenic karstification. | Crystalline carbonates, breccias, and mudstones. | 9.2 | 5.1 | 24.6 |
| 2 | Well-developed in-situ facies/ in-situ shrubs | | Well-developed calcitic shrubs exhibiting vertical to sub-vertical growth (>2mm). Dome-like or rounded geometries are frequently observed at the tops of these layers. | Inorganic mineralization and/or biologically influenced organomineralization (Dupraz et al., 2009) occurring in a high-alkalinity, moderate-to-high-energy subaqueous environment. | Carbonate aggregates. | 8.6 | 4.7 | 36 |
| 3 | Poorly-developed in-situ facies with shrub-like or crust-like textures/ in-situ incipient | | Poorly developed calcitic shrubs elements (<2mm), often associated with spherulites that can amalgamate to form millimetric crustiform levels. | Inorganic mineralization and/or biologically influenced organomineralization (Dupraz et al., 2009) in a moderate-energy, high-alkalinity subaqueous environment. | Carbonate aggregates. | 6.9 | 4.8 | 8 |
| 4 | Reworked Carbonates | | Grain-supported fabric with grain sizes varying from very coarse to coarse sand and medium to good selection. | Subaqueous traction flow in high-to-moderate-energy environments. | Intraclastic grainstones. | 11.1 | 5.2 | 12.3 |
| 5 | Reworked Carbonates with siliciclastic content | | Grain-supported fabric with the presence of more than 10% siliciclastic material, including igneous rocks clasts. | Subaqueous traction flow in high-to-moderate-energy environments and occasionally subaqueous gravitational flow. | Intraclastic grainstones. | 7.1 | 4.7 | 2 |
| 6 | Low-energy Facies Lithologies related to low-energy environments in general | | Spherulites in a clayey matrix of brown to greenish color. Thin siliciclastic material associated. | Inorganic mineralization and/or biologically influenced organomineralization (Dupraz et al., 2009) in a low-energy underwater environment, with high alkalinity and high concentrations of magnesium and silica. Settling in a low-energy underwater environment with possible biologically influenced organomineralization (Dupraz et al., 2009) and trapping and binding process (Black, 1993). | Spherulites, spherulitic claystones, mudstones to wackstones, laminites. | 4.8 | 3.6 | 1.2 |
| | | | Laminated structure formed by the intercalation of fine, light-colored to greenish sediments. Centimetric to decimetric levels of silica are also observed. | | | | | |
| 7 | Clayey Facies - with a significant presence of Mg-rich clay minerals - Carbonates with clay minerals | | Characterized by an abundance of preserved Mg-rich clay minerals in its internal structure. Also, there are other clay minerals and various fines present. Commonly referred to as partially dolomitized or silicified, and they typically exhibit no observable porosity. Differentiated from other low-energy facies by exhibiting specific petrophysical behavior. | Inorganic mineralization and/or biologically influenced organomineralization (Dupraz et al., 2009) in an underwater environment with low-to-very-low-energy, high alkalinity, and high magnesium concentration. | Rock from any of the mentioned lithologies with a significant presence of Mg-rich clay minerals, leading to the obliteration of rock porosity. | 4.1 | 3.2 | 0.16 |

Modified from Pedrinha et al. (2018), Pedrinha et al. (2024) and Pedrinha and Artagão (2024)

Petrophysical measurements

Table 1 – Summary chart of the seven facies associations identified within the study area and the Tupi Field. This classification is based on genetic, environmental, and reservoir quality considerations, following the nomenclature suggested by Pedrinha et al. (2018). The rock sample images represent wells examined in this study. Included are average effective porosity and median permeability values derived from basic laboratory petrophysical tests. Due to their specific petrophysical properties, carbonates with clay minerals have been distinctly grouped in the clayey facies association (7), setting them apart from other low-energy facies (6).

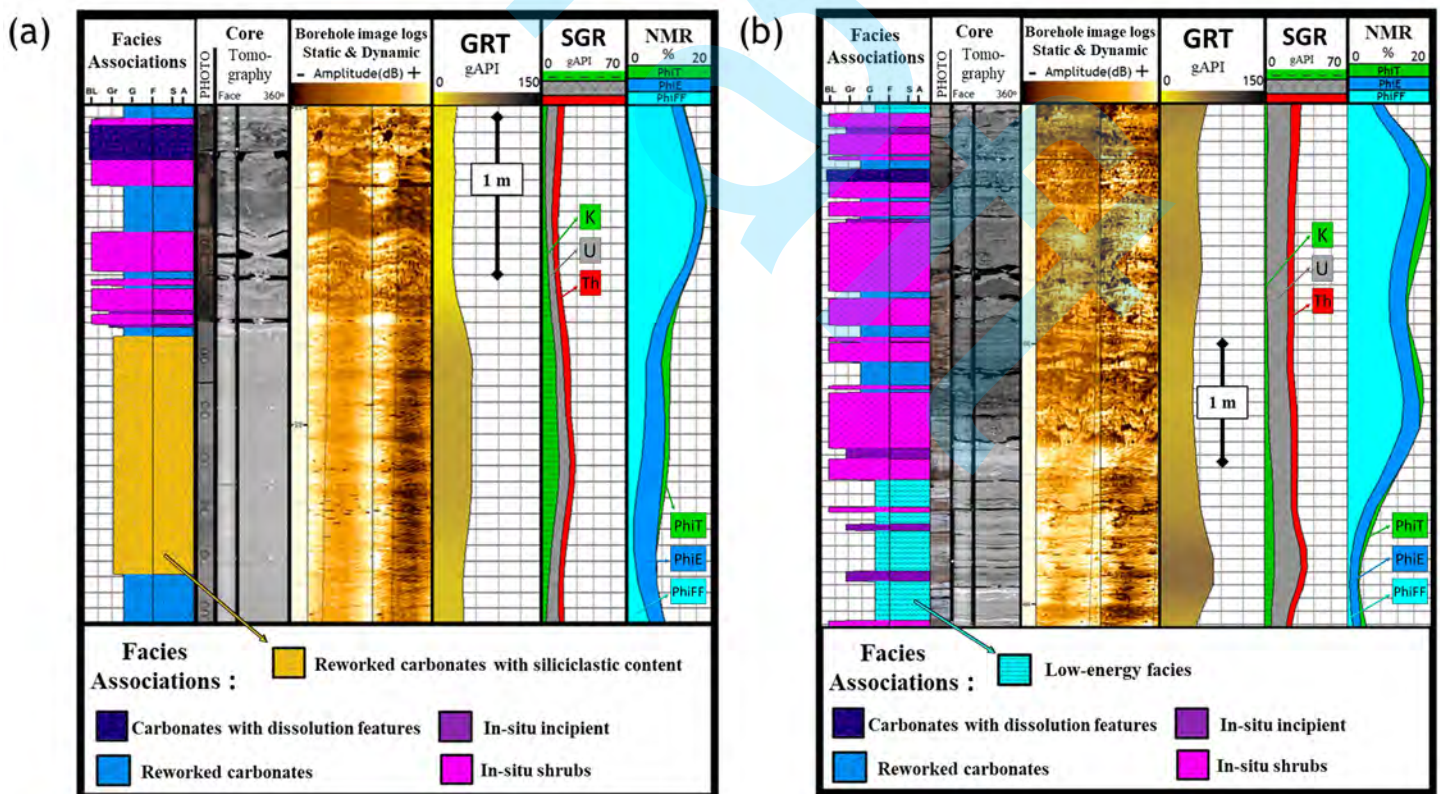


Figure 12 – The interpretation of carbonate facies associations concerning reworked, in-situ, low-energy and dissolution features using acoustic borehole image logs, complemented by rock core samples. Reworked facies with high siliciclastic content are differentiated from other reworked facies due to their elevated potassium (K) values (a), which are highlighted in green on the spectral gamma-ray [SGR (K.U.Th)] log. When compared to

adjacent intervals, the low-energy facies exhibit a more laminated pattern and higher values in the total gamma-ray (GRT) log (b). In the nuclear magnetic resonance (NMR) porosity logs, PhiT represents the total porosity (filled in green), PhiE represents the effective porosity (filled in blue), and PhiFF represents the free fluid porosity (filled in cyan).

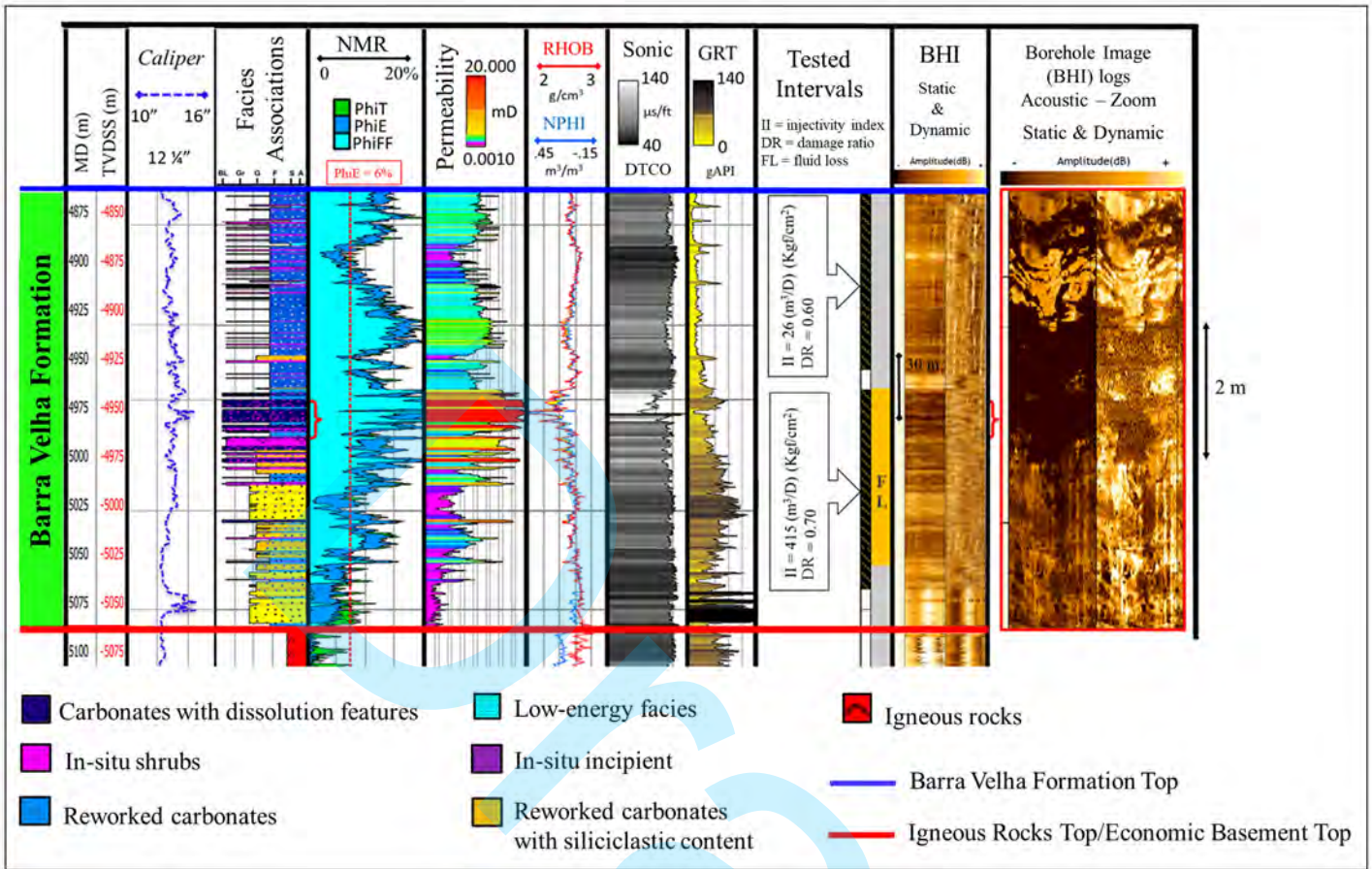


Figure 13 – Integrated analysis of carbonates with dissolution features, combining acoustic BHI logs, other electric logs, and results from fluid injectivity tests. In well P23 (Eastern Edge), a karstification feature can be observed (refer to the red brackets), which has a vertical extension of approximately two meters and can thus be interpreted as a cave (see the enlarged acoustic image for reference). The most porous and permeable interval is highlighted in the density (RHOB), neutrons (NPHI), and compressional sonic (DTCO; with a notably observed "bright spot") logs. In the acoustic image log, zones of low amplitude are emphasized in dark brown tones. During drilling, the tested interval containing the cave experienced significant fluid loss (FL) and displayed an injectivity index (II) approximately 15 times greater than that of the upper interval, which is composed of reworked carbonate facies with lesser associated dissolution.

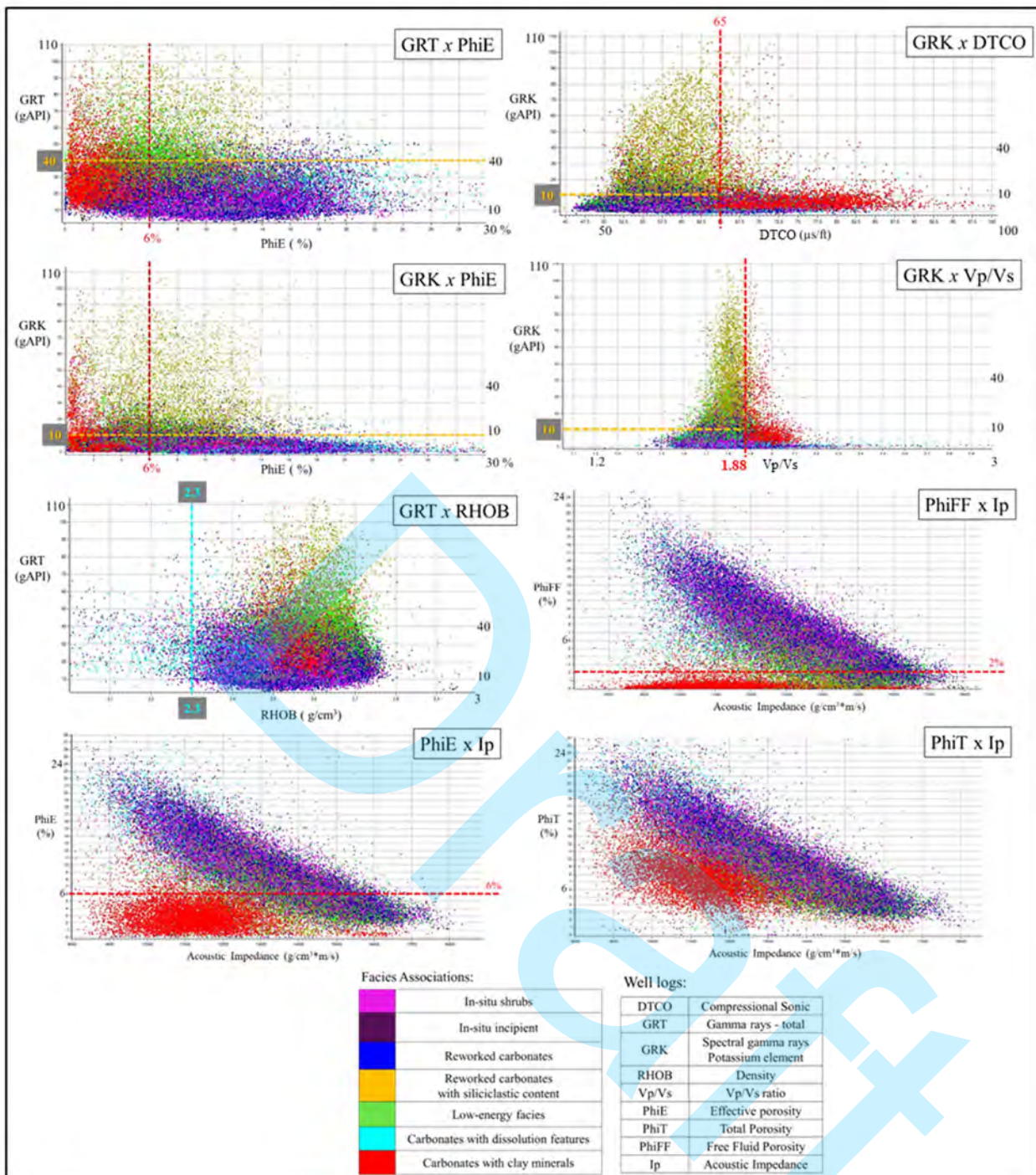


Figure 14 – Crossplot graphs analyzed during the feasibility studies, considering data from 44 wells with available borehole image logs for continuous facies interpretation. Despite a significant degree of overlap among the points forming the clusters of each facies association, distinctive trends are observed for carbonates with clay minerals, low-energy facies, reworked carbonates with siliciclastic content, and carbonates with dissolution features. Among these, carbonates with clay minerals stand out as the most distinct group, exhibiting the least overlap with other facies. This distinction is particularly evident in the GRK versus DTCO, GRK versus Vp/Vs, and Ip versus NMR porosity graphs. The in-situ and reworked carbonate facies do not exhibit specific clustering. The well-log scale corresponds to one sample every 0.24 cm. Exclusively for the crossplot graphs, to better signal the facies associations clusters, carbonates with clay minerals are highlighted in red, low-energy facies are represented in green, and carbonates with dissolution features are distinctly assigned in cyan.

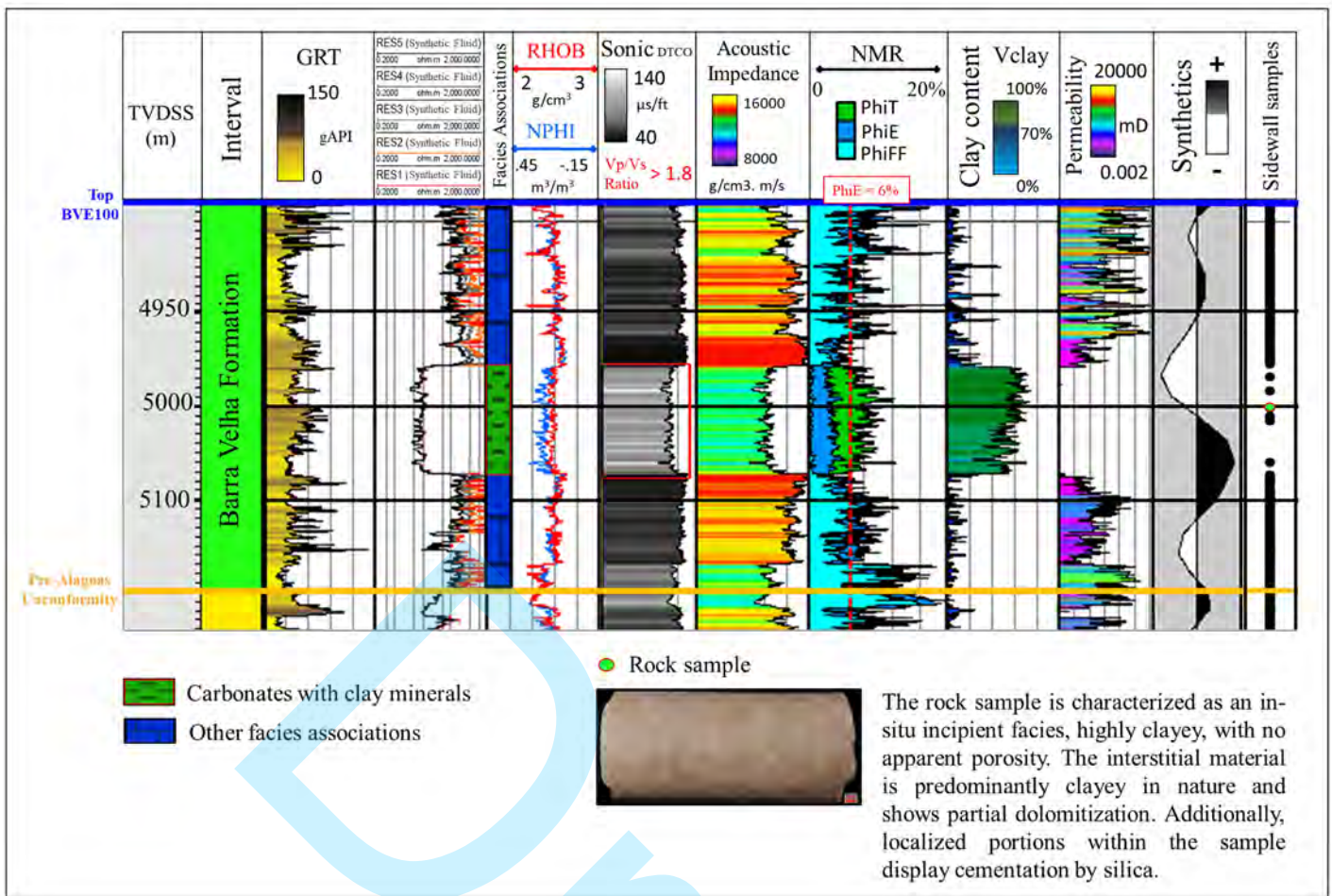


Figure 15 – Interpretation of the clayey intervals observed in well P6 (flank of the Main Structural High). The facies association referred to as carbonates with clay minerals, rich in magnesian clays, is primarily interpreted using the porosity and clay content profiles derived from nuclear magnetic resonance (NMR) logs, supported by descriptions of rock sidewall samples and cores. Even in the absence of a significant and diagnostic increase in gamma-ray log values, auxiliary discriminating responses can be identified in the resistivity (RES1 to RES5), density (RHOB), neutron (NPHI), acoustic impedance, and permeability logs (notable decreases). Typically, intervals of carbonates with clay minerals can also be demarcated by increased sonic travel times and Vp/Vs ratios. Depending on the thickness of the interval and the seismic resolution, the tops of these intervals can align with strong negative amplitude troughs (as illustrated in the synthetic seismogram).

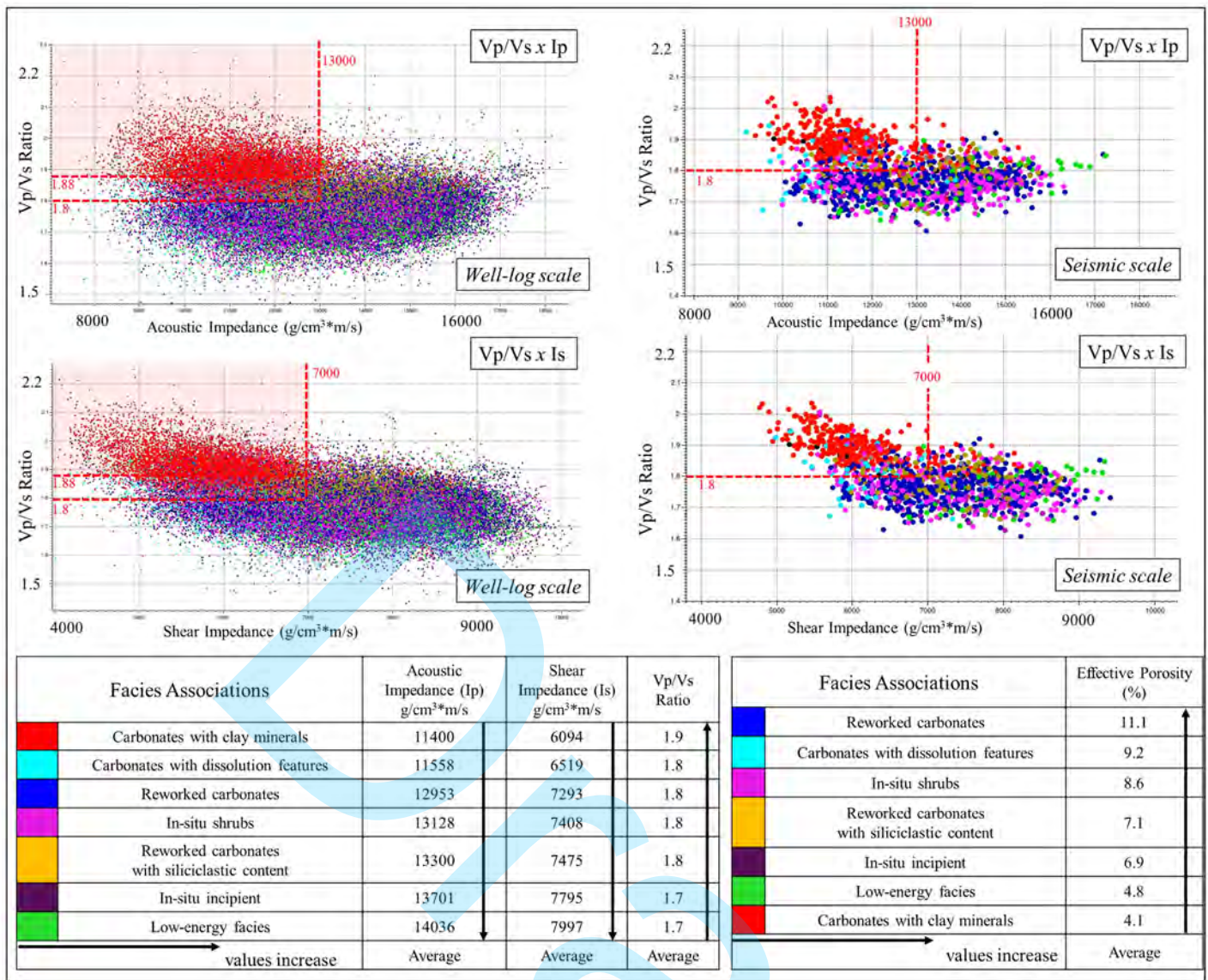


Figure 16 – Crossplot graphs and tables evaluated during the feasibility studies, involving 44 wells with available borehole image logs for continuous facies interpretation. Displays the relationships of $I_p \times I_s$, $I_p \times V_p/V_s$, and $I_s \times V_p/V_s$ in relation to the facies associations. The tables show average values of I_p , I_s , V_p/V_s , and effective porosity for each facies association. The carbonates with clay minerals exhibit a distinct clustering that sets them apart from other facies, notwithstanding the continued presence of overlapping samples, especially between the V_p/V_s values of 1.8 and 1.88. For the other facies, despite the lack of clear separation, there is a trend of increasing low-energy facies association towards the higher I_p and I_s values, and a relative increase of in-situ shrubs (less perceptible), reworked carbonates, and those with dissolution features (more perceptible) towards their respective lower values. In the tables, the average values of I_p , I_s , V_p/V_s , and effective porosity reinforce the trends observed in the graphs. The well-log scale corresponds to one sample every 0.24 cm, with 4 ms seismic scale, and 60-80 Hz high-cut filter. Exclusively for the crossplot graphs, to better signal the facies associations clusters, carbonates with clay minerals are highlighted in red, low-energy facies are represented in green, and carbonates with dissolution features are distinctly assigned in cyan.

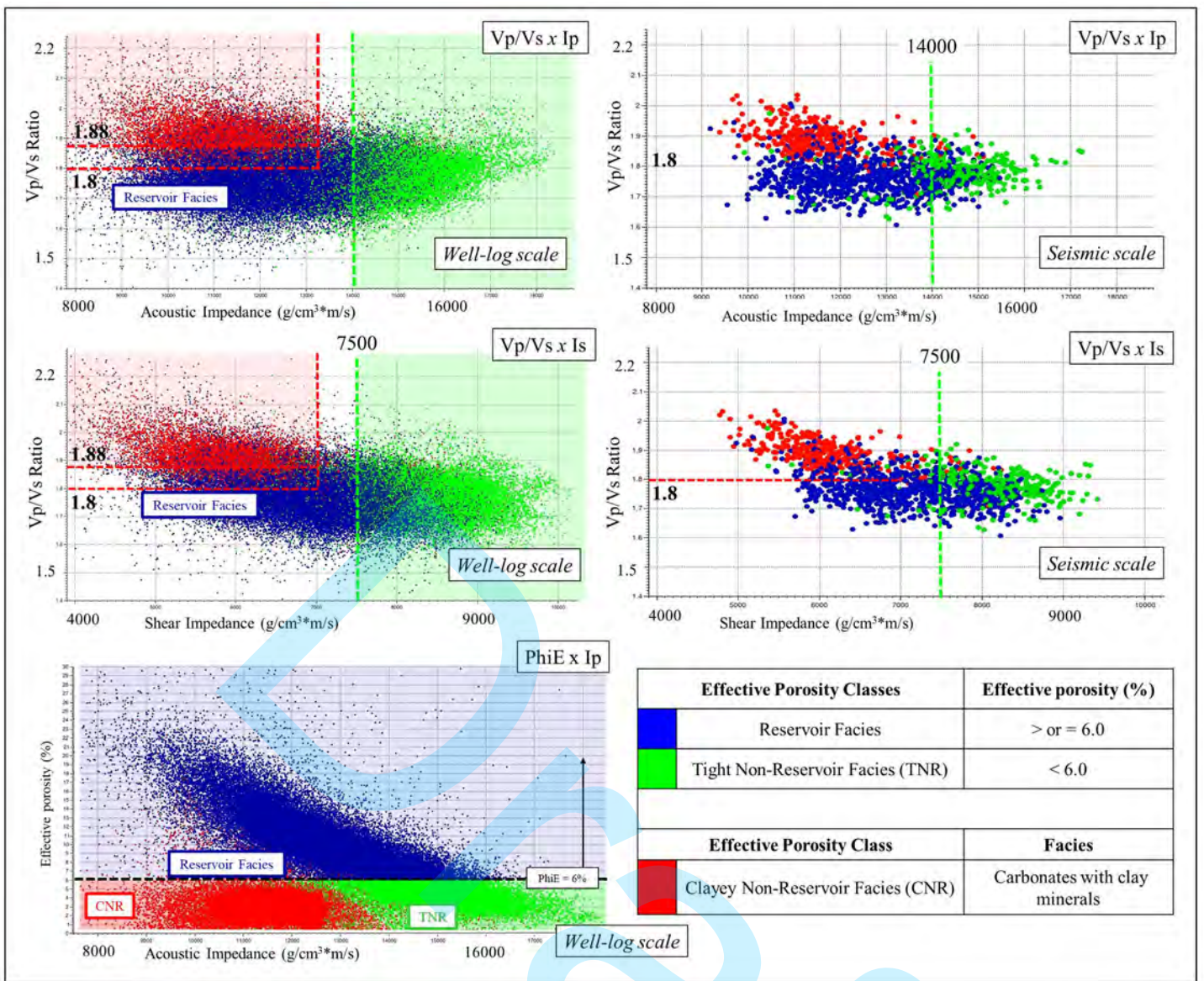


Figure 17 – Crossplot graphs and tables evaluated during the feasibility studies, involving 44 wells with available borehole image logs for continuous facies interpretation. The relationships of $I_p \times I_s$, $I_p \times V_p/V_s$, and $I_s \times V_p/V_s$ in association with effective porosity (ΦE) are displayed. The points on the graphs are colored according to their categorization into effective porosity classes. The 'Reservoir Facies' porosity class (blue shaded) consists of samples with a value of effective porosity of 6% or greater. For values below 6% effective porosity and higher impedance (green shaded), the 'Tight Non-Reservoir Facies' porosity class is distinguished. The carbonates with clay minerals are identified as 'Clayey Non-Reservoir Facies' regardless of the associated effective porosity value, though they are predominantly associated with ΦE values below 6% and high V_p/V_s values (red shaded), with few spurious samples deviating from this pattern. The well-log scale corresponds to one sample every 0.24 cm, with 4 ms seismic scale, and 60-80 Hz high-cut filter.

| Effective Porosity Classes (%) | | Acoustic Impedance Trends | Vp/Vs Ratio Trends | Facies Associations Predominance |
|--------------------------------|-----------------------------|------------------------------------------------|------------------------|------------------------------------------------------------------------------|
| | | Usual average values (g/cm ³ · m/s) | Usual average values | |
| PhiE ≥ 6% | Reservoir Facies | Low to moderate; < 14000 | Low to moderate; < 1.8 | In-situ shrubs, reworked carbonates and carbonates with dissolution features |
| PhiE < 6% | Clayey Non-Reservoir Facies | Low to moderate; < 14000 | High; > 1.8 | Carbonates with clay minerals |
| PhiE < 6% | Tight Non-Reservoir Facies | High; > 14000 | Low to moderate; < 1.8 | Low-energy facies |

Table 2 – Correlations between the predominance of certain facies associations (depositional and diagenetic), the effective porosity classes proposed in this study, and the average values trends of the acoustic impedance and Vp/Vs ratio seismic attributes. It's important to note that, although in-situ shrubs, reworked carbonates, and carbonates with dissolution features predominantly compose the Reservoir Facies porosity class, smaller proportions of in-situ incipient facies, reworked carbonates with siliciclastic content, and occasionally, low-energy facies may also be present. Similarly, while low-energy facies often dominate the Tight Non-Reservoir Facies class, significant proportions of in-situ incipient facies may occur, and other non-clayey facies can appear in subordinate proportions.

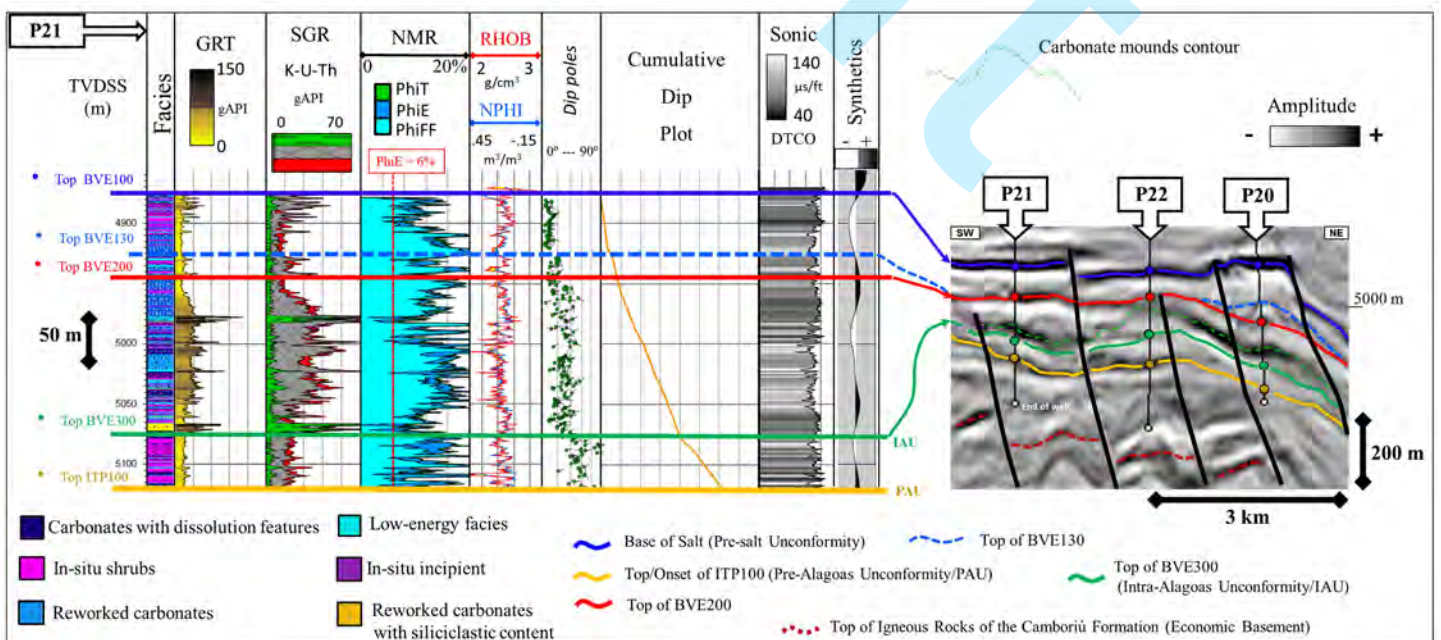


Figure 18 – Interpretation of the tops of the stratigraphic intervals BVE100, BVE130, BVE200, BVE300, and ITP100, based on well logs from well P21 and the seismic amplitude section intersecting wells P21, P22, and P23, on the Eastern Edge of the Tupi Field. Noteworthy are the differences in the trends of the gamma-ray logs, the behavior of the dip poles, and the flexion of the cumulative dip plot. This area is predominantly characterized by reworked facies (mostly) and in-situ shales, along with a higher occurrence of carbonates with dissolution features. The alternation of these facies, combined with varying levels of siliciclastic content and cave features, leads to changes in the typical seismic responses at the tops of the BVE200 (shifting from negative troughs to positive peaks in wells P21 and P22) and BVE300 (shifting from positive peaks to negative troughs in well P21). Additionally, mound-like seismic features, related to basement faults and highs, are observed in both the upper intervals (P20) and the BVE200 and BVE300 intervals (P21, P22, P20).

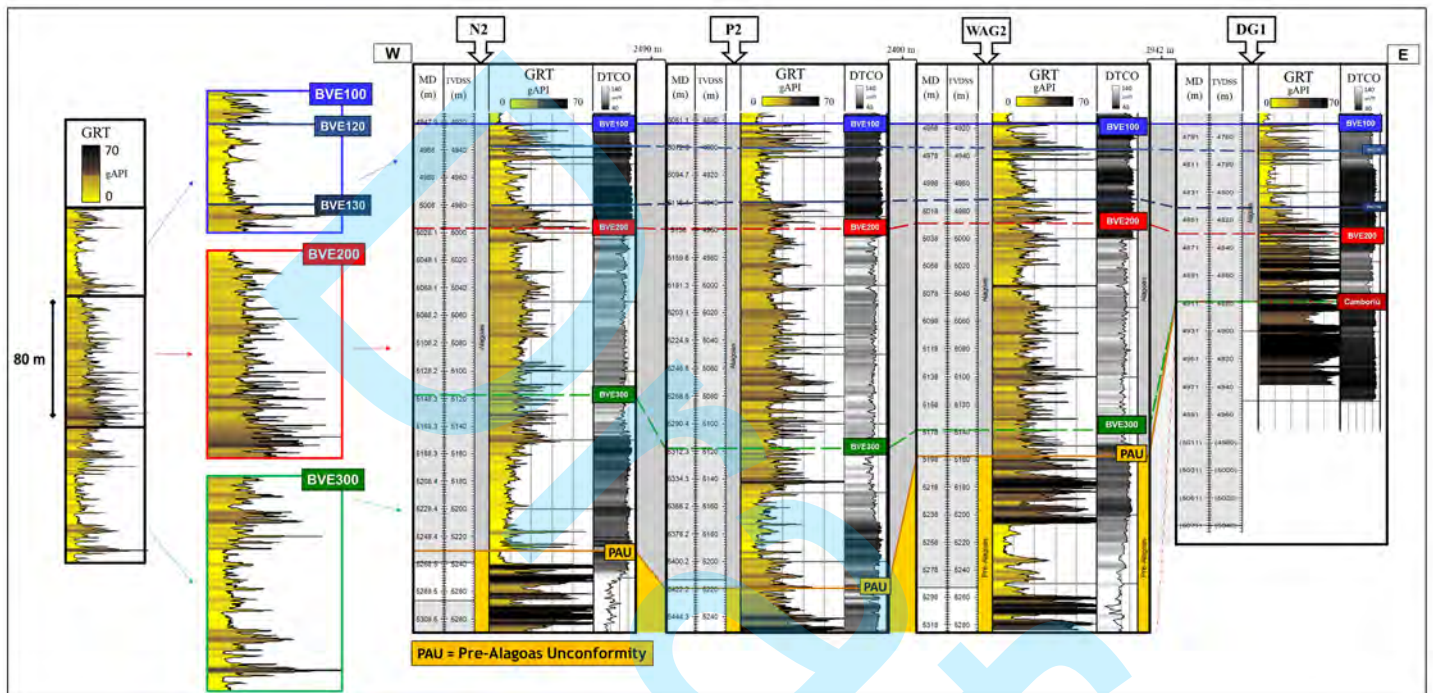


Figure 19 – Recognition of typical signatures in total gamma-ray (GRT) and compressional sonic (DTCCO) logs for intervals BVE100, BVE200, and BVE300. The stratigraphic correlation section between wells N2, P2, the water-alternating-gas injection well number 2 (WAG2), and the gas disposal well number 1 (DG1) exemplifies how these signatures have been identified, despite subtle variations, and tracked over long distances (kilometers) throughout the study area. Towards the structural highs, recurrent pinch-outs or thinning of the stratigraphic intervals BVE200 and BVE300 are observed in the wells, supported by seismic sections, and interpreted as a result of erosion or non-deposition. These intervals also exhibit significant thickness variations. In contrast, within the BVE100 interval, only minor thickness variations are noted. The basal limit of the Barra Velha Formation is defined by the Pre-Alagoas Unconformity (PAU) in wells N2, P2, and WAG2, and by the onset of the Camboriú Formation igneous rocks in well DG1.

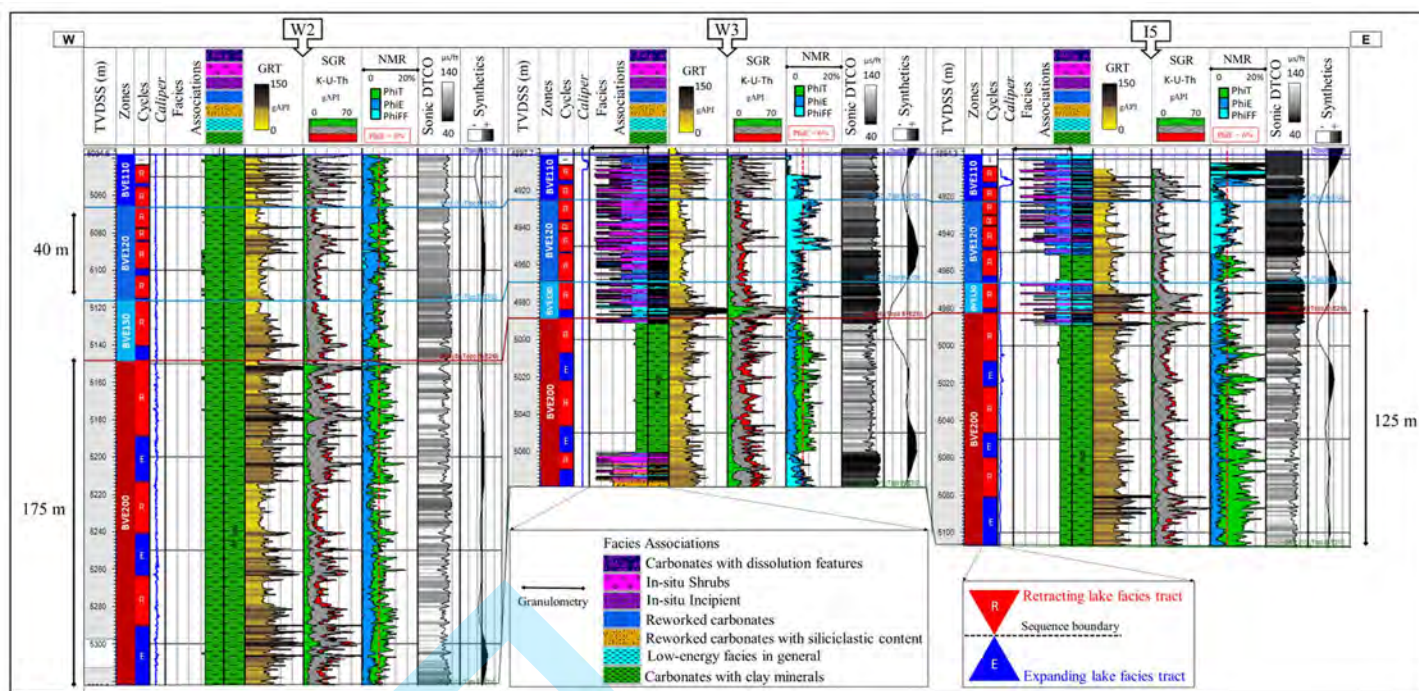


Figure 20 – Interpretation of the tops of the BVE110, BVE120, BVE130, and BVE200 stratigraphic intervals, in accordance with the tops of lake retraction cycles and lower GRT values, as observed in wells W2 (Regional Structural Low), and W3 and I5 (Western Edge). Notice the relative increase of low-energy facies within the BVE130, as well as the thickening and predominance of carbonates with clay minerals within the BVE200. Towards the structural lows, the notable occurrence of clayey facies boosts the average sonic log values, and the onset of the BVE200 interval is reflected as a negative amplitude trough in the synthetic seismograms. It is also noteworthy that the BVE200 exhibits moderate thickness variations, which in this wells correlation section, exceed 50 meters. Additionally, observe the lower amplitude contrasts in the W2 synthetic seismogram, a well where the displayed BVE100 and BVE200 intervals are entirely filled by carbonates with clay minerals.

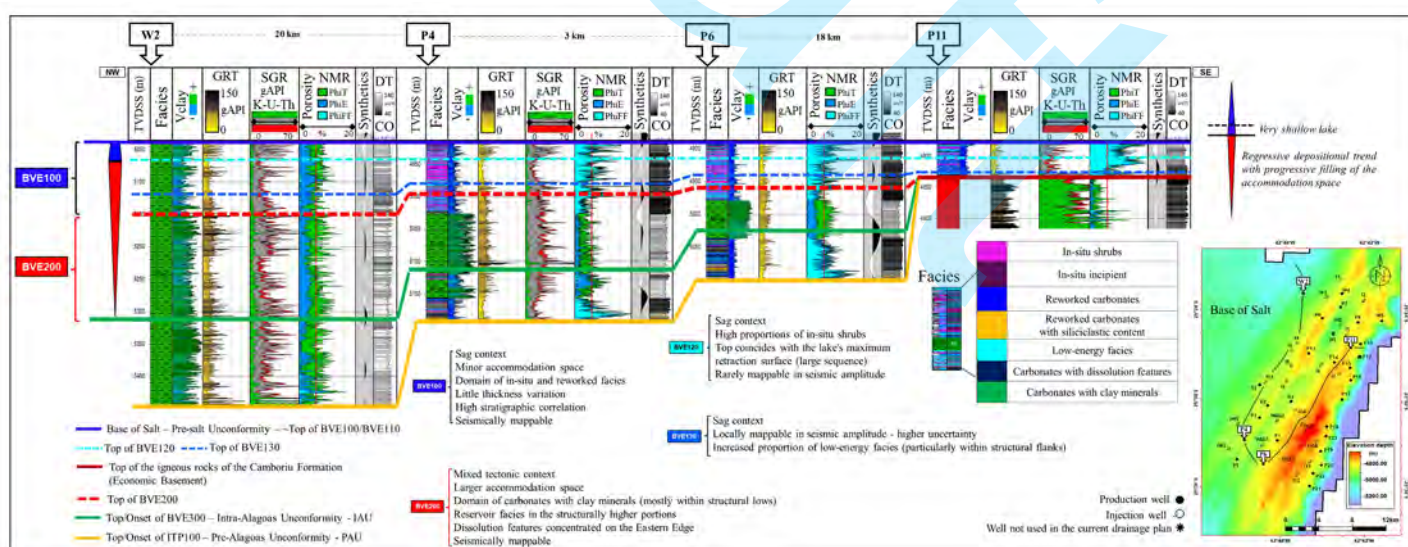


Figure 21 – This visualization encapsulates the results obtained from the stratigraphic zonation of the Barra Velha Formation, exemplified through a correlation section between wells W2 (Regional Structural Low), P4 and P6 (flanks of the Secondary and Main Structural Highs), and P11 (Main Structural High). The location of these wells is highlighted on the Base of Salt structural map (arbitrary section). The wells logs and annotations provide a synthesis of the main tectono-sedimentary, paleoenvironmental, and petrogeophysical characteristics observed, with a focus and detail on the upper portion of the Barra Velha Formation, zones BVE100 and

BVE200. Notice the pronounced increase in the carbonates with clay minerals and the decrease in free fluid porosities towards the structural lows. The degradation of reservoir quality is represented by the relative increase in the overall values of the compressional sonic (DTCO) and total and spectral gamma-ray (GRT and SGR) logs. The greatest thickness variations are observed in the lower intervals of the Barra Velha Formation (BVE300 and BVE200 zones), with progressive wedging of the packages towards the Main Structural High. In wells W2 and P6, the BVE200 zone is predominantly filled with Non-Reservoir Clayey Facies and its top is associated with a negative amplitude trough. Within the BVE100 interval, thickness variations are significantly reduced, with more noticeable variations observed in the BVE130 zone.

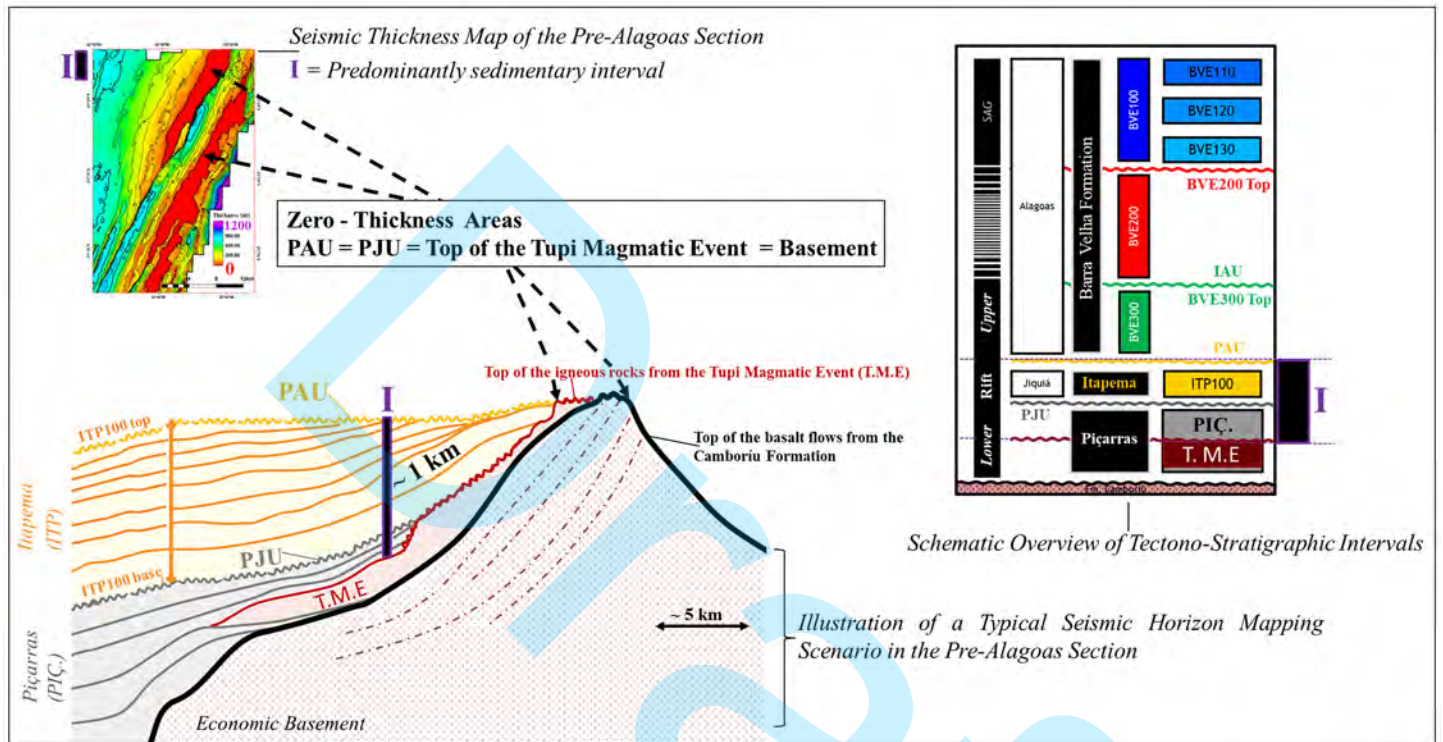


Figure 22 – Schematic chart illustrating key aspects of the stratigraphic interpretation of the pre-Alagoas section in the study area. On the upper left, a seismic thickness map of the pre-Alagoas section shows zero-thickness areas (depicted in red), where there is a coincidence of PAU, PJU, the top of the Tupi Magmatic Event (T.M.E.), and/or the Economic Basement within a single seismic reflection. The seismic thickness map highlights predominantly sedimentary intervals (I), with thickness measurements taken from the PAU (orange horizon) to the top of the T.M.E. (darker red surface), as depicted in the typical scenario illustration (bottom left).

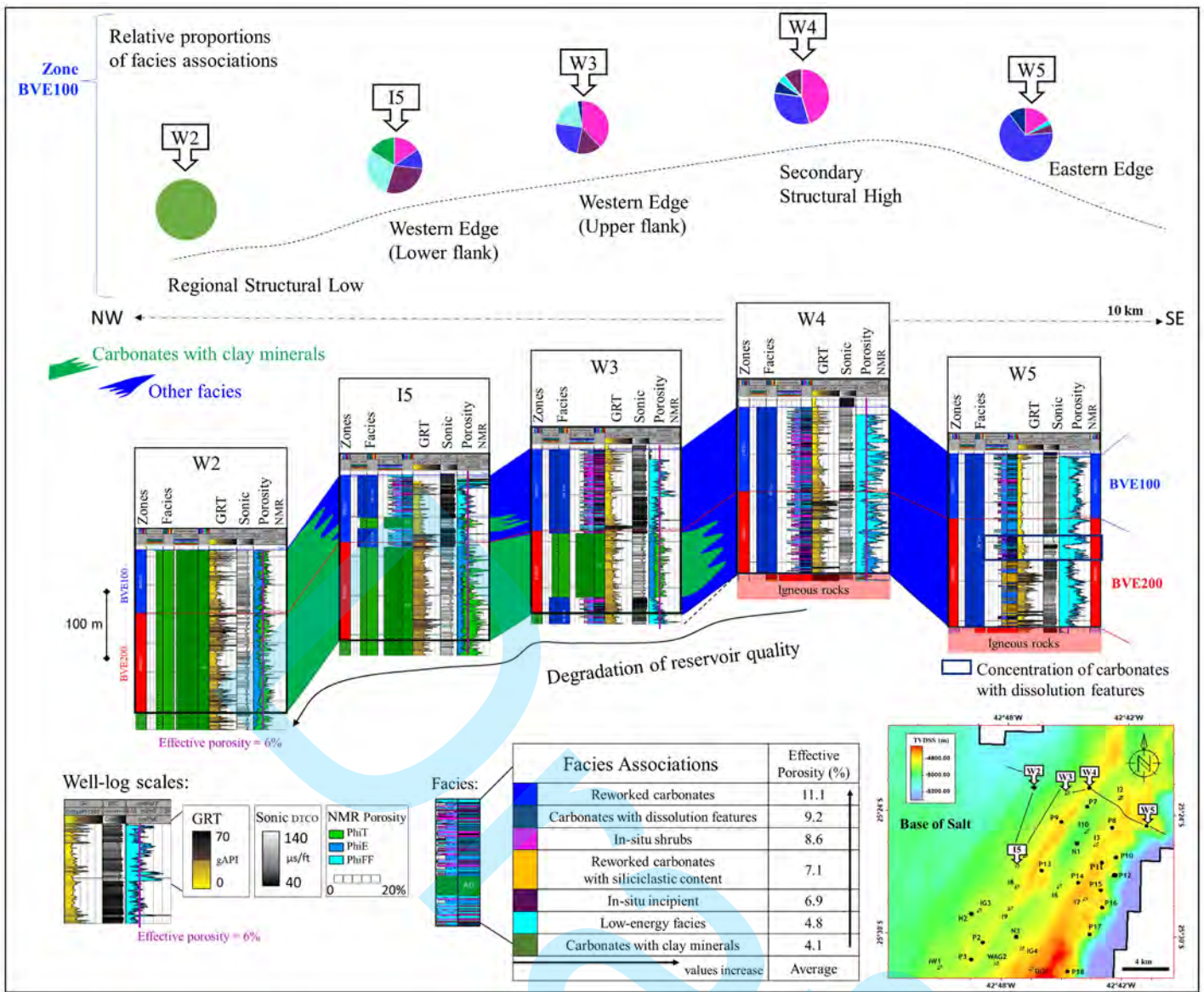


Figure 23 – Seismostratigraphic zoning and lateral variations of facies associations across the upper portion of the Barra Velha Formation, specifically the BVE100 and BVE200 zones, illustrated through a wells correlation section between W2 (Regional Structural Low), I5 and W3 (Western Edge), W4 (Secondary Structural High), and W5 (Eastern Edge). The locations of these wells are highlighted on the Base of Salt structural map (arbitrary section). The pie charts display the proportional distributions of facies associations within the BVE100 zone. Towards the Regional Structural Lows, reservoir quality declines, marked by an increase in low-energy facies and carbonates with clay minerals. This degradation is accompanied by relatively higher values in the sonic logs (notably for clayey facies) and total gamma-ray (GRT) logs (for both clayey and low-energy facies). Conversely, towards the Eastern Edge, there is a higher proportion of reworked facies and carbonates with dissolution features, reflecting increased depositional energy and relatively more favorable paleoenvironmental conditions for karstification. The effective and free-fluid porosity values observed in the logs align with the proportions of Reservoir, Non-reservoir Clayey, and Tight Facies. Within the BVE100 zone, the highest effective and free-fluid porosity values are associated with wells that have higher proportions of in-situ shrubs, reworked carbonates, and carbonates with dissolution features, combined with lower proportions of low-energy facies (e.g., W5 and W4).

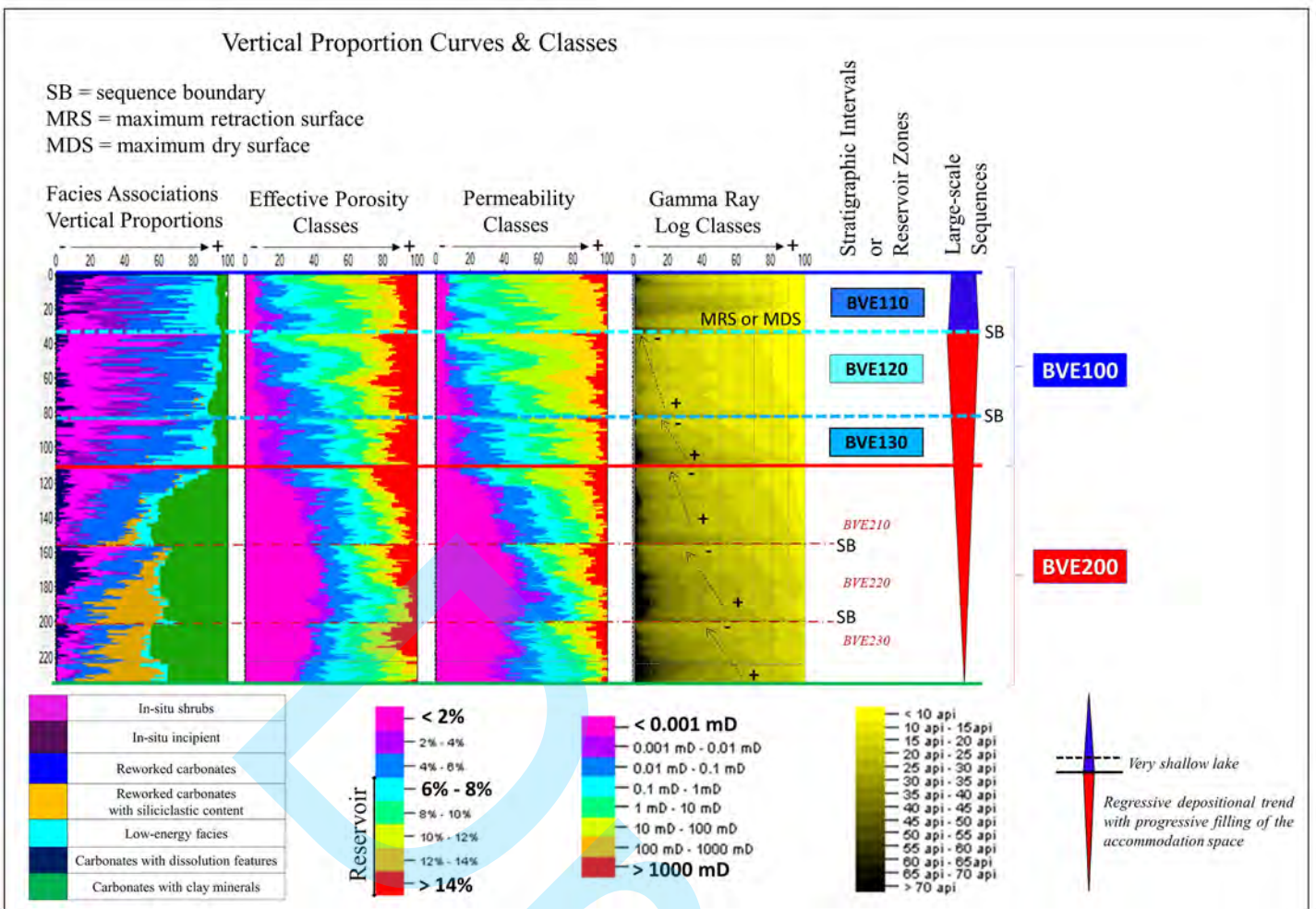


Figure 24 – Vertical stacking patterns of facies associations and corresponding distributions of effective porosity, permeability, and total gamma-ray log classes, associated with the stratigraphic zoning of the reservoir, paleoclimate fluctuations, and changes in the lake's paleogeography. The vertical facies proportions curves and the classes of porosity, permeability, and total gamma-ray logs were computed from the 51 wells studied, adopting 1 m layering. The arrows indicate a recurring decrease in gamma-ray values towards the tops of medium-scale sequences, culminating in very low values at the top of the BVE120 stratigraphic zone, which is marked in concordance with the maximum lake retraction/dry surface (MRS or MDS), along with a high proportion of in-situ shrubs. The vertex of the red triangle (refer to the base of the graphs; top of the BVE300 zone or IAU) signifies a larger accommodation space and a wetter depositional period, with enhanced preservation of clayey facies within the BVE200 zone. An increase in reworked carbonates with siliciclastic content is also noticeable towards the base of the BVE200 zone. These results mirror those found by Pedrinha et al. (2018) and depicted in Figure 4.

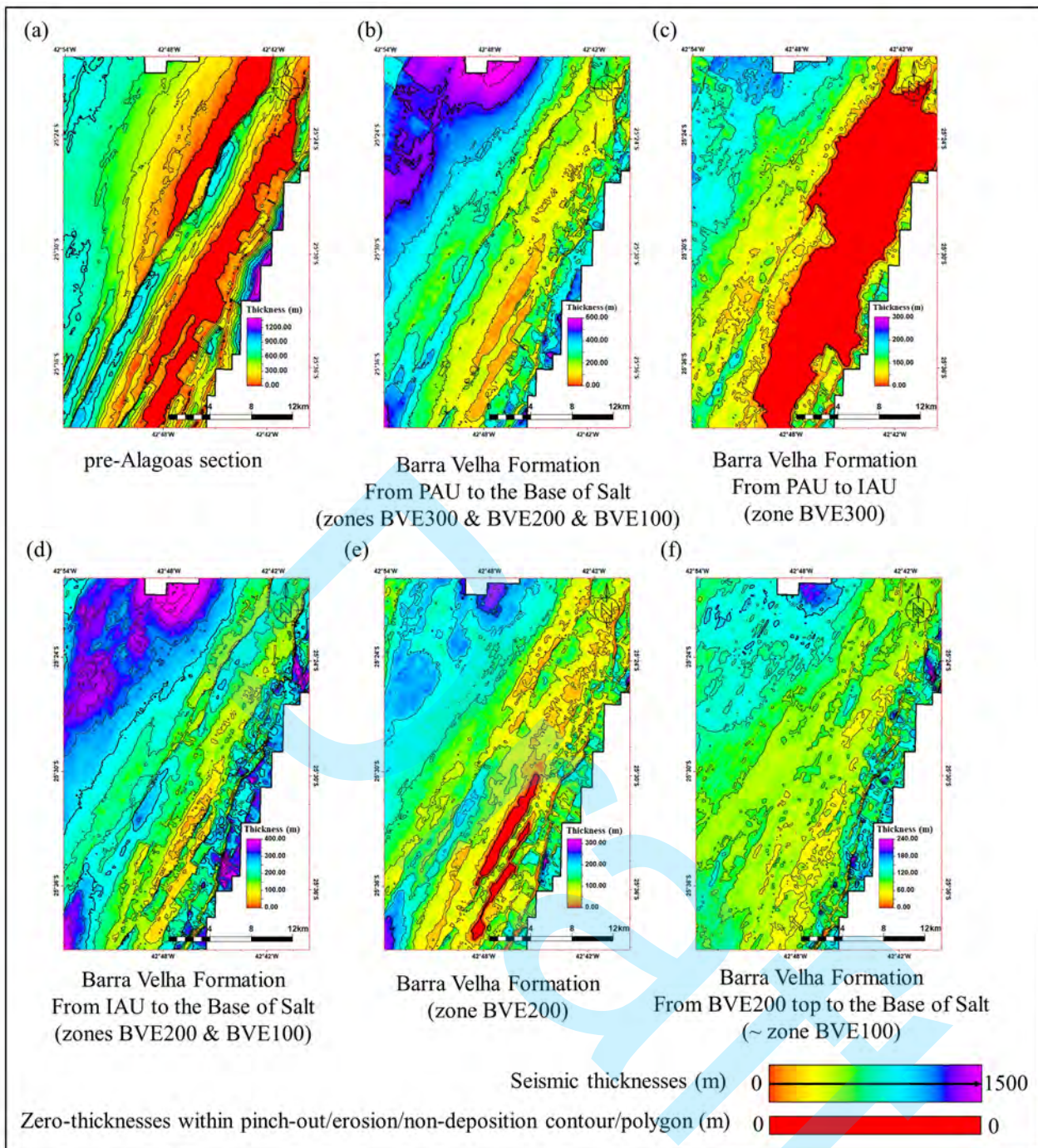


Figure 25 – Seismic thickness maps derived from detailed seismostratigraphic interpretation of the pre-Alagoas (a) and Alagoas (b) sections, showing the individual thicknesses of the BVE300, BVE200, and BVE100 zones, as well as the combined thicknesses of the BVE100 and BVE200 zones. Seismic thickness estimates were calculated based on differences between seismic horizons and are consistent with the thicknesses recorded in the wells. The pre-Alagoas section thickness shown in panel (a) was calculated from the top of the igneous rocks of the Tupi Magmatic Event to the Pre-Alagoas Unconformity (PAU). The BVE300 zone thickness (c) was computed from the PAU to the Intra-Alagoas Unconformity (IAU), while the combined seismic thickness of the BVE100 and BVE200 zones (d) was calculated from the IAU to the Base of Salt seismic horizon. The BVE200 zone thickness (e) was measured from the IAU to the Top of the BVE200 seismic horizon, and the BVE100 zone thickness (f) was calculated from the Top of the BVE200 seismic horizon to the Base of Salt. Areas with zero-thickness are highlighted in dark red, indicating locations where strata were either eroded or not deposited [(a), (c), and (e)]. Within the Regional Structural Lows, the seismic thickness of the Barra Velha Formation can reach

up to 600 meters [purple shades; (b)]. In contrast, minor thickness variations in the BVE100 zone suggest deposition under a predominantly sag tectonic context (f).

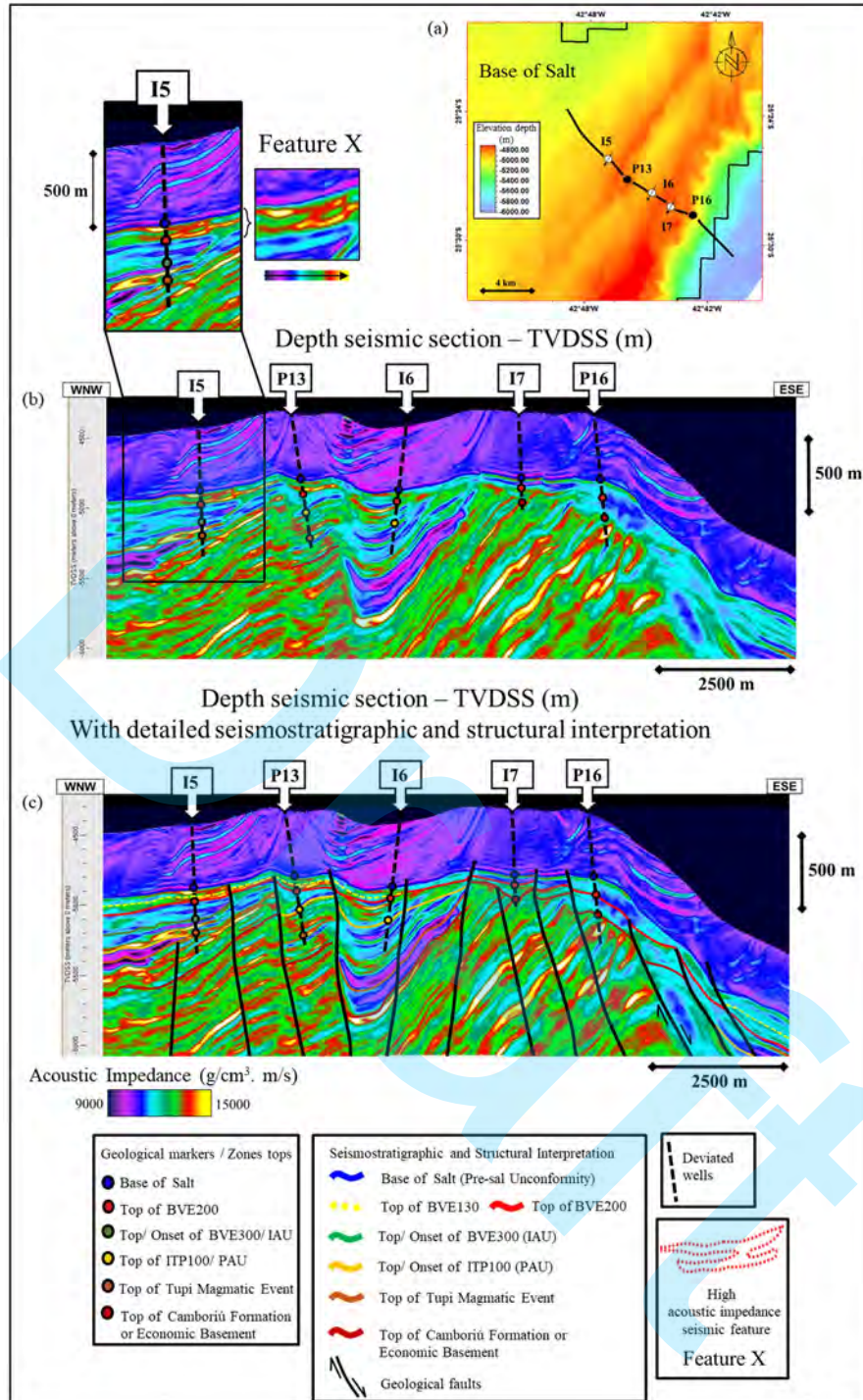


Figure 26 – Results of detailed seismostratigraphic and structural interpretation around wells I5 (Western Edge), P13 (Secondary Structural High), I6 (Relative Structural Low), I7 (Main Structural High), and P16 (Eastern Edge). The location of the arbitrary seismic section is depicted on the Base of Salt structural map (a). Variations in acoustic impedance can be associated with changes in reservoir properties and facies. For instance, the high acoustic impedance seismic feature crossed by well I5 (Feature X; represented by the dotted red geometry) suggests an increase in the Tight Non-Reservoir Facies, especially low-energy facies within the western flanks of the BVE100 zone. Feature X also assists in defining this zone (a). Within the interpreted seismic section (c), the tracing of the BVE130 subzone (indicated by the yellow dashed line) is notable across a significant part of the seismic section, including positions of the Secondary Structural High (well P13). Its interface signifies a relative increase in low-energy facies towards the basal part of the BVE100 zone. On the Eastern Edge, at well

P16, note the significant low acoustic impedance values that populate the interface between the BVE100 and BVE200 zones, as well as a large part of the BVE200 zone [(a) and (b)]. These exceedingly low values correlate with the increase in carbonates with dissolution features, amid the prevalence of reworked carbonates.

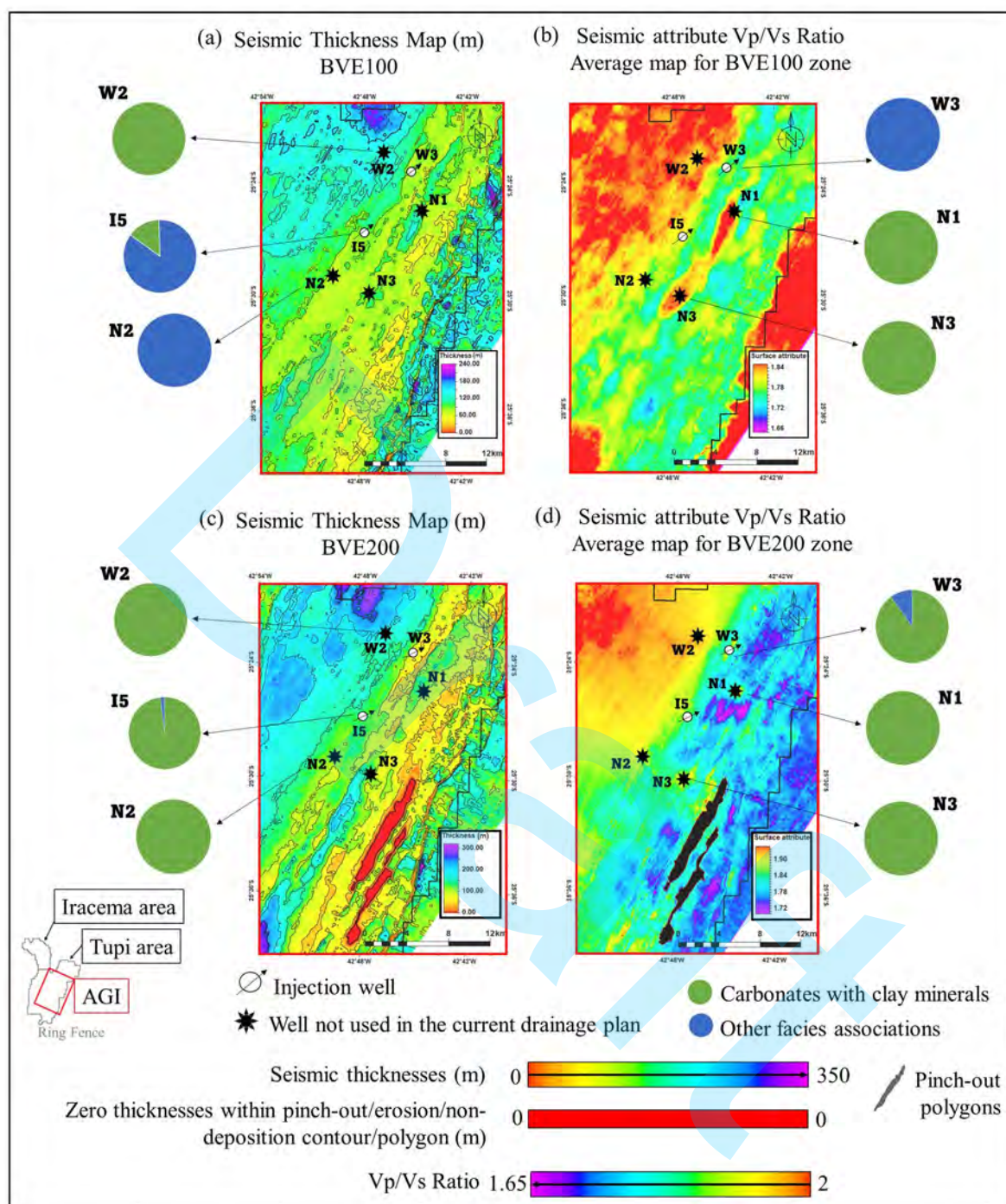


Figure 27 – Seismic thickness maps [(a) and (c)] and average Vp/Vs ratio values [(b) and (d)], calculated for the BVE100 and BVE200 zones. The areas of null thickness [in dark red tones; (c)] and the pinch-out polygons [in dark grey tones; (d)] indicate the highest portions of the Main Structural High where the strata of the BVE200 zone were either eroded or not deposited. The pie charts [(a), (b), (c) and (d)] inform the relative proportions of the Clayey Non-Reservoir Facies (in light green) compared to the other facies associations (in light blue), as interpreted in the wells W2 (Regional Structural Lows), W3, I5, N2 (Western Edge), N1, and N3 (Relative Structural Lows). In the Regional and Relative Structural Lows, the greatest thicknesses are associated with higher average values of the Vp/Vs ratio seismic attribute and elevated proportions of Clayey Non-Reservoir Facies. The wells drilled within these regions of high Vp/Vs ratio could not be used for injection or production

(wells not used in the current drainage plan). Towards the structural flanks, the V_p/V_s ratio average values decrease, while the proportions of other non-clayey facies associations increase. N2 was not incorporated into the drainage plan due to operational issues.

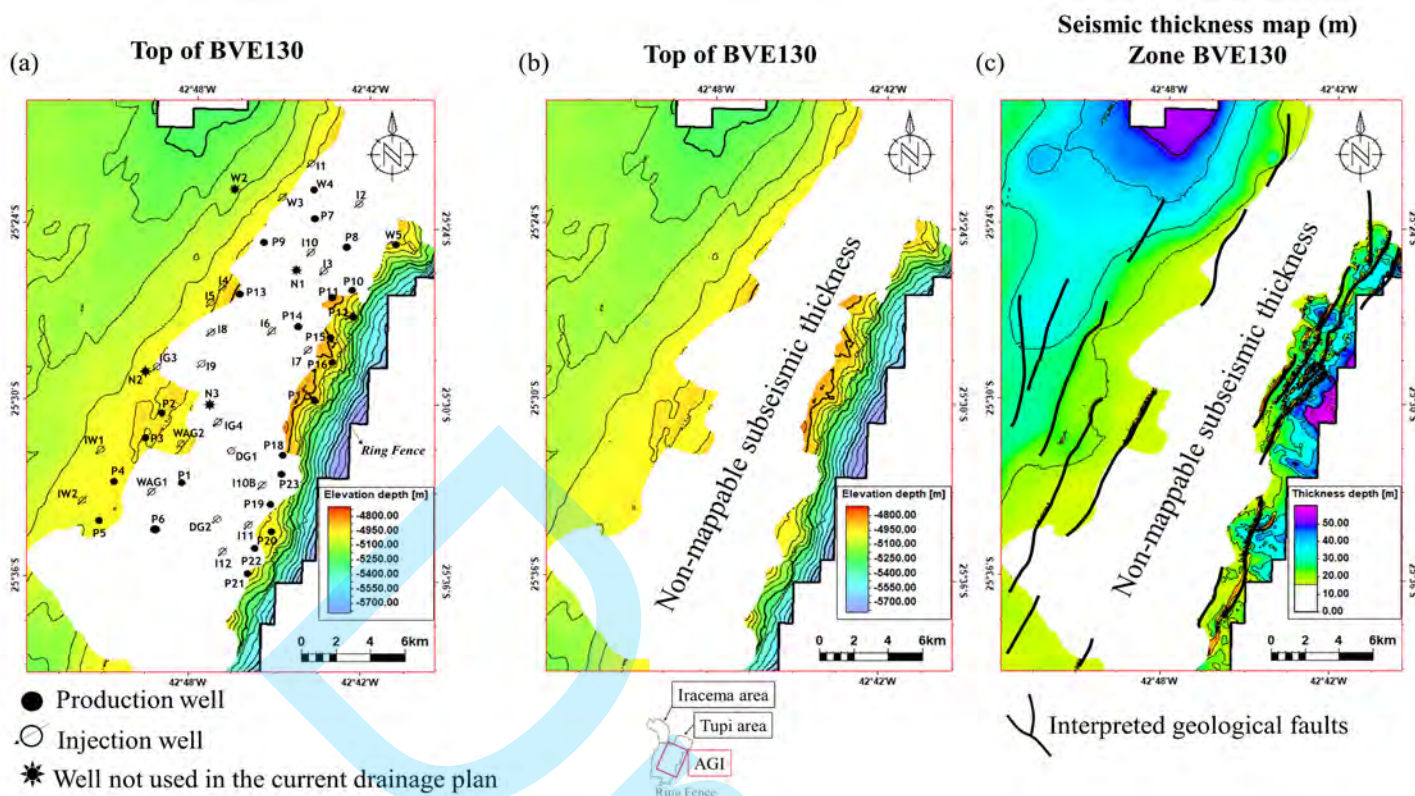


Figure 28 – Structural [(a) and (b)] and seismic thickness maps (c), derived from the high-resolution seismostratigraphic mapping and detailed structural interpretation of the BVE130 zone (or subzone/stratigraphic interval). The maps highlight the locations of the drilled wells (a), the polygon of subseismic thicknesses [(a), (b), and (c)], and the representation of geological faults (c), which are primarily normal faults with oblique slip, oriented predominantly NE-SW. The polygon of subseismic thicknesses [in white; (a), (b), and (c)] signifies the regions where the sediments of the BVE130 zone were eroded, not deposited, or have a thickness below the vertical resolution of the available seismic data, even those seismic attributes with higher frequency content, such as acoustic impedance and Iterdec. The interpretations are clipped within the boundary of the Tupi Field's ring fence, indicating that the interpretations are confined to the area with improved seismic coverage.

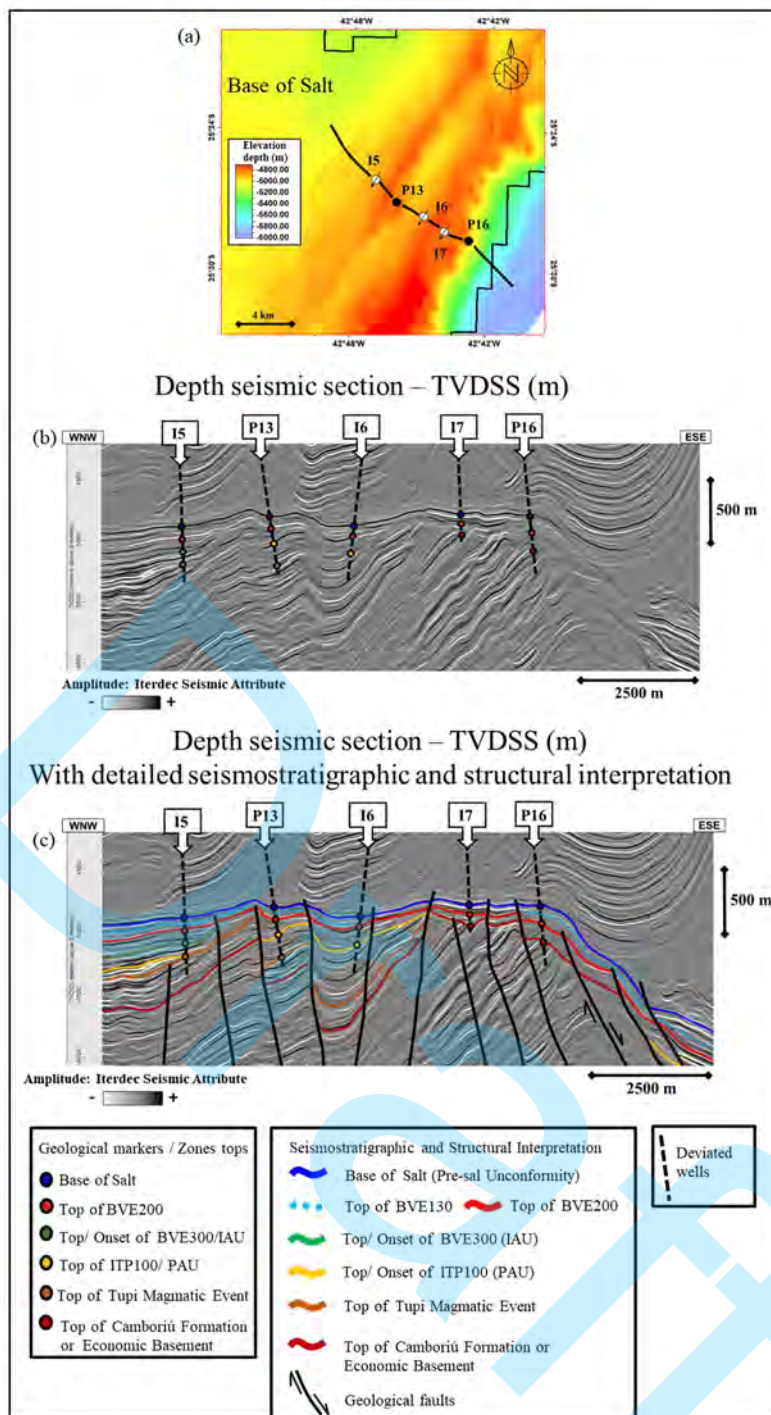


Figure 29 – Results of detailed seismostratigraphic and structural interpretation around wells I5 (Western Edge), P13 (Secondary Structural High), I6 (Relative Structural Low), I7 (Main Structural High), and P16 (Eastern Edge). The location of the arbitrary seismic section is depicted on the Base of Salt structural map (a). The high-frequency seismic attribute, Iterdec, due to its superior vertical seismic resolution, displays a larger number of seismic reflections, which can be associated with the tops of large and medium-scale stratigraphic sequence boundaries (b). In the interpreted seismic section (c), note the tracking of the BVE130 zone (light blue dashed line) throughout almost the entire seismic section, including positions of the Secondary Structural High (well P13) and the Eastern Edge (well P16), a feat not achievable using the other seismic attributes with a narrower frequency range. Additionally, observe that part of the faults crossing the BVE100 stratigraphic interval are restricted to its most basal portion, terminating within the BVE130 subzone [e.g., geological faults between wells I5 and P13; (b)].

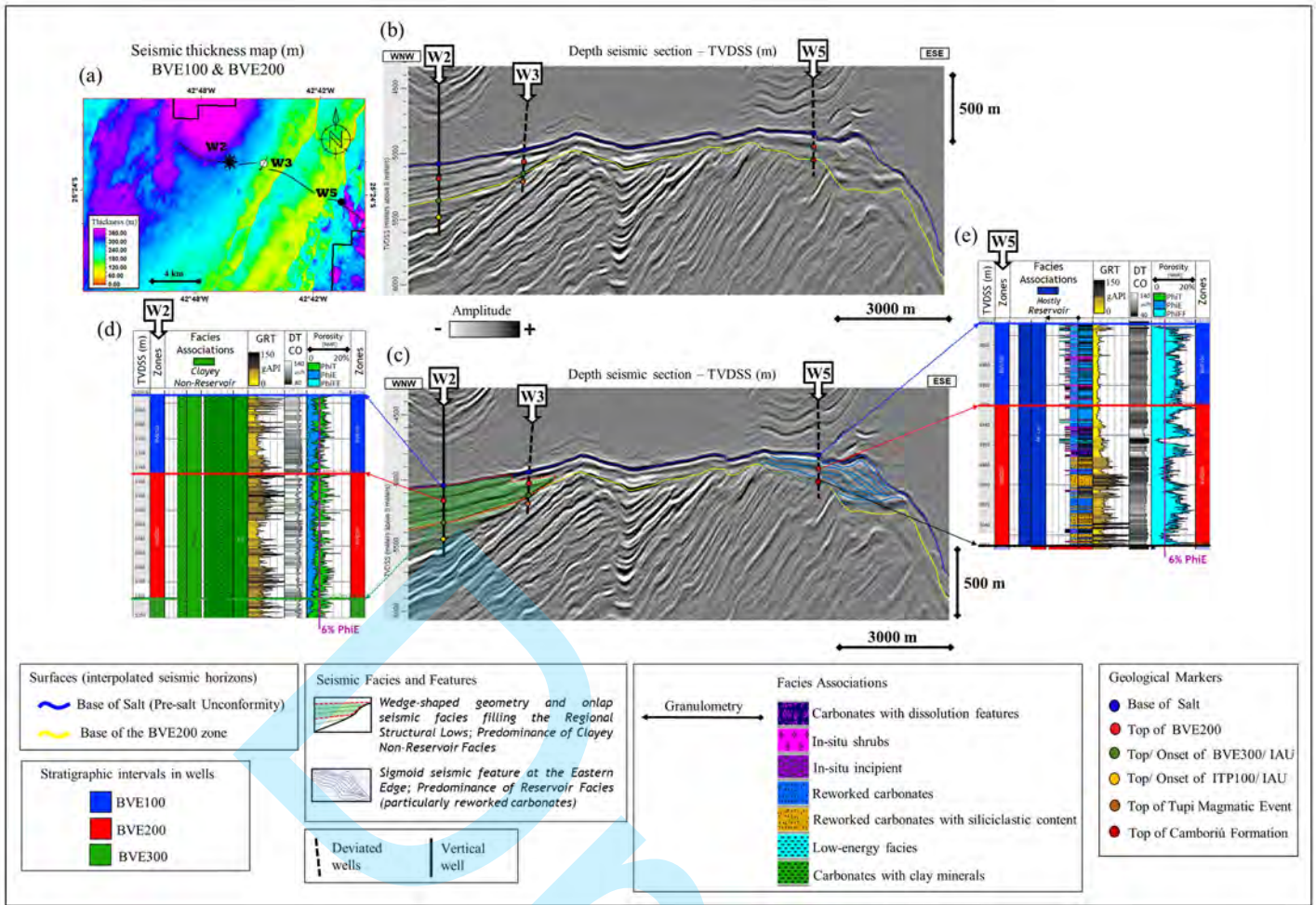


Figure 30 – Results of seismostratigraphic, facies, and seismic features interpretations around wells W2, W3, and W5. The location of the arbitrary seismic section is displayed on the seismic thickness map of the ‘BVE100 & BVE200’ package, calculated from the Top of the BVE200 seismic horizon to the Base of Salt (a). The greatest seismic thicknesses of the package [blue and purple tones; (a)] occur in regions influenced by plane-parallel seismic facies and onlap filling of the Regional Structural Lows [wells W2 and W3; (b), (c), and (d)] and sigmoid seismic features observed on the Eastern Edge [well W5; (b), (c), and (e)]. Both sediment thickening and seismic features are related to low to moderate amplitude values and high total porosity values. In the Regional Structural Lows, carbonate with clay minerals, the Clayey Non-Reservoir Facies [well W2; (d)], prevail, while reworked carbonates, the Reservoir Facies [well W5; (e)], dominate in the structurally higher portions of the Eastern Edge.

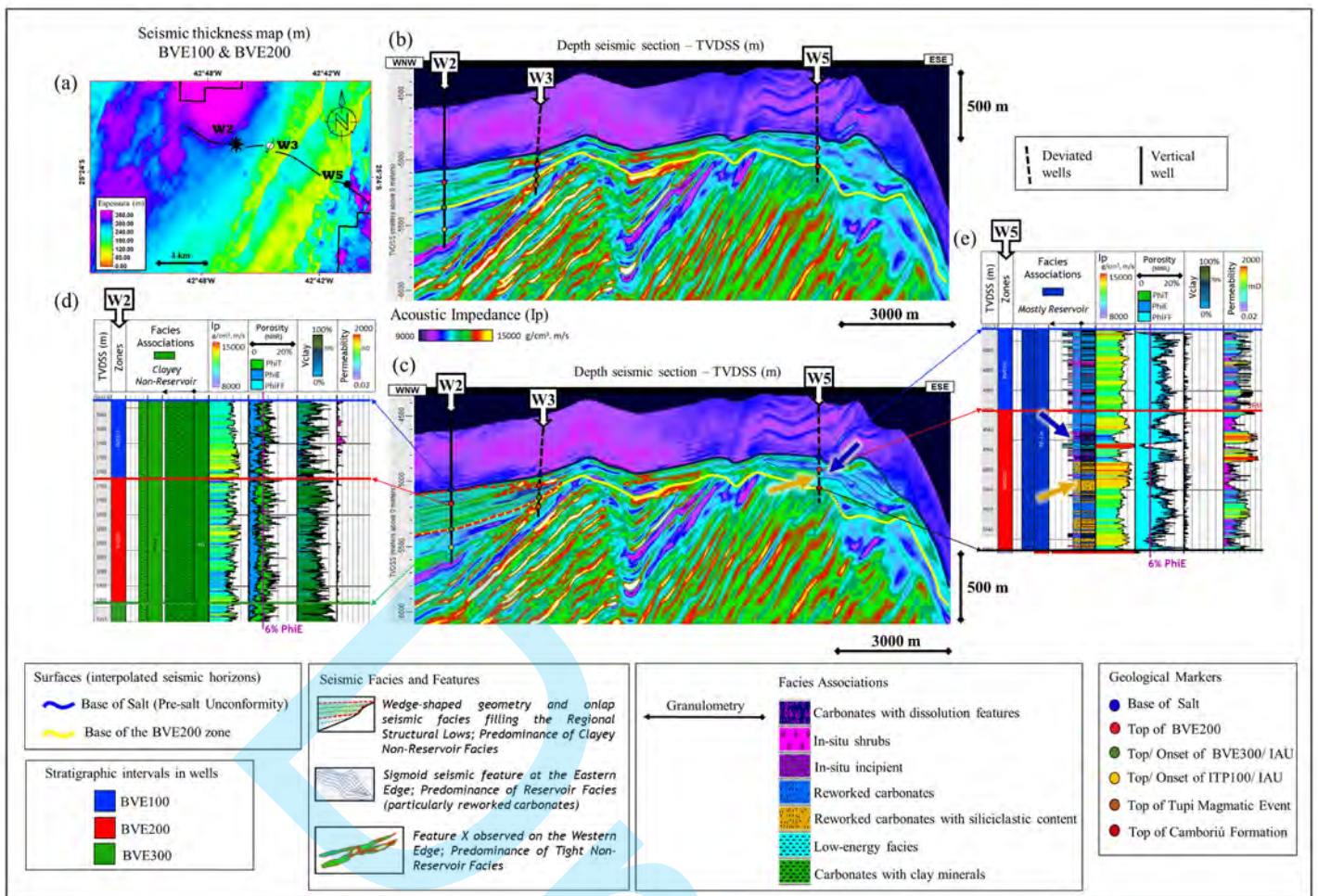


Figure 31 – Results of the seismostratigraphic, facies, and seismic features interpretations around wells W2, W3, and W5. The location of the arbitrary seismic section is displayed on the seismic thickness map of the "BVE100 & BVE200" package (a). The greatest seismic thicknesses of the package [blue and purple tones; (a)] occur in regions influenced by plane-parallel seismic facies and onlap filling of the Regional Structural Lows [wells W2 and W3; (b), (c), and (d)] and sigmoid seismic features observed on the Eastern Edge [well W5; (b), (c), and (e)]. Both sediment thickening and seismic features are related to low to moderate acoustic impedance values and high total porosity values. In the Regional Structural Lows, carbonate with clay minerals [well W2; (d)] prevail, while in the structurally higher portions of the Eastern Edge, reworked carbonates [well W5; (e)] dominate. On the Western Edge, within the BVE100 zone, note that the updip limit of the Clayey Non-Reservoir Facies is signaled by the high acoustic impedance anomaly crossed by well W3 [Feature X; (b) and (c)]. On the Eastern Edge, within the sigmoid feature, observe how the lowest values of acoustic impedance can be qualitatively associated with the carbonates with dissolution features [blue arrow; (c) and (e)], while the highest values of acoustic impedance might be related to an increase in reworked carbonates with siliciclastic content at the base of the seismic feature [orange arrow; (c) and (e)].

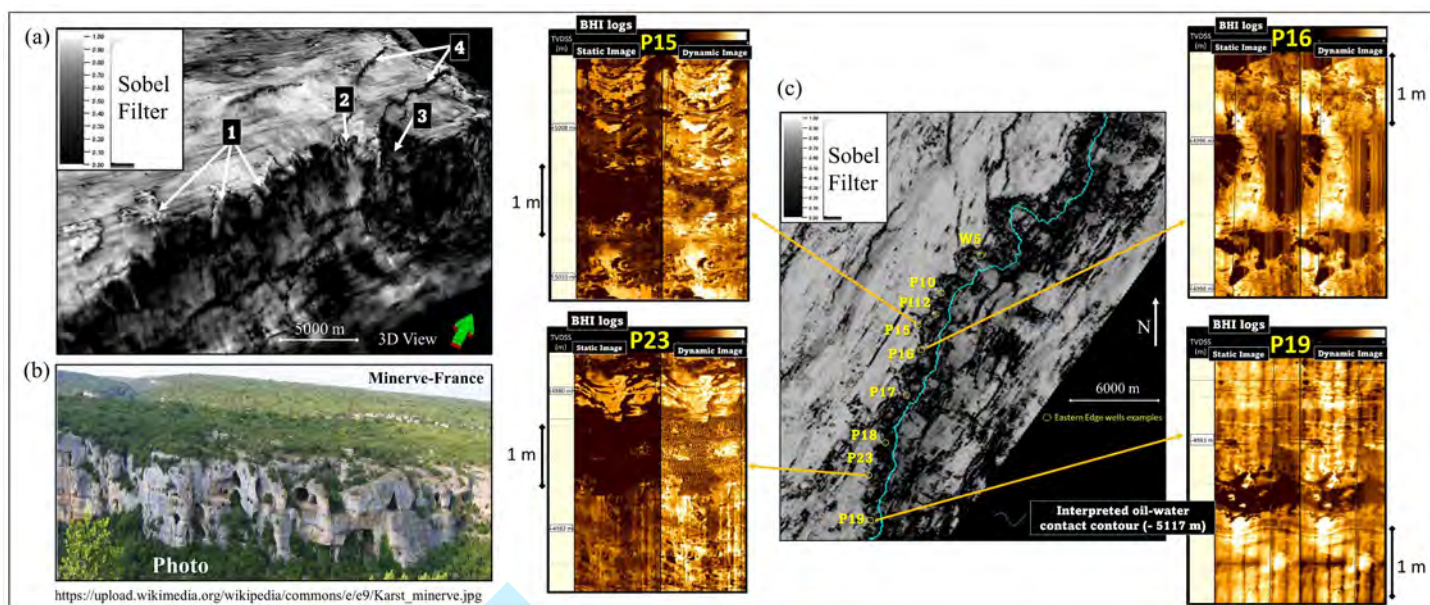


Figure 32 – Different views of the Sobel Filter geometric seismic attribute support the interpretation that the Eastern Edge may be a high-energy, steep, reworked structural edge, under the strong influence of fluid percolation and circulation (e.g., meteoric waters). In the 3D view of the attribute extracted on the Base of Salt seismic horizon [horizon slice; (a)], various rugosities, distorted, irregular, and even "dendritic" seismic features are observed. These resemble the geological features of the karst landscape in Minerve, France [photo; (b)]. The term "dendritic" refers to the tree-branch-like appearance of grooves, potentially created by water as it percolated through the porous rock [1; (a)]. Wells that intersected these seismic features exhibit a high relative proportion of reworked carbonates and carbonates with dissolution features in the BVE100 and BVE200 zones. The borehole image (BHI) logs from these wells clearly display levels of disseminated vugular porosity (primarily within the BVE100 zone), intense dissolution intervals, and even caves (more common within the BVE200 zone), exemplified in the BHI logs of wells P15, P16, P19, and P23 [in larger darker brown tones; (c)]. In the 2D view, the average map calculated for the BVE200 zone shows an increased accumulation of distorted seismic features near the estimated oil-water contact [contour in cyan; (c)]. Besides the karstic connotations, the Sobel Filter seismic attribute suggests other geological and physiographic elements, such as sediment slumping features [2; (a)], collapse of the carbonate platform margin features [3; (a)], and geological faults [4; (a)]. In the BHI logs of the example wells, the static images are positioned on the left track, and the dynamic images on the right (c).

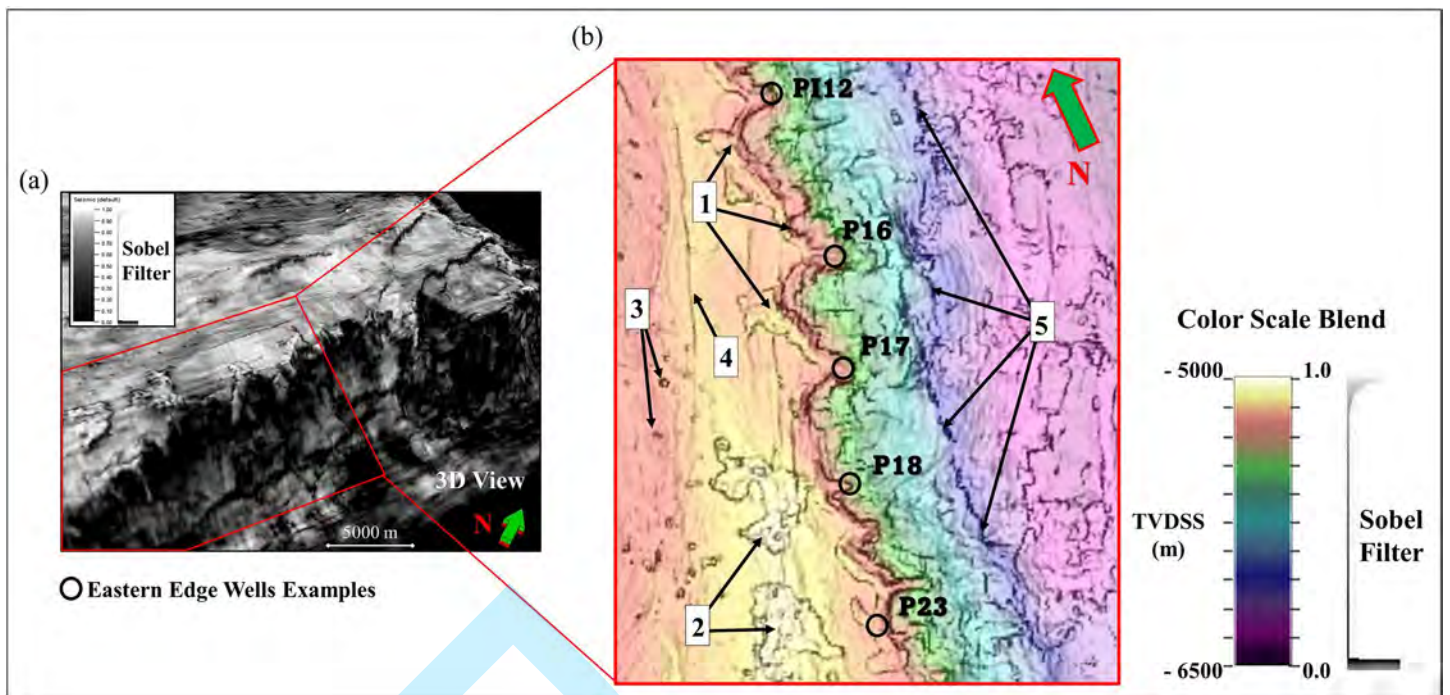


Figure 33 – A three-dimensional view of the extraction of the Sobel Filter seismic attribute on the Base of Salt seismic horizon [horizon slice; (a)] is paired with a 2D zoomed view of the blend between the Sobel Filter seismic attribute and the topography of the Base of Salt (b). The 2D zoomed view (b) emphasizes various seismic features [(1, 2, 3, 4 and 5); (b)] that form the structure and karstified physiography of the Eastern Edge. This includes multiple rugosities, distorted, irregular, and "dendritic" seismic features [1 and 2; (b)], as well as several circular marks potentially indicating dolines, sinkholes, or concretions [3; (b)]. These features can all be related to the formation processes of either epigenic or hypogenic karsts. Geological faults [4 and 5; (b)] are also interpreted, including a subset that separates the Eastern Edge from the Regional Structural Lows [depicted in shades of pink and purple; 5; (b)]. Wells P12, P16, P17, P18 and P23 (b) intersected high relative proportions of carbonates with dissolution features in the BVE100 (mainly disseminated levels) and BVE200 zones (including several caves), providing evidence to support these interpretations.

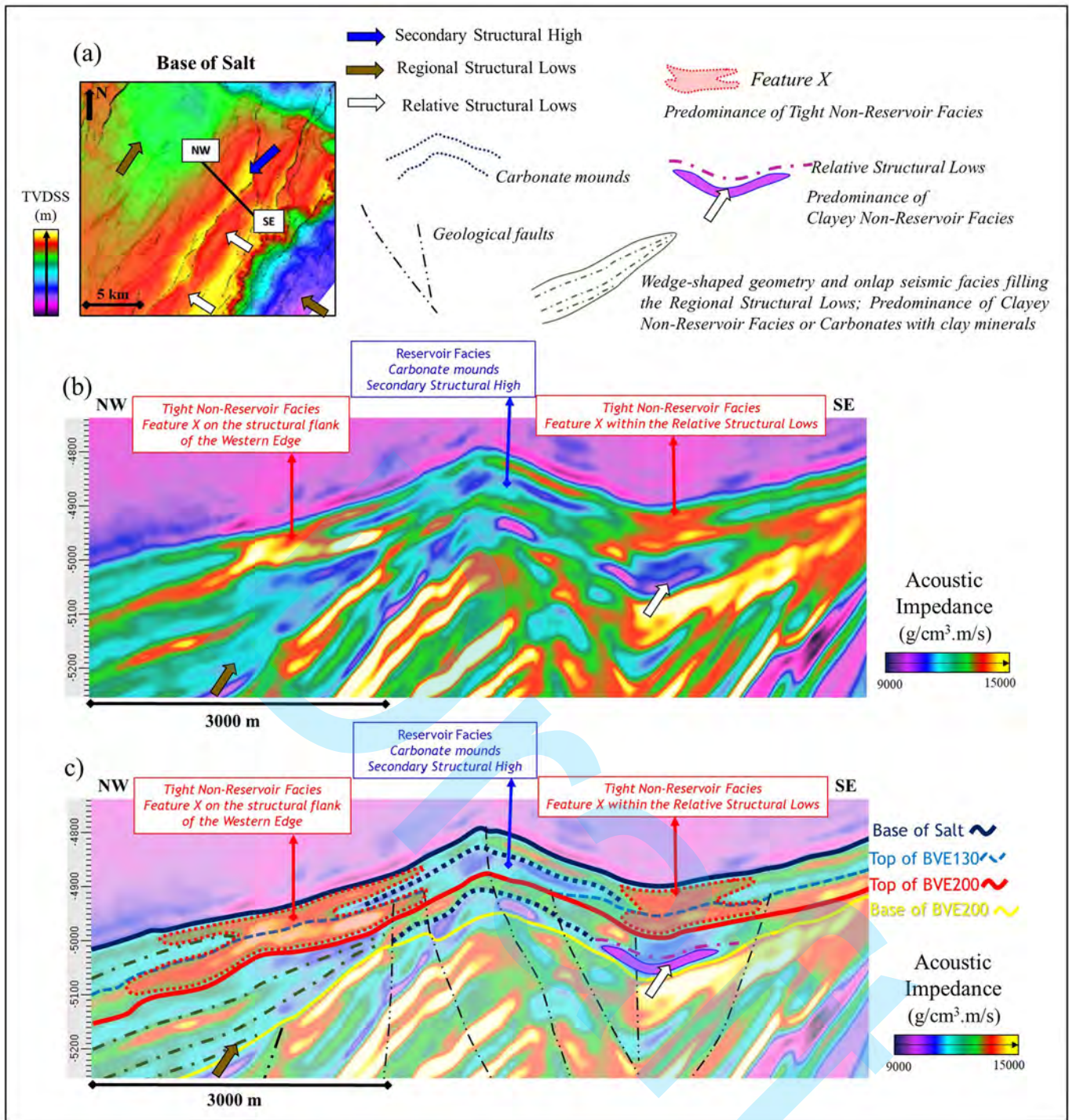


Figure 34 – High-resolution and detailed seismostratigraphic, structural, facies, and seismic features interpretations around the Secondary Structural High [blue arrows; (a), (b) and (c)] with a focus on BVE100 and BVE200 zones. The location of the seismic arbitrary section is indicated on the Base of Salt structural map (a). Variations in acoustic impedance have been correlated with changes in reservoir properties and facies, helping in delineating boundaries of large and medium-scale stratigraphic sequences. On the Secondary Structural High, note the low acoustic impedance values associated with the convex geometries of carbonate mounds and the predominance of Reservoir Facies [blue arrows; (b) and (c)]. In the Regional [brown arrows; (a), (b) and (c)] and Relative Structural Lows [white arrows; (a), (b) and (c)], note the onlap seismic facies (represented by dark green dash-dotted lines) and the internal basin-shaped format (magenta dash-dotted line and fuchsia polygon), predominantly filled with low to moderate acoustic impedance values and associated with Clayey Non-Reservoir Facies. Specifically, in the SE BVE100 zone, pay attention to the high acoustic impedance anomalies, which resemble the letter X of the alphabet [Feature X; red arrows and shapes; (b) and (c)] and border the Secondary

Structural High. Feature X is seen as an important indicator of reservoir quality degradation and the increase of Tight Non-Reservoir Facies within structural flanks, relative lows, and towards the Regional Structural Lows. In the interpreted seismic section (c), observe further how the relative increase in acoustic impedance values in the basal portion of the BVE100 zone aids in distinguishing the BVE130 subzone.

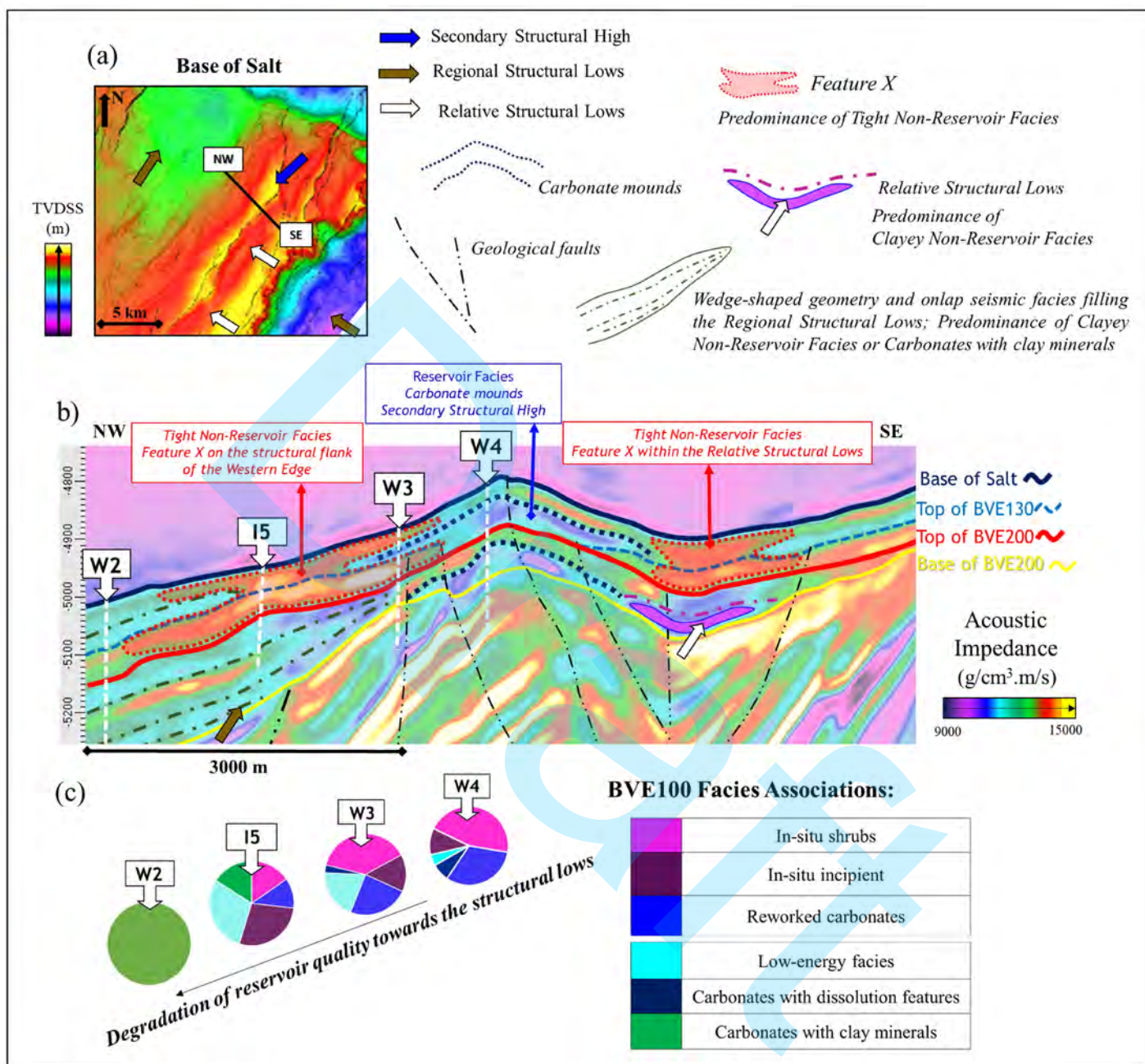


Figure 35 – High-resolution and detailed seismostratigraphic, structural, facies, and seismic features interpretations around the Secondary Structural High [blue arrows; (a) and (b)] with a focus on BVE100 and BVE200 zones. The seismic section location is indicated on the Base of Salt structural map (a). Variations in acoustic impedance correlate with changes in reservoir properties and facies [(b) and (c)]. On the Secondary Structural High, note the low acoustic impedance values associated with high porosity carbonate mounds and the predominance of Reservoir Facies, mostly in-situ shrubs within BVE100 [blue arrow; W4; (b) and (c)]. In the Regional [brown arrows; (a) and (b)] and Relative [white arrows; (a) and (b)] Structural Lows observe the onlap seismic facies (represented by dark green dash-dotted lines) and the internal basin-shaped format (magenta dash-dotted line and fuchsia polygon) predominantly displayed with low to moderate acoustic impedance values and associated with Clayey Non-Reservoir Facies (e.g., well W2). In the BVE100 interval, high acoustic

impedance anomalies resembling the letter X border the Secondary Structural High [Feature X; wells I5 and W3; red arrows; (b)]. The variation in facies proportions within BVE100, represented from wells W4 to W2 (c), highlights the importance of recognizing Feature X for well positioning, as it indicates reservoir quality degradation and possible fluid-flow baffles within flanks and structural lows [Feature X; red arrows and shapes; (b)].

Draft